UNIVERSITÄTSKLINIKUM HAMBURG-EPPENDORF

Institut für Neuroimmunologie und Multiple Sklerose

Prof. Dr. Manuel A. Friese

Translatome analysis of inflammatory neurodegeneration

Dissertation

zur Erlangung des Grades eines Doktors der Medizin
an der Medizinischen Fakultät der Universität Hamburg.

vorgelegt von:

Constantin Michael Dimitri Volkmann
aus Wiesbaden

Hamburg 2019

Angenommen von der
Medizinischen Fakultät der Universität Hamburg am: 24.04.2019

Veröffentlicht mit Genehmigung der
Medizinischen Fakultät der Universität Hamburg.

Prüfungsausschuss, der/die Vorsitzende: Prof. Dr. Manuel Friese

Prüfungsausschuss, zweite/r Gutachter/in: Prof. Dr. Matthias Kneussel

Contents

List of Figures

List of Tables

1 Introduction

1.1 Multiple sclerosis

The first known clinical description of a patient suffering from multiple sclerosis (MS) was published by CP d'Angieres Ollivier in 1824. In his diary, he reported neurological symptoms, such as bilateral neuritis, weakness in the legs, perineal numbness, urinary retentions, constipation and paralysis converting into a secondary progressive form of the disease (Compston, 1988). In 1868, the French neurologist Jean-Martin Charcot identified multiple sclerosis as a distinct disease in his work 'Histologie de la sclérose en plaques', which is why it was called Charcot disease until 1921 (Compston and Coles, 2008), before being named multiple sclerosis in 1955 (Compston and Coles, 2008). Today, MS is considered a chronic inflammatory disease of the CNS, in which focal lymphocytic infiltrates lead to demyelination and neuronal as well as axonal degeneration, resulting in a myriad of neurological symptoms and functional deficits (Compston and Coles, 2008). It is the leading cause for non-traumatic neurological disability in young adults in North America and Europe (Trapp and Stys, 2009) and affects around two and a half million individuals worldwide (Kingwell et al., 2013). Albeit extensive research, there is currently no curative treatment available.

1.1.1 Clinical presentation

In 80% of cases, multiple sclerosis first manifests itself as the so-called clinically isolated syndrome. The patients present themselves with an isolated neurological deficit that can affect motor, sensory, visual and autonomic systems (Compston and Coles, 2008). These transient impairments usually reoccur episodically, thus defining the relapse-remitting course of the disease (RRMS). The episodes emerge at random intervals, averaging at around one per year. In between the attacks, the patients initially recover fully but typically acquire persistent deficits over time, hence entering the secondary progressive MS (SPMS) phase of the illness. This applies to about 65% of patients. 20% of patients present a progressive disease character from onset (Primary progressive MS or PPMS) (Compston and Coles, 2002). In both cases, the disease progression starts at around 40 years of age (Lovas et al., 2000). Because the CNS lesions can occur in many different locations, patients may suffer from a manifold of different symptoms. RRMS usually starts with sensory disturbances, unilateral optic neuritis, diplopia (internuclear ophthalmoplegia), Lhermitte's sign (trunk and limb paresthesias evoked by neck flexion), limb weakness, clumsiness, gait ataxia, and neurogenic bladder and bowel symptoms (Noseworthy et al.,

2000). The progressive form is primarily a spinal disease but can also affect optic nerve, cerebrum and brain stem. The lifetime frequency of depression is 50%, the median time to death is 30 years from onset, while death is attributable to MS in 2/3 of cases, due to increased risk of infection and complications (Compston and Coles, 2008). The diagnosis of multiple sclerosis is made based on the modified McDonald criteria, which require dissemination in time and location of lesions and the exclusion of alternative causes. It considers clinical appearance, MRI scan results and the presence of oligoclonal bands in the cerebrospinal fluid (Polman et al., 2011).

1.1.2 Etiology

Despite all efforts in the last decades, the cause of multiple sclerosis has not yet been identified. Today, MS is considered a multifactorial disease, in which environmental factors trigger the illness in predisposed individuals.

Genetics

Already in the 19th century, a genetic component was assumed in the development of multiple sclerosis (Eichhorst, 1896). Epidemiological studies show that the prevalence of MS is about three times as high in women (Haghikia et al., 2013) and there is a familial recurrence rate of 20%, the relative risk being 9.2 for siblings and 3.4 for children of affected parents (Compston and Coles, 2008; Sawcer et al., 2014). The percentage of concordance for monozygotic twins is approximately $25 - 30\%$, whereas that for dizygotic twins is $3 - 5\%$, indicating a genetic influence (Sawcer et al., 2014). Genome-wide-association-studies (GWAS) have revealed dozens of gene loci that are associated with an increased risk of developing MS (IMSGC and WTCCC, 2011). Immunologically relevant genes are significantly overrepresented (IMSGC and WTCCC, 2011), with genetic variation within the major histocompatibility complex (MHC) exerting the greatest individual effect on risk (IMSGC, 2005). Furthermore, genes involved in cytokine pathway, co-stimulatory and signal transduction molecules of immunological relevance and genes linked to environmental risk factors such as vitamin D where found to predispose for MS (IMSGC and WTCCC, 2011). So far, few genes have been identified as predisposing to MS and being involved in neurodegeneration independent of inflammation (GALC, KIF21B) (IMSGC and WTCCC, 2011).

Exogenic factors

MS has been associated with many extrinsic factors. The prevalence of MS is strongly correlated with the distance to the equator (Simpson et al., 2011). Studies show that infections with the Epstein Barr virus are associated with the development of MS (Sumaya et al., 1980). Further environmental risk factors include month of birth (Willer et al., 2005) and smoking (Hawkes, 2007).

1.1.3 Pathology

Characteristic for MS is the formation of sclerotic plaques in the CNS. They represent the end stage of a process involving inflammation, demyelination and remyelination, oligodendrocyte depletion, gliosis and neuronal and axonal degeneration (Compston and Coles, 2008). These lesions have predilection for the optic nerves, periventricular white matter, brain stem, cerebellum and spinal cord white matter. The usually round lesions often have finger like extensions, called Dawson's fingers (Noseworthy et al., 2000), MRI imaging shows focal or confluent abnormalities in white matter in more than 95% of cases. T1 images show hypo-intense 'black holes', cortical lesions, atrophy of the brain and spinal cord. The grey matter lesions represent demyelinated cortical plaque, transected axons, apoptotic neurons and reduced neuronal density with atrophy. The CSF shows oligoclonal bands in more than 95% of cases that represent the intrathecal immunoglobuline production (MS et al., 2005). While akute white matter lesions are characteristic for the relapses of MS, there are also changes in the normal appearing white matter (NAWM). A slowly progressive axonal injury and cortical demyelination in the whole brain can be observed (Kutzelnigg et al., 2005; Popescu and Lucchinetti, 2012), which are not directly associated with the inflammatory lesions.

1.1.4 Pathophysiology

MS is traditionally considered an autoimmune disease that is triggered by autoreactive T-lymphocytes that cross the blood-brain barrier and initiate a self-directed immune reaction and inflammation in the CNS. This process it thought to lead to a continuous activation of innate immune cells such as macrophages and microglial cells in the brain parenchyma with ensuing demyelination and neurodegeneration (Compston and Coles, 2008). This is regarded as the *outside-in model*, meaning that the autoimmune process precedes neurodegeneration. Anti-inflammatory properties have therefore been in the focus of early trials and all available treatment options target the immune system. Corticosteroids as

well as plasmapheresis can be applied for the management of acute attacks (Compston and Coles, 2008) and the so-called disease modifying drugs (DMDs) are used to reduce the frequency of attacks. Disease modifying treatment of RRMS mainly aims at a reduction of relapses. Yet, long-term clinical data, MRI data and neuropathological studies show that neuronal and axonal damage occurs i) in absence of acute relapses, ii) outside MS lesions on MRI and iii) in chronic progressive stages of the disease without relapse activity, hinting at independent neurodegenerative features of the disease (Salmen and Gold, 2014). Even though the circumscribed dysfunctions during the RRMS phase are closely correlated to active white matter plaques, these lesions do not account for the diffuse brain injury and spinal cord atrophy that accumulate over time (Lassmann, 1999). In the past years, an alternative theory, the *inside-out model*, has therefore been proposed, in which MS is regarded a primarily neurodegenerative disorder (Stys et al., 2012). Indeed, in addition to the sites of acute inflammation, there seems to be a latent, subliminal process that drives neurodegeneration diffusely. It is characterised by microglial activation, astrocytic gliosis, mild demyelination and axonal loss in normal appearing white matter (Kutzelnigg et al., 2005). This latent neurodegenerative process might play an important role in the disease progression, as the number of relapses does not have a significant influence on the development of chronic disability (Confavreux et al., 2000). Further evidence for a distinct neurodegenerative process is drawn from the fact that current treatment options all affect relapse frequency and severity but have little impact on the progression rate of the disease (Haghikia et al., 2013). Even though some drugs are able to reduce neuro-axonal degeneration, it is still unclear if any drug can delay the onset of the progressive phase of the disease. In order to develop more efficacious therapies and bring the disease progression to a halt, it is thus crucial to improve the understanding of the processes underlying neurodegeneration.

1.1.5 Evidence for neurodegeneration in MS

The notion that inflammation and neurodegeneration may be two partly independent processes is supported by genome-wide association studies (GWAS), in which no correlation between genes associated with disease severity and any of the genes known to predispose to MS onset could be found (Baranzini et al., 2009; IMSGC, 2011). The mechanisms that lead to axonal and neuronal injury are not fully understood. The following section will briefly review the current state of research regarding neurodegeneration in MS.

Ion channels dysfunction

Glutamate, the main excitatory neurotransmitter in the CNS, has been described to be involved in Ca^{2+}-mediated excitotoxicity, formation of NO, mitochondrial dysfunction but also cellular survival pathways (Hardingham and Bading, 2010). Glutamate seems to be secreted by dying neurons and activated immune cells (Stranahan and Mattson, 2012), leading to elevated levels in the CSF (Sarchielli et al., 2003; Stover et al., 1997) and brains (Baranzini et al., 2010) of MS patients. In MS lesions, an up-regulation of NMDAR, AMPA and kainate receptors can be observed (Newcombe et al., 2008). During CNS inflammation a redistribution of sodium channels along demyelinated axons can be observed, probably in order to compensate for the loss of saltatory conduction. Co-localization of voltage-gated Na^+ channel Na(v)1.6 and Na^+/Ca^{2+} exchanger (NCX) subunits along demyelinated axons can be seen in MS plaques (Craner et al., 2004). Na(v)1.2 (SCN2A) is redistributed as a result of axonal injury (Craner et al., 2004) and its up-regulation during experimental autoimmune encephalomyelitis (EAE, a mouse model of MS) is associated with axonal loss (O'Malley et al., 2009). The NCX operates in reverse when Na^+ levels rise in axons, further increasing intracellular Ca^{2+} and Ca^{2+}-dependent neurotoxicity (Craner et al., 2004). The loss of saltatory conduction may result in a lesser energy efficiency of action potential, leading to a neuronal energy deficit. Deficiency of Na(v) channels and Nav/NCX blockers have been proven to reduce axonal degeneration and disability in mice (O'Malley et al., 2009; Morsali et al., 2013; Black et al., 2007). Furthermore, the pharmacological blocking of the ion channels Asic1 and Trpm4 had no impact on inflammatory infiltrates but decreased EAE severity (Friese et al., 2007; Schattling et al., 2012). The Trpm4-mediated ion-influx may lead to cell death mediated by oncotic swelling of the cells (Schattling et al., 2012).

Radical oxidation species

Immunohistochemical studies show that signs of oxidative damage are present in MS lesions. Neurons that stain positive for oxidised phospholipids reveal signs of degeneration and disturbed fast axonal transport (Haider et al., 2011). Reactive oxygen (ROS) and nitric oxide species (RNS) are produced by activated macrophages and microglial cells in an inflammatory environment, the producing enzymes are also found to be up-regulated in MS lesions (Fischer et al., 2012). Additionally, the neutralisation of ROS and RNS has been shown to rescue degenerating axons and neurodegeneration can be triggered without axonal damage by the application of NO donors (Nikic et al., 2011). Anti-oxidant

enzymes are increased in MS lesions (van Horssen et al., 2008) and in the CSF (Pennisi et al., 2011) of MS patients and the MS drug dimethylfumarate seems to work through antioxidant effects (Linker et al., 2011).

Trophic factors

Several neurotrophic factors that are released during CNS inflammation have been shown to influence the survival and death of neurons. The brain-derived neurotrophic factor (BDNF) is released by resident and infiltrating immune cells, a polymorphism in this gene has been shown to be associated with lower brain damage in MS patients (Zivadinov et al., 2007). Furthermore, endogenous cannabinoids might be involved in neuroprotection. In *Cb1*-deficient mice, EAE course is more severe and cannabinoid receptor agonist treatment is able to ameliorate EAE course and axonal loss. Interestingly, this neuroprotective effect has been shown to be moderated through neurons, not immune cells (Croxford et al., 2008).

Cell death

During MS, apoptotic pathways are activated and might contribute to neurodegeneration in NAWM (Fischer et al., 2013). Oxidative stress-induced necrosis is mediated by P53 and Cypd and through changes in mitochondrial permeability (Vaseva et al., 2012). P53 dysfunction may result in mitochondria-associated cellular dysfunction in Huntington's disease (Bae et al., 2005). Mice neuronally overexpressing the anti-apoptotic *Bcl2* are resistant to MOG-induced EAE (Offen et al., 2000). Neurons are able to influence and modulate immune cell responses during CNS inflammatory processes, for example by suppressing monocytes (Chitnis et al., 2007).

Mitochondrial dysfunction and energy deficit

The physiological cellular respiration yields radical oxygen species (ROS) as by-products. These are involved in multiple cellular responses, such as proliferation, metabolism, differentiation, apoptosis, antioxidant and anti-inflammatory response, iron homeostasis, and DNA damage response as well as mitochondrial stress (Ray et al., 2012). The mitochondrial DNA lacks protective histones and is thus vulnerable to oxidative stress that can cause mutations and DNA damage. Mitochondrial damage and dysfunction have been shown to be involved in neurodegenerative processes (Trapp and Stys, 2009; Quintanilla

and Johnson, 2009). Mitochondrial pathology might in fact precede changes in axon morphology in MS and EAE (Nikic et al., 2011). The phenol resveratrol activates sirtuin1 (a NAD^+ dependent deacetylase that promotes mitochondrial function) and has been shown to reduce neuronal loss during EAE without affecting inflammatory infiltrates (Fonseca-Kelly et al., 2012), although some studies show an exacerbation of disease course under resveratrol medication (Sato et al., 2013). CyPD is a protein involved the mitochondria permeability transition (mPT), a process considered crucial in necrotic and apoptotic cell death. *Cypd*-deficient mice are resistant towards Ca^{2+}-overload and ROS (Nakagawa et al., 2005) and show a milder EAE course (Forte et al., 2007). PGC1a is the master regulator of mitochondrial biogenesis and has been linked to neuroprotection (Farshbaf et al., 2016; Witte et al., 2013) by regulation of FNDC5. FNDC5 stimulates the expression of BDNF in the hippocampus, which in turn leads to an up-regulation of PGC1a in neurons (Farshbaf et al., 2016). AMPK, which is an activator of PGC1a (Cantó and Auwerx, 2009), has been shown to be neuroprotective (Kamoshita et al., 2016) and its loss exacerbates EAE disease severity (Nath et al., 2009). AMPK is activated by falling energy levels by detection of decreasing AMP/ATP and ADP/ATP ratios as well as dropping glucose levels (Lin and Hardie, 2018).

Protein misfolding and accumulation

Proteins possess a tertiary structure that is established by protein folding. Eukaryote cells are under constant protein quality control, ensured by proteins such as chaperones. When cells are under stress, certain proteins can change their configuration and thereby transform into toxic agents (Ciechanover and Kwon, 2017). To prevent an accumulation of these toxic substrates, misfolded proteins are either refolded or degraded via the ubiquitin-proteasome system or the autophagy-lysosome system (Ciechanover and Kwon, 2017). If these systems fail, the misfolded proteins may aggregate and lead to a number of neurodegenerative disorders, such as Alzheimer's disease, Parkinson's disease, Huntington's disease and amyotrophic lateral sclerosis (Chiti and Dobson, 2017). For example, hyperphosphorylation and accumulation of tau protein are hallmarks of neurodegenerative diseases like fronto-temporal dementia and Parkinson's, as well as Alzheimer's disease (Spillantini and Goedert, 2013). Abnormally phosphorylated protein tau has also been associated with axonal and neuronal loss in MS and EAE (Anderson et al., 2008). Proteins with a high percentage of disordered residues, such as tau or alpha-synuclein, are particularly prone to malformation and pathological aggregation, thus leading to cellular toxicity. Disordered regions or residues are parts of proteins that lack a fixed tertiary structure

(Chiti and Dobson, 2017). These protein regions can be predicted using prediction models such as the VSL algorithm (Peng et al., 2006).

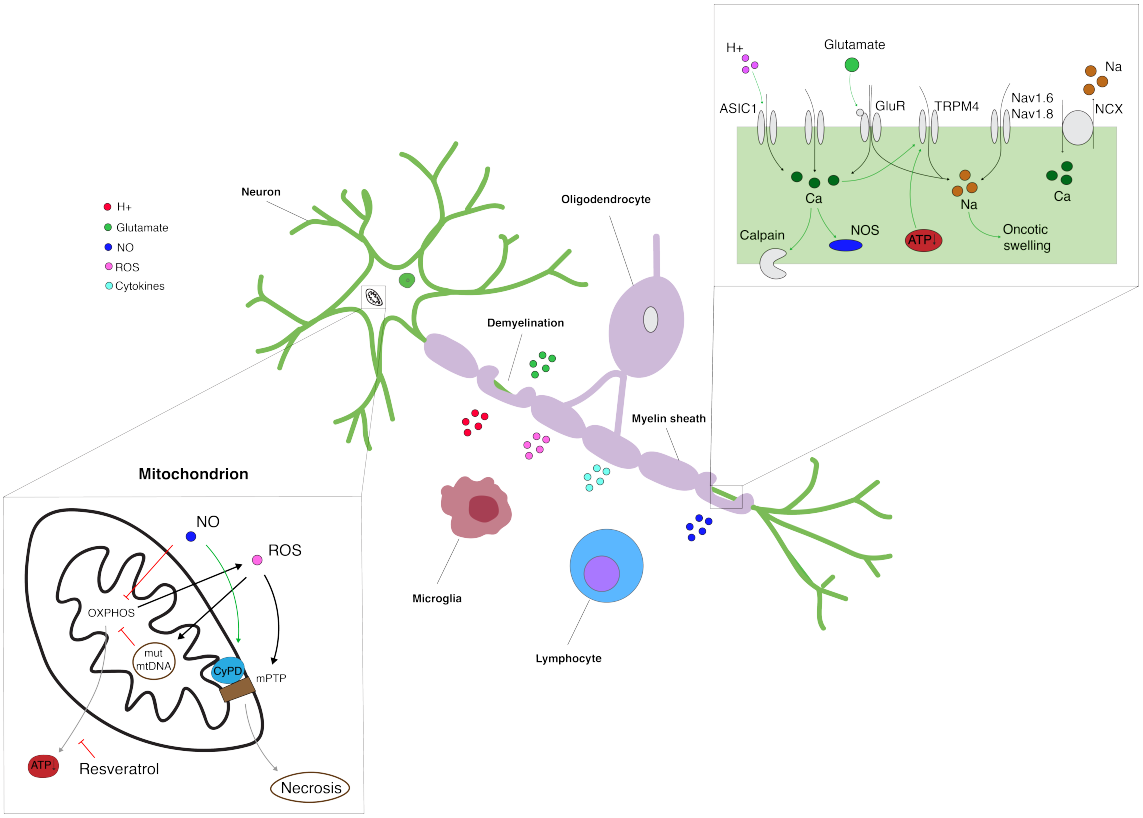

Figure 1.1: Model of neurodegerative processes during MS. The image was inspired by Friese et al. (2014). OXPOS = oxidative phosphorylation; mut mtDNA = mutated mitochondrial DNA; CyPD = Cyclophilin D; mPTP = mitochondrial permeability transition pore.

1.2 Animal models

While human studies, such as post-mortem brain sections and imaging techniques, can provide some insight into disease mechanisms, the study of molecular mechanisms underlying neurodegeneration requires *in vivo* studies of nervous tissue. To this end, animals models are frequently used. Experimental autoimmune encephalomyelitis (EAE) is a widely utilised animal model for human demyelinating diseases, such as MS. Its development can be traced back to Louis Pasteur who first accidentally induced an ascending paralysis in humans when immunising his patients against Rabies by the injection of spinal cord ma-

terial of infected rabbits (Baxter, 2007). Post-mortem histology showed encephalomyelitis characterised by lymphoid infiltrates and demyelination in the CNS of those patients (Peter Bassoe, 1929). In rodents, EAE can be induced by immunisation with a component of the myelin sheath, such as myelin basic protein (MBP), myelin oligodendrocyte glycoprotein (MOG) or proteolipid protein (PLP) in an emulsion with complete Freund′s adjuvant. In SJL mice, the disease is characterised by a relapsing-remitting course of paralysis, which allows assessment of the efficacy of various immuno-regulatory strategies. In C57BL/6 mice, the disease displays a mono-phasic clinical course. The illness is a $CD4^+$ T cell-mediated autoimmune disease characterised by perivascular $CD4^+$ T cell and mononuclear cell inflammation and subsequent primary demyelination of axonal tracks in the central nervous system (CNS), leading to progressive hind-limb paralysis (Robinson et al., 2014). The degree of disease affection is evaluated on a scale of 0 to 5. This animal model has been criticised, as the pathophysiology differs significantly from MS (Sriram and Steiner, 2005). On the other hand, all FDA-approved MS-therapies are effective to some extend in EAE and some disease-modifying drugs have been identified in EAE (Robinson et al., 2014).

1.3 Translatome versus transcriptome

Proteins are macromolecules which perform a myriad of functions in living organisms, like enzymatic reactions, transport, receptors, ion channels and many more. The protein-encoding DNA-sequence is first transcribed into messenger-RNA (mRNA) and then - if required - translated into a protein via protein complexes called ribosomes. This process of protein biosynthesis is strongly regulated at many different stages, starting from DNA-methylation down to post-translation modification and folding of proteins. The profile of all proteins in a cell (the proteome of a cell) determines its phenotype, it adapts according to the cells requirements driven by intra- and extracellular stimuli. One widely-used approach in predicting the proteome of a cell or tissue, is to analyse its transcriptome (profile or sum of all mRNA) via microarray or sequencing analysis but it has been shown that there is no direct link between the two profiles (Dhingra et al., 2005). A more accurate way of predicting the proteome of a cell is to study its translatome, which represents the entirety of all mRNA, which are actually (in the process of being) translated into proteins. A study conducted in a cancer cell line (HeLa cells) showed a high degree of uncoupling between the transcriptome and the translatome (ribosome-bound mRNA transcripts), up to anti-directional changes (Conceptualised in fig. 1.2). The degree of homo-directional changes was as low as 5% in EGF (epidermal growth factor)-treated HeLa-cells (Tebaldi

et al., 2012). Intriguingly, 85% of the changes were seen in the translatome only, which suggests a higher sensitivity of translatome-analysis in predicting changes in protein profiles.

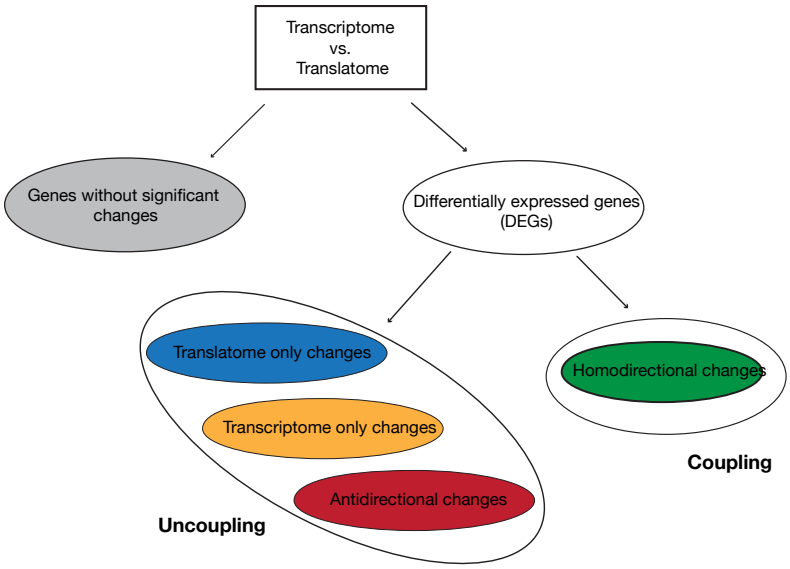

Figure 1.2: Illustration was inspired by Tebaldi et al. (2012), depicting the coupling and uncoupling of changes in the translatome and transcriptome.

1.4 Analysis of neuronal gene expression profiles

The above mentioned mechanisms do not fully explain the inflammatory neurodegenerative processes in MS and EAE. In order to illuminate the molecular processes contributing to neurodegeneration, it is necessary to study the changes in neuronal gene expression profiles. This goal poses methodological problems, as it requires the isolation of neuronal material from a mixed CNS tissue. Conventional research methods like PCR, microarray or RNA/cDNA sequencing of whole tissue homogenates will detect transcripts from all cell types and cannot distinguish between their origin. During EAE, many of the detected changes in the mRNA profile are likely to be due to the altered cell composition, as infiltrating immune cells and activated resident immune competent cells import high amounts of immunological genes into the inflamed tissue (Raddatz et al., 2014). Different methods have been applied in order to analyse neuronal expression profiles *in vivo*, each having limitations. Single-cell *in vitro* analysis of neurons (Tietjen et al., 2003) can't

imitate the complex environment of a CNS. Other methods for *in vivo* analysis involve laser-capture microdissection (LCM) (Rossner et al., 2006) and fluorescence activated cell sorting (FACS) (Lobo et al., 2006). These methods are limited by prolonged tissue processing *ex vivo*, which may lead to changes in gene expression and mRNA levels. Moreover, tissue fixation for LCM poses problems on high-quality RNA isolation (Rossner et al., 2006) .

1.4.1 BacTRAP

Because of the limitations of conventional isolation techniques, a novel approach called bacTRAP was applied in this study to extract neuronal mRNA from a mixed CNS tissue. The transgenic *Chat* bacTRAP mouse line uses a bacterial artificial chromosome (BAC) to express a fusion protein of an enhanced green fluorescent protein (EGFP) and the ribosomal protein L10a under the motor neuron-specific choline acetyltransferase (*Chat*) promotor. This allows to harvest ribosome-bound, i.e. translating, mRNA specifically from neuronal cells via anti-eGFP antibodies coupled to magnetic beads, a method termed translating ribosome affinity purification or TRAP (Heiman et al., 2008). This denotes a major advantage of bacTRAP over conventional gene expression analysis techniques, as the mRNA yielded by the precipitation of translating ribosomes incorporates the translatome rather than the transcriptome of a cell line.

1.5 Aims

Multiple sclerosis is a chronic neurological disease which poses a major burden for many individuals and the public healthy system. Neurodegenerative processes substantially contribute to disease severity and long-term disability. In order to abate disease progression, a more thorough understanding of the processes preceding and contributing to neurodegeneration is needed. To this end, it is necessary to identify protective and maladaptive molecular pathways in neurons during CNS inflammation. The required extraction of neuron-specific mRNA *ex vivo* poses methodological issues, which have thus far been solved only unsatisfactorily. The so-called *Chat* bacTRAP methodology holds the promise of achieving this aim with unparalleled accuracy.
The goal of this thesis was to establish the *Chat* bacTRAP method and validate its cell-specificity using immunohistochemistry and qPCR analyses. After successful implemen-

tation of the method, the objective was to identify changes in the neuronal translatome in response to neuroinflammation by comparing gene expression profiles of motor neurons of healthy and EAE mice via qPCR and whole translatome analysis. The aim was to uncover protective and maladaptive neuronal responses in order to identify potential therapeutical targets for MS patients.

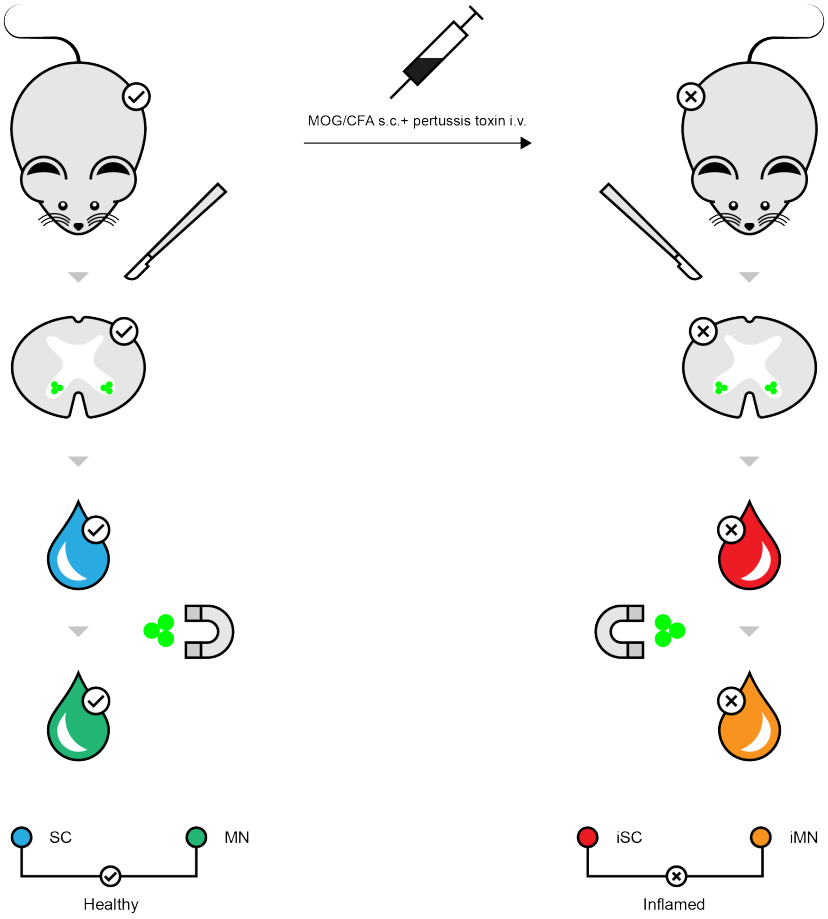

Figure 1.3: Graphical abstract of experimental approach. *Chat* L10a-eGFP transgenic mice are either healthy (tick) or immunised in order to induce EAE (cross). The cervical spinal cords are dissected, RNA extraction is conducted on whole tissue before (blue drop for healthy spinal cord (SC) and red drop for inflamed spinal cord (iSC)) and after (green drop for healthy motor neurons (MN) and orange drop for inflamed motor neurons (iMN)) immunoprecipitation via TRAP (symbolised by magnet collecting mRNA from L10a-eGFP expressing motor neurons). The four retrieved samples are then used for further analysis via qPCR and RNA-seq.

2 Materials and Methods

2.1 Materials

2.1.1 Reagents

Table 2.1: Reagents for animal experiments

Reagent	Company
Freund's adjuvant, complete	Difco laboratories
Mouse/rat $MOG_{35–55}$ peptide MEVGWYRSPFSRVVHLYRNGK-NH2	Schafer-N
Mycobacterium tuberculosis H37	Difco laboratories
Pertussis toxin, from Bordetella pertussis	Calbiochem

Table 2.2: Reagents for RNA extraction, cDNA synthesis and real-time PCR

Reagent	Company
2-Mercaptoethanol	Gibco
Ethanol, absolute	Th. Geyer
RevertAid H Minus first Strand Synthesis Kit	Thermo Scientific
RNA isolation columns, RNeasy Micro Kit	Quiagen
TaqMan Gene Expression Master Mix	Life Technologies

Table 2.3: Reagents for anaesthesia and tissue preparation

Reagent	Company
Esketamin Hydrochlorid (Ketanest)	Pfizer
Isopentan	Roth
PFA	AppliChem
Saccharose	Roth
Tissue Freezing Medium	Jung
Xylazin Hydrochlorid (Rompun 2%)	Bayer

Table 2.4: Reagents for immunhistochemistry

Reagent	Company
Triton X-100	Roth
Normal donkey serum	Chemikon
PBS	Gibco

Table 2.5: Chemicals

Product	**Manufacturer**
0,9% NaCl solution	Braun
1M $MgCl_2$	Ambion
2M KCl	Ambion
Biotinylated Protein L	Pierce
Cycloheximide	Sigma
DEPC-treated water	Ambion
DHPC	Avanti
Dithiothreitol	Sigma
Fluoromount-G	Southern Biotech
Glucose	Roth
Glycoblue	Ambion
Hank's Balanced Salt Solution (10x)	Invitrogen
HEPES	Roth
IgG-free BSA	Jackson
Potassium hydroxide	Roth
$NaHCO_3$	Roth
Paraformaldehyd (PFA)	AppliChem
PBS	Ambion
Protein Solubilizer 40, Sterile 10% of NP-40	AG Scientific
Recombinant Rnasin	Fisher
Research plus pipette	Eppendorf
RNA Pico Chip	Agilent
RNase Zap	Ambion
RNeasy mini kit	Qiagen
S-ketamine hydrochloride	Pfizer
SafeSeal RNase-free 1,5 ml tube	Sarstedt
Streptavidin MyOne T1 Dynabeads	Invitrogen
Superasin	Promega
TriZol-LS reagent	Invitrogen
Xylazine hydrochloride	Bayer

2.1.2 Antibodies

Table 2.6: Antibodies (Ab) for immunohistochemistry

Product	clone	dilution	Manufacturer
Anti-Bsn, mouse IgG	SAP7F407	1:400	Enzo Life Sciences
Anti-Cd31, rat IgG	550274	1:50	BD Pharmingen
Anti-Cnpase, mouse IgG	C5922	1:500	Sigma-Aldrich
Anti-Egfp, chicken polyclonal	ab13970	1:1000	Abcam
Anti-Gfap, chicken polyclonal	ab4674	1:1000	Abcam
Anti-Iba1, goat IgG	ab107159	1:500	Abcam
Anti-Neun, mouse IgG	MAB377	1:200	Millipore
Cy2-coupled donkey anti-chicken IgG	715-166-150	1:300	Jackson
Cy3-coupled donkey anti-mouse whole IgG	703-225-155	1:300	Jackson
Dye549-coupled donkey anti-rat F(ab)	712-506-150	1:300	Jackson

Table 2.7: Antibodies for immunoprecipitation

Product	Manufacturer
HtZ-GFP 19C8 Memorial	Sloan-Kettering Monoclonal Ab Facility
HtZ-GFP 19F7 Memorial	Sloan-Kettering Monoclonal Ab Facility

2.1.3 Primers

Table 2.8: Primers for PCR

Gene name	Primer	Manufacturer
Ampk	Mm01264789_m1	Applied Biosystems
Arc	Mm00479619_g1	Applied Biosystems
Chat	Mm01221882_m1	Applied Biosystems
Clcn5	Mm00443851_m1	Applied Biosystems
Cnp	Mm01306640_m1	Applied Biosystems
Fndc5	Mm01181543_m1	Applied Biosystems
Gapdh	Mm99999915_g1	Applied Biosystems
Gfap	Mm01253033_m1	Applied Biosystems
Hif1	Mm00468869_m1	Applied Biosystems
Hvcn1	Mm01199507_m1	Applied Biosystems
Ncam	Mm00456815_m1	Applied Biosystems
P53	Mm01731287_m1	Applied Biosystems
Pgc1a	Mm01208835_m1	Applied Biosystems
Scn2a1	Mm01270359_m1	Applied Biosystems
Sesn2	Mm00460679_m1	Applied Biosystems
Trpm4	Mm00613159_m1	Applied Biosystems
Ucp2	Mm00627599_m1	Applied Biosystems

2.1.4 Solutions

Table 2.9: Blocking solution

Starting	Final concentration
Triton X-100	0,01%
Normal donkey serum	10%
PBS	

Table 2.10: 0.15 M KCl IP wash buffer (30 ml stock)

Starting	Amount to add	Final concentration
1 M HEPES	600 μl	20 mM
1 M $MgCl_2$	150 μl	5 mM
2 M KCl	2.25 ml	150 mM
10% NP-40	3 ml	1%
DEPC-treated water	24 ml	
Immediately before use:		
1 M Dithiothreitol	5 μl	0.5 mM
Cycloheximide	30 μl	100 μg/ml

Table 2.11: 0.35 M KCl wash buffer (30 ml stock)

Starting	Amount to add	Final concentration
1 M HEPES	600 μl	20 mM
1 M $MgCl_2$	150 μl	5 mM
2 M KCl	5.25 ml	350 mM
10% NP-40	3 ml	1%
DEPC-treated water	21 ml	

Table 2.12: Dissection buffer (50 ml stock)

Starting	Amount to add	Final concentration
10 x HBSS	5 ml	1 x
1 M HEPES-KOH (pH 7.4)	125 μl	2.5 mM
1 M Glucose	1.75 ml	35 mM
1 M $NaHCO_3$	200 μl	4 mM
DEPC-treated water	42.875 ml	
Immediately before use:		
1000 x Cycloheximide	50 μl	100 μg/ml

Table 2.13: Lysis buffer (10 ml)

Starting	Amount to add	Final concentration
1 M HEPES-KOH (pH 7.4)	200 μl	20 μl
2 M KCl	750 μl	2.5 mM
1 M $MgCl_2$	50 μl	5 mM
DEPC-treated water		
Immediately before use:		
1 M Dithiothreitol	5 μl	0.5 mM
Protease Inhibitor	1 tablet	
1000 x Cycloheximide	10 μl	100 μg/ml
RNasin	100 μl	40 U/ml
Superasin	100 μl	20 U/ml

2.1.5 Equipment

Table 2.14: Equipment

Product	Manufacturer
DynaMag-2	Invitrogen
Freezing microtome CM3000	Leica Jung
TCS SP2 confocal microscope	Leica
Bioanalyzer 2100	Agilent
Centrifuge 5417 R	Eppendorf
ABI Prism 7900 HT Fast Real-Time PCR	Applied Biosystems
Fridges (4°C) and freezers (-20°C and -80°C)	Liebherr, Sanyo
Nanodrop Nd-1000	Peqlab
PCR cycler, FlexCycle	Analytik Jena
PCR tanks and power supply	Peqlab, Biometra
Pipets and pipette controllers	Gilson, Eppendorf, Brand

2.1.6 Consumables

Table 2.15: Consumables

Product	Manufacturer
Eppendorf tubes	Sarstedt
Falcon tubes, 15 and 50 ml	Greiner
PCR plate, 96 well and PCR plate sealing tape	Sarstedt
Pipette tips	Sarstedt
Syringes and needles	Braun

2.1.7 Software

Table 2.16: Software

Product	Company
BibDesk bibliography manager for Mac	
Illustrator	Adobe
NanoDrop ND-1000 V3.5.2	Thermo Scientific
RStudio	
TeXShop	

2.2 Methods

2.2.1 Mice

ChAT bacTRAP hemizygous ($^{+/-}$) and littermate WT ($^{-/-}$) transgenic mice (Chat BACarray line DW165) on a C57BL/6J background were used. All animal experiments were approved by the local ethics committee (Behörde für Soziales, Familie, Gesundheit und Verbraucherschutz in Hamburg).

2.2.2 Experimental autoimmune encephalomyelitis

EAE was induced by injecting 200 μg of MOG_{35-55} peptide in complete Freund's adjuvant containing 4 mg/ml mycobacterium tuberculosis in each flank of the mice. Furthermore, 200 ng of pertussis toxin in 100 μl 0,1 M Dulbecco's phosphate buffered saline were injected intravenously on the day of immunisation and 48 h later. Mice were scored for clinical signs by the following system: 0: no clinical deficits; 1: tail weakness; 2: hind limb paresis; 3: partial hind limb paralysis; 3.5: full hind limb paralysis; 4: full hind limb paralysis and forelimb paresis; 5: premorbid or dead. Mice were killed at a score >=4. The mice were supplied with soft food.

2.2.3 Immunohistochemistry

Mice were anaesthetised by intraperitoneal injection of 100 μl Ketamine/Xylazine in PBS (10 mg/ml S-Ketamine hydrochloride, 1.6 mg/ml Xylazine hydrochloride) per 10 g of body weight. Intracardial perfusion was implemented using cold PBS for 3 minutes followed by 4% paraformaldehyde (PFA) in PBS for 7 minutes in order to fixate the tissue using a peristaltic pump. The preparation of the spinal cord tissue was performed manually and post fixation was conducted for 30 minutes in 4% PFA. The tissue was then placed in 30% sucrose in PBS and stored at 4°C for 24 hours for cryoprotection. The spinal cord probes

were then embedded in Jung Tissue Freezing Medium and cut into 10 μm thick sections using a freezing microtome and stored at -80°C. For immunohistochemistry, the sections were incubated in blocking solution (10% normal donkey serum in PBS) containing 0.01% Triton X-100 at room temperature for 45 min and subsequently stained overnight at 4°C with antibodies against the following structures: Egfp, NeuN, Gfap, Cd31, Iba1, Cnpase or Bsn. As secondary antibodies, Cy2-coupled donkey antibodies recognising chicken whole IgG, Cy3-coupled donkey antibodies recognising mouse whole IgG and Dye549-coupled donkey antibodies were used. DNA was stained with Hoechst 33258 (Invitrogen), sections were analysed with a Leica TCS SP2 confocal microscope.

2.2.4 Translating ribosome affinity purification (TRAP)

The following protocol was applied for 1 Immunoprecipitation (IP): 300 μl Streptavidin-labeled magnetic beads (Streptavidin MyOne T1 Dynabeads, Invitrogen) were collected on a DynaMag-2 magnet (Invitrogen), then washed in 1 ml PBS and recollected on magnet for 1 min. The supernatant was removed and the beads were resuspended in 1 ml of PBS. 120 μl of biotinylated Protein L in PBS were then added to the solution and incubated for 35 min at room temperature using end-over-end rotation. The beads were subsequently washed five times with 1 ml PBS containing 3% IgG- and protease-free BSA. Next, the beads were incubated with a total of 100 μg of two monoclonal anti-eGFP antibodies for 1 hour using end-over-end rotation. For this purpose, 83 μl of HtZ-GFP 19C8 at 0.6 μg/μl and 22 μl HtZ-GFP 19F7 at 2.2 μg/μl (clone 19F7 and 19C8; Memorial Sloan-Kettering monoclonal antibody facility) were suspended in 1 ml 0.15 M KCl buffer and added to the biotinylated Protein L - beads mix. The antibody-solutions were stored at -80°C in single-use aliquots. After incubation, the beads were again collected on the magnet, washed three times in 1 ml of and resuspended in 200 μl of 0.15 M KCl IP wash buffer and then stored on ice. Mice were anaesthetised by intraperitoneal injection of 100 μl Ketamine/Xylazine in PBS per 10 g of body weight. Intracardial perfusion was implemented for 1 minute using chilled dissection buffer. Spinal cords were quickly dissected and stored in dissection buffer on ice. Cervical spinal cord tissues of three mice were pooled and homogenised in 1 ml lysis buffer using a hand homogeniser with 12 strokes applied. Homogenates were centrifuged for 10 minutes at 2,000 x g and 4°C in order to pellet large cell debris, and NP-40 and DHPC were added to the supernatant at a final concentration of 1% and 30 mM, respectively. After incubation on ice for 5 minutes, the clarified lysate was centrifuged for 10 minutes at 20,000 x g to pellet insoluble material. 100 μl of each probe was extracted before further processing and used as Input for normalisation and control

purposes. The previously prepared antibody-coated beads were added to the supernatant and the mixture was incubated at 4°C with end-over-end rotation overnight. The beads were subsequently collected on a magnetic rack, washed four times with 0.35 M KCl wash buffer and immediately placed in 800 μl TriZol-LS reagent (Invitrogen) and incubated at room temperature for 5 minutes.

TriZol preparation

In order to extract the bound rRNA and mRNA from polysomes, 200 μl of chloroform were added. The tubes were shaken vigorously for 15 seconds and then incubated for another 3 minutes at room temperature. The mix was centrifuged at 12,000 x g and 4°C for 15 min and the RNA-containing, colourless upper phase was carefully collected and transferred to new tube.

Sodium acetate precipitation

In order to pellet RNA, 30 μl of sodium acetate to a final concentration of 0.3 M and 300 μl of isopopanol were added. For better visualisation, 5 μl of Glycoblue (Ambion) were applied. The solution was stored at -80°C overnight, then spun down at 13,000 x g at 4°C for 15 minutes. The pellet was washed twice in 70% ethanol, spinning down in between at 13,000 x g at 4°C for 5 minutes, then air-dried for 15 minutes under a cell culture hood. For resuspension, 20 μl of RNase-free water were added to the pellet, tubes were stored at -80°C.

RNA isolation

The RNA was subsequently purified using the Quiagen Micro Kit with on-column DNA-digestion. 10 μl buffer RDD and 2,5 μl DNase I stock solution were added to the probe and volume was adjusted to 100 μl using RNase-free water. The tube was incubated on the benchtop (20-25°C) for 10 min. First 350 μl of buffer RLT containing 1% 2-mercaptoethanol, then 250 μl of 100% ethanol were added and the solution was mixed by pipetting up and down several times. The sample was transferred to a spin column placed in a 2 ml collection tube, which was centrifuged for 15 s at 8000 x g. The RNA was then washed using 700 μl RW1 buffer (15 s at 8,000 x g), 500 μl RPE buffer (15 s at 8,000 x g) and 500 μl of 80% ethanol (2 min at 8,000 x g) and consecutively redistributed in 14 μl of RNase-free water.

2.2.5 Reverse transcription of RNA

The cDNA was synthesised using the RevertAid H Minus First Strand cDNA Synthesis Kit (Fermentas). 1 μl of random hexamer primers was added to the isolated RNA, the volume was adjusted to 12 μl per reaction with RNase-free (DEPC treated) water and the samples were denatured at 65°C for 5 min. Subsequently, 4 μl 5 x reaction buffer, 1 μl RiboLock RNase Inhibitor (20 U/μl), 2 μl 10 mM dNTP Mix and 1 μl RevertAid H Minus M-MuLV Reverse Transcriptase (200 U/μl) were added. The mix was incubated at 25°C for 5 min followed by 60 min at 42°C for reverse transcription. The reaction was terminated by heating at 70°C for 5 min.

Table 2.17: Solution for incubation step

Input	**Final concentration**
RNA	
Random hexamers (50 μM)	1 μl
DEPC H_2O	add up to 12 μl

Incubation at 65°C for 5 minutes, followed by cooling on ice. Then, the following ingredients were added to the solution:

Table 2.18: Solution for reverse transcription

Input	**Final concentration**
5 x Reaction buffer	4 μl
RiboLock RNase Inhibitor	1 μl
dNTP Mix 10 mM	2 μl
RevertAid H- M-MuLV RT (200 U/μl)	1 μl
RNA solution	12 μl

The solution with a total of 20 μl was then carefully mixed, centrifuged briefly and subsequently incubated in cycler, using the following programme:

Table 2.19: Incubation step of reverse transcription

Temperature	**Duration**
25°C	5 min
42°C	60 min
70°C	5 min

The yielded cDNA was stored at -20°C.

2.2.6 Real-time PCR

The polymerase chain reaction (PCR) is a method used to amplify DNA fragments utilising the DNA polymerase enzyme. The DNA is first denatured to single strands at 90-95°C, complementary oligonucleotides (primers) then bind to the DNA in the annealing step at 50 - 65°C. In the subsequent elongation step, the polymerase enzyme copies the DNA single strands by incorporating dNTP, usually at a temperature of 69 - 72°C. This cycle is repeated several times which yields an exponentially increasing amount of DNA.

Table 2.20: Solution for rtPCR

Input	**Final concentration**
20 x TaqMan gene expression assay	0.5 μl
2 x TaqMan gene expression master mix	5.0 μl
RNase-free water	2.5 μl
cDNA template	2 μl

Thermal profile, 40-45 cycles of:

Table 2.21: Incubation step of rtPCR

Temperature	**Duration**
50°C	2 min
95°C	10 min
95°C	15 sec
60°C	1 min

Analysis of all results was performed using the $\Delta\Delta Ct$ method for relative quantification. Values were normalised to *Gapdh* and the respective Input (WT Input, Transgenic (GFP) Input) to correct for different compositions of starting material.

2.2.7 Quantification of DNA and RNA

The concentration of double-stranded DNA (plasmids, PCR and restriction digestion fragments) and RNA was determined spectrophotometrically by absorbance at 260 nm using the conversion factor: A260 = 1 = 50 μg/ml for DNA and A260 = 1 = 40 μg/ml for RNA. The ratio of A260/A280 was used as a marker for purity. Preparations with an A260/A280 value of $1.8 - 2.0$ for DNA and $2.0 - 2.2$ for RNA were considered pure.

2.2.8 Deep sequencing analysis

The probes for the deep sequencing analysis were cooled down to -80°C and sent to the deep sequencing facility Göttingen (Transcriptome and genome analysis laboratory, microarray and deep-sequencing facility Göttingen), which conducted the deep sequencing and preparation of the raw data. The following settings were used:

Basic data:
Illumina HiSeq 4000 50 bp single end run + 7 bp for Index, mRNA 20 samples: 4 groups with 5 replicates.

Processing and analysis pipeline:

1. Demultiplexing: CASAVA v1.8.2, 1MM allowed for index, indices different in at least 2 bases
2. Alignment: STAR (2.3.0), local alignment; mm10 transcriptome reference of Ensembl, 2MM allowed
3. Conversion + sorting via samtools 0.1.19
4. Counting reads per gene via htseq version 0.5.4.p5
5. Data analysis via R/Bioconductor (3.0.2/2.14)
    a) DESeq (1.14.0) => normalisation, dispersion estimation, negative binomial distribution
        i. Normalisation: scaling factor calculated as the median of the ratio gene/geometric mean of all samples for all genes (see DESeq paper)
        ii. gene filtering: raw counts > 3 counts at least for one sample in pair-wise comparison; addition of 1 for each gene count for fc computation
        iii. filter: fc> 2 x, pFDR< 0.05
    b) further annotation: ensembl biomart (2.18.0) via R
    c) goseq (1.14.0), GO.db (2.10.1),: GO enrichment test on candidate genes

Automation pipeline 1.-4. in cooperation with the DZNE.

Description:

Sequence images were transformed with Illumina software BaseCaller to bcl files, which were demultiplexed to fastq files with CASAVA (v1.8.2). Reads were aligned by STAR (2.3.9e) to the Ensembl Mus musculus transcriptome (mm10). Counting the reads to each gene was done via HTSeq python scripts. Data was preprocessed and analysed in the R environment (3.0.2/2.14) loading DESeq, gplots, and biomaRt packages. After filtering the genes exceeding more than 3 counts for at least one sample, normalisation, estimation of dispersions and testing for differentially expressed genes based on a test assuming negative binomial data distribution was computed via DESeq. Candidate genes were filtered to a minimum of 2 x fold change and FDR-corrected pvalue$<$ 0.05. Everything in the section **Deep sequencing analysis** was conducted by the deep sequencing facility Göttingen.

2.2.9 Data analysis

The yielded raw data was analysed by us using R Studio, version 1.0.136. GO term analysis was conducted using the integrated tool on http://www.geneontology.org/page/go-enrichment-analysis and the GeneAnswers package in R. All plots were done using the ggplots2 package or the GeneAnswers package.

Lower threshold

In order to minimise the non-specific background, a lower threshold for the IP/Input fold change was set. Genes with a fold change below this threshold were excluded from analysis. The threshold was calculated as follows, based on negative control genes taken from (Dougherty et al., 2010). The negative control genes were:

- *Plp1*
- *Slc1a3*
- *Vim*
- *Mbp*
- *Cnp*
- *Gfap*
- *Clp*

$$threshold = \mu + 2 * \sigma$$

where

$$\mu = \frac{\sum_{n=0}^{j} \log_2 \frac{IP_{\mathrm{j}}}{\mathrm{Total_j}}}{j}$$

and

$$\sigma = \sqrt{\frac{1}{j} * \sum_{n=0}^{j} \mu - \log_2 \frac{IP_{\mathrm{j}}}{Total_{\mathrm{j}}}}$$

Adjusted p-value

For the 'Neuron up' and 'Neuron down' gene list, the included genes were required to fulfil the following criteria:

- iMN/MN > 2, p-value < 0.05 and
- iMN/iSC > 2, p-value < 0.05

Let A and B the following events:
A: MN/MN > 2 is a false positive
B: iMN/iSC > 2 is a false positive
Then :
p(A $\cup$ B) = p(A) + p(B) - p(A $\cap$ B)

In words:

The probability of either iMN > MN or iMN > iSC being a false positive equals to the added probability of either event minus the probability of both being false positives. As it is not known to which degree both events are dependent, a conservative approach was chosen by applying the following restriction:
p(A) + p(B) < 0.05 , the adjusted p-value for 'Neuron up' to was set to:
p('Neuron up') = p(iMN vs MN) + p(iMN vs iSC)
and for 'Neuron down' accordingly:
p('Neuron down') = p(iMN vs MN) + p(MN vs SC)

2.2.10 Statistical analysis

All data are presented as mean values ±SEM. Mean differences between two experimental groups were determined by unpaired or paired, two-tailed Student's t-test. Comparison of three or more groups was performed by one-way analysis of variance (ANOVA) with Bonferroni's post hoc test. All statistical analyses were performed using R Studio for Mac. Significant results are indicated by asterisks: $*P < 0.05$; $**P < 0.01$;$***P < 0.001$.

2.2.11 Prediction of natural disordered regions

Disordered regions are defined as entire proteins or regions of proteins that lack a fixed tertiary structure and were evaluated using the predictor of natural disordered regions (PONDR) VSL2 algorithm (Peng et al., 2006) available through http://www.pondr.com. The plots were graphically improved using Adobe Illustrator.

2.2.12 Gene Ontology analysis

The Gene Ontology (GO) is a major bioinformatics initiative which developed a computational representation of the knowledge of all genes and their functions in different organisms. It integrates the combined knowledge about a genes and their functions of experiments reported in over 100,000 peer-reviewed scientific papers. If a gene is shown to be involved in a certain function, it receives an annotation referring to that function. Three independent ontologies have been constructed: biological process, molecular function and cellular component (Ashburner et al., 2000). The GO library is under constant improvement (The Gene Ontology Consortium, 2017).

Statistical analysis of GO frequency

The statistical analysis of the GO frequency in a given gene list was done by a hypergeometric statistic using the GeneAnswers package in R (Feng et al., 2010). Enrichment maps summarise overlapping gene sets into interconnected clusters, in which each node represents a significantly regulated gene set. For the visualisation of GO and KEGG enrichment maps, the GeneAnswers package (Feng et al., 2010) in R Studio was applied. To increase legibility, very general and thus highly interconnected GO terms that gave no additional biological insight with regard to their child terms were removed. The following settings were used: pvalueT=0.1 , FDR-correction=TRUE, hypergeometric G statistics, removed noncritical layers of GO IDs: 3 (5 in the case of whole transcriptome changes, because of many unspecific terms).

2.2.13 CSEA

Using bacTRAP data of different cell-lines, the so-called specificity index (SI) (Dougherty et al., 2010) can be used to identify genes enriched in specific cell populations across a large number of profiles based on gene expression levels. For any given cell-type, a list of specific genes, dependent on a specificity index p-value (pSI) threshold, can now be generated, a method called cell-type specific expression analysis or CSEA (Xu et al., 2014). The CSEA was used to determine the cell-specificity and cell-composition of the *Chat* bacTRAP material.

2.2.14 GSEA

The gene set enrichment analysis (GSEA (Subramanian et al., 2005)) is a computational method that determines wether the expression levels of genes within a given set vary significantly between two conditions. Specifically, it determines wether the members of a given gene set are significantly over or under-represented at the top or bottom of a ranked gene list. The enrichment score (ES) represents how strong this association is, it corresponds to a Kolmogorov-Smirnov-like statistic (Hollander and Wolfe, 1973). The GSEA was utilised to determine the enrichment of gene clusters in neurons of EAE mice. The sets of marker genes for the gene-set enrichment analysis were retrieved from public sources (Bader lab website, $http://download.baderlab.org/EM/Genesets/current\_release/$)
or custom compiled from the literature (Lein et al., 2006). The gene set collection for cell types was compiled from published astrocyte, oligodendrocyte and neuron signatures and genes associated with the GO term 'immune response' (GO:0006955). A ranked list of genes from the TRAP and total mRNA differential transcript expression analyses were generated from the log2 fold change between conditions. The analysis was done using the web-based version with default parameters. The designs were improved using Adobe Illustrator.

3 Results

3.1 Establishment of the bacTRAP methodology

The goal of this work was to analyse translating mRNA from motor neurons specifically by applying the *Chat* bacTRAP methodology. This method relies on a cell-specific (in this case, motor neuron-specific) activation of the bac driver. In order to verify the neuronal expression of the eGFP-L10a transgene, immunohistochemical (IHC) stainings were conducted. Spinal cord sections of bacTRAP$^{+/-}$transgenic mice were stained for different cell type markers occurring in the CNS and the co-localisation of eGFP with these markers was analysed.

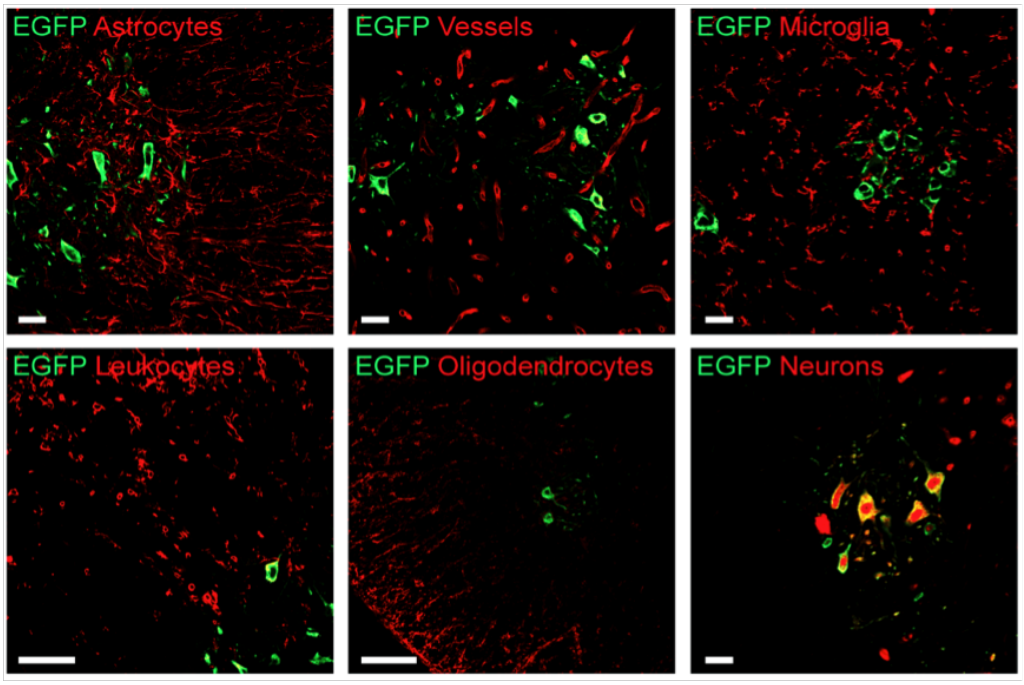

Figure 3.1: Representative immunohistochemical (IHC) stainings of eGFP and (a) Gfap (astrocytes), (b) Cd31 (endothelial cells), (c) Iba1 (microglia), (d) Cd45 (leukocytes), (e) Cnpase (oligodendrocytes) and (f) NeuN (neurons) in cervical spinal cord sections of healthy (a, b, c, e, f) and EAE sick (d) L10a-eGFP transgenic mice. Co-localisation of eGFP could only be detected with Neun. The stainings were conducted in collaboration with Dr. Benjamin Schattling.

No co-localisation with eGFP was found for Cnpase (oligodendrocytes), Gfap (astrocytes), Cd31 (endothelial cells), Iba1 (microglia) or Cd45 (leukocytes). For NeuN (neu-

rons) however, a significant overlay was detected (Fig. 3.1). This supports the premise that the eGFP-L10a transgene is expressed exclusively in neurons. Notably, no evidence was found for the expression of the transgene in infiltrating and activated immune cells during EAE.

To prove the efficacy of the bacTRAP method, the immunoprecipitation (IP) protocol was performed on a 3-set of bacTRAP transgenic (bacTRAP$^{+/-}$) and WT littermate (bacTRAP$^{-/-}$) mice. The WT mice served as a control condition, as they do not express eGFP and thus no mRNA should be detected in that sample after TRAP. This experiment was conducted for establishment purposes in collaboration with Katherine Miller. The mice were anaesthetised, spinal cords were dissected and TRAP was performed as described in the methods section. The quality of the RNA probes before (input) and after (IP) immunoprecipitation (bacTRAP$^{+/-}$ input and IP and bacTRAP$^{-/-}$ input and IP) was assessed using the Agilent Bioanalyzer. Figure 3.2a depicts an exemplary purification of the 18S and 28S rRNA of spinal cord material after immunoprecipitation via TRAP. Fig. 3.2b shows the electrophoresis results of four different RNA materials. Sample 1, 2, 3 and 4 correspond to bacTRAP$^{-/-}$ input, bacTRAP$^{-/-}$ IP, bacTRAP$^{+/-}$ input and bacTRAP$^{+/-}$ IP, respectively. The gelelectrophoresis performed by the Bioanalyzer showed peaks for 18S and 28S rRNA in the input material as well as the bacTRAP$^{+/-}$ IP, which were not found in the bacTRAP$^{-/-}$ IP probe, as no rRNA was precipitated.

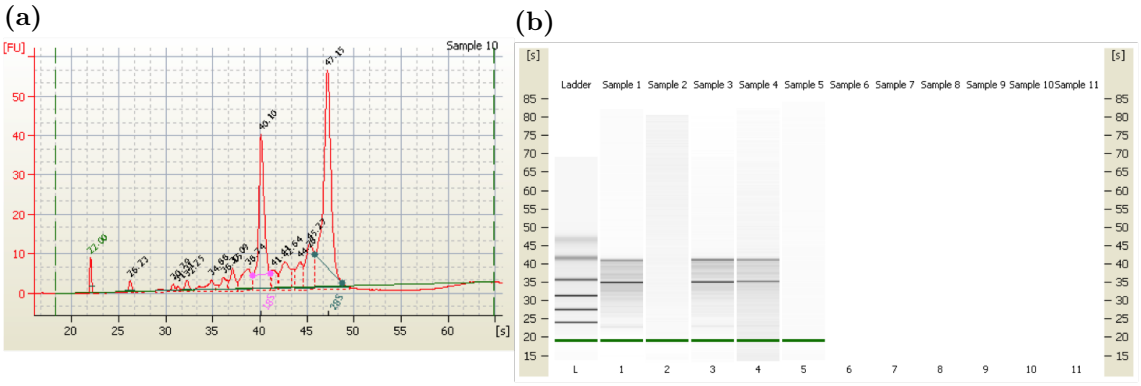

Figure 3.2: (a) Exemplary purification of 18S and 28S rRNA from *Chat* BAC array transgenic animals as detected by the Bioanalyzer PicoChip (Agilent Technologies). (b) Bioanalyzer results of WT whole tissue (1), WT after immunoprecipitation (IP) (2), transgenic whole tissue (3) and transgenic IP (4) RNA.

In order to verify the efficacy of the pull-down, the degree of enrichment of neuron-specific mRNA was determined using qPCR analysis. The expression level of *Chat* (a specific marker for motor neurons), normalised to *Gapdh*, was measured in input and IP material of wild type and *Chat* bacTRAP transgenic mice. As fig. 3.3a shows, the expression level of *Chat* was highest in the transgenic IP probe, reflecting an overabundance of mRNA from motor neurons. The *Chat* transcript was increased by a factor of 14, meaning that neuronal mRNA was overrepresented by the factor 14 in the IP material compared to the input. In the RNA material of wild type mice this enrichment was not observed.

In order to examine wether the RNA pull-down was neuron-specific and minimised non-specific background, different cell-specific markers were used as primers (Fig. 3.3b). In particular, the degree of contamination by lymphocytes (*Cd45*), oligodendrocytes (*Cnp*), astrocytes (*Gfap*) and $Chat^-$ neurons (*Kcnn1*) was determined. For the analysis of *Cd45* (leucocyte marker), mice suffering from EAE were used with the aim of increasing the concentration of $Cd45^+$ cells in the analysed tissue. For each probe set of EAE sick mice 5 bacTRAP$^{+/-}$ mice were immunised in order to account for the incomplete penetration of EAE. At day 12-14 after immunisation, 3 clinically sick mice were chosen for dissection. For the all other markers, 3 healthy bacTRAP$^{+/-}$ mice were used.

As fig. 3.3b demonstrates, the relative abundance of *Chat* was greatened by a factor of $\sim$15, while the fold enrichments of *Cd45*, *Cnp*, *Gfap* and *Kcnn1* were < 0.5, in the case of *Cd45* and *Gfap* the depletion was statistically significant. This result supports the notion that the bacTRAP method enriched RNA from $Chat^+$ neurons specifically, while signatures from other CNS-resident or infiltrating cell types were depleted, thus proving the validity of the implemented approach. After having established the bacTRAP methodology in healthy and EAE mice, the aim was to identify evidence for and mechanisms contributing to neurodegeneration using immunohistochemistry, PCR and deep sequencing analysis.

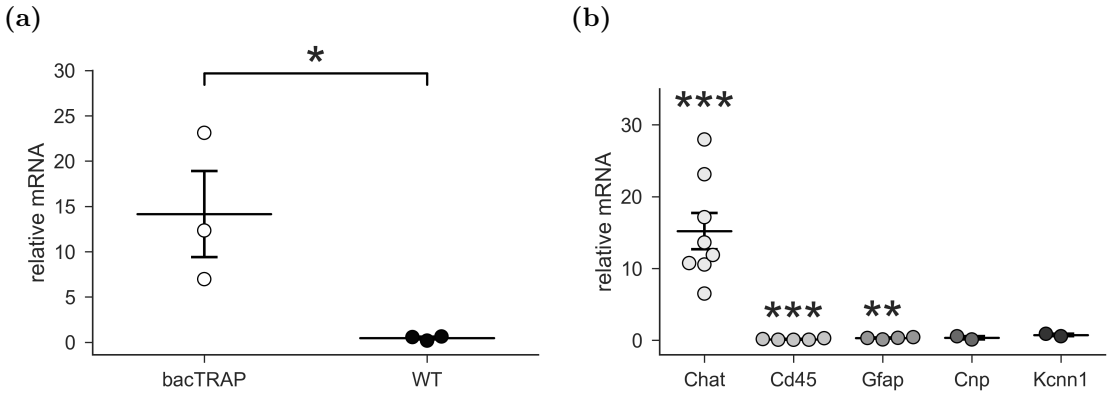

Figure 3.3: a) Dotplot depicting enrichment (IP/input ratio) of *Chat* gene normalised to *Gapdh* ($\Delta\Delta Ct$ method) as detected by qPCR in cervical spinal cord material of *Chat* bacTRAP transgenic and WT littermate mice. b) $\Delta\Delta Ct$ values of cervical spinal cord material of transgenic *Chat* bacTRAP$^{+/-}$ mice depicting the enrichment of cell type specific genes. *Chat* (Cholinacetyltransferase; motor neurons); *Cd45* (Protein tyrosine phosphatase, receptor type, C; immune cells); *Cnp* (2',3'-cyclic nucleotide 3'-phosphodiesterase; oligodendroglial cells); *Gfap* (glial fibrillary acidic protein; astrocytes); *Kcnn1* (potassium intermediate/small conductance calcium-activated channel, subfamily N, member 1; *Chat*$^{-}$ neurons). Bars show mean values ±SEM. Statistical analysis was performed using a two-tailed (a) and paired (b) Student's t-test. $^{*}P < 0.05$; $^{**}P < 0.01$; $^{***}P < 0.001$. Benjamini-Hochberg correction was conducted for multiple testing.

3.2 Evidence for neurodegeneration using IHC

In search of evidence for neuronal cell death, immunohistological stainings of spinal cord sections of healthy and EAE mice were conducted. The following images show exemplary immunohistological stainings for eGFP in healthy and inflamed spinal cord tissue. A significant reduction in the number of eGFP-positive neurons per ventral horn was found during EAE (fig. 3.4). The mean number of neurons per ventral horn was reduced from 18 in healthy cervical spinal cord tissue to 13 in inflamed spinal cord.

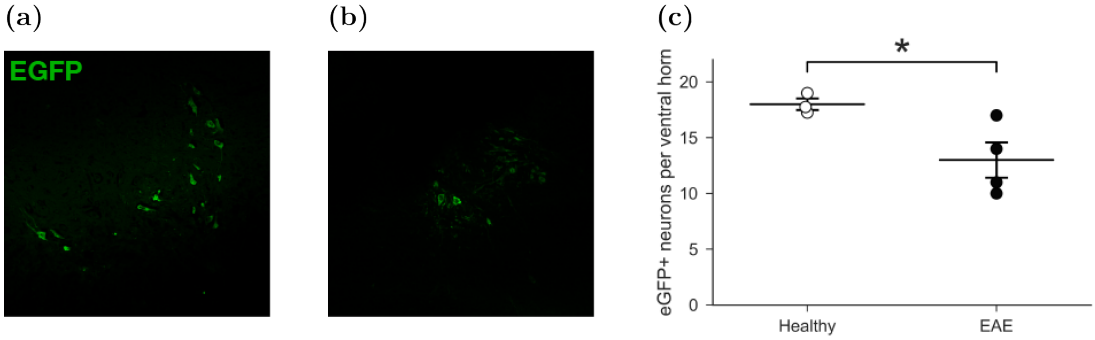

Figure 3.4: Cell count (c) of eGFP-positive motor neurons in cervical spinal cord sections of healthy (n = 3, (a)) and acute EAE (n = 4, (b)) *Chat*-L10a-eGFP mice. Bars show mean values ±SEM. Statistical analysis was performed using two-tailed Student's t-test. $^{*}P < 0.05$; $^{**}P < 0.01$

3.3 Validation of previously reported genes via qPCR

Following the validation experiments, the aim was to perform the TRAP method on spinal cord material of healthy mice and mice suffering from EAE and screen the translatome for alterations in neuronal gene expression. For each probe set of EAE sick mice, 5 *Chat* bacTRAP$^{+/-}$ mice were immunised in order to account for the incomplete penetration of EAE. At day 12 after immunisation, three clinically sick mice were chosen for dissection. For the control group, 3 healthy *Chat* bacTRAP$^{+/-}$ mice were used. Mice were anaesthetised, spinal cords were dissected and TRAP was performed as described in the methods section. The RNA probes were named 'SC' (spinal cord) for the input and 'MN' (motor neuron) for the IP material. For the probes of the mice suffering from EAE, the probes were named 'iSC' (inflamed spinal cord) and 'iMN' (inflamed motor neuron), accordingly. These four groups allow for several different comparisons. Comparing 'iSC' to 'SC' represent the whole tissue transcriptional changes during EAE; the difference in mRNA profiles between 'MN' and 'SC' (resp. 'iMN' and 'iSC') are caused by TRAP, thus representing the neuron-specific genes in the spinal cord tissue.

First, qPCR experiments were performed considering genes that have previously been described to be associated with mitochondrial dysfunction and excitotoxicity in neurons. Pgc1a, which acts through its downstream target Fndc5, is the master regulator of mitochondrial biogenesis and has been linked to neurodegenerative diseases such as Hunting-

ton's disease, Parkinson's disease, Alzheimer's disease and ALS (Farshbaf et al., 2016). Ampk, which is an activator of Pgc1a (Cantó and Auwerx, 2009), has been shown to be neuroprotective (Kamoshita et al., 2016) and its loss exacerbates EAE disease severity (Nath et al., 2009). Uncoupling proteins (UCP) are proteins located at the inner mitochondrial membrane and separate the oxidative phosphorylation from ATP synthesis (Andrews et al., 2005). They help reduce ROS production (Arsenijevic et al., 2000) and have been shown to be neuroprotective in stroke (Lindholm et al., 2004). Hypoxia may induce the hypoxia-sensing protein Hif-1a, its impaired functioning has been associated with ALS in mice (Sato et al., 2012). Dysfunction of tumour suppressor gene *p53* may result in mitochondria-associated cellular dysfunction in Huntington's disease (Bae et al., 2005). Furthermore, ion channels that have previously been described in the pathogenesis of MS/EAE were considered. Scn2a1, a sodium channel, that is known to be redistributed in neurons as a result of axonal injury (Craner et al., 2004) and its up-regulation during EAE is associated with axonal loss (O'Malley et al., 2009). Neuronal ion-influx via Trpm4 mediates cell death in EAE (Schattling et al., 2012).

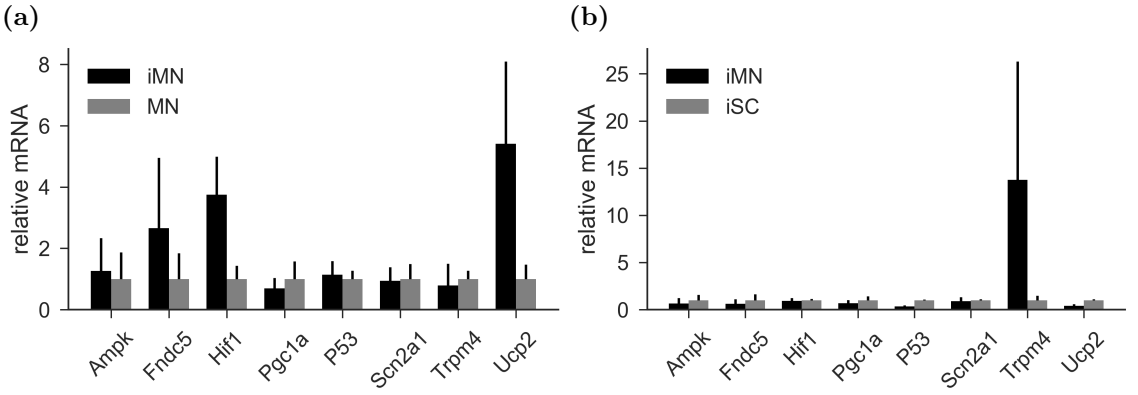

Figure 3.5: $\Delta\Delta Ct$ values of cervical spinal cord material of transgenic *Chat* bacTRAP$^{+/-}$ mice depicting the up-regulation of potential genes of interest in TRAP probes. *Ampk* (5' adenosine monophosphate-activated protein kinase); *Fndc5* (Fibronectin type III domain-containing protein 5) n=2; *Hif1* (Hypoxia-inducible factor 1) n=4; *Pgc1a* (Peroxisome proliferator-activated receptor gamma coactivator 1-alpha) n=3; *Scn2a1* (Sodium voltage-gated channel alpha subunit 2) n=3; *Trpm4* (Transient receptor potential cation channel subfamily M member 4) n=2; *Ucp2*(uncoupling protein 2) n=4; *p53* (Tumor protein *p53*) n=4. Bars show mean values ±SEM. Statistical analysis was performed by two-tailed Student's t-test. $^{*}P < 0.05$; $^{**}P < 0.01$; $^{***}P < 0.001$. Benjamini-Hochberg correction was conducted for multiple testing.

The quantitative PCR analysis didn't yield significantly altered neuronal expression levels during EAE for any of the analysed candidate genes.

3.4 Deep sequencing analysis of the inflamed spinal cord

After this hypothesis-driven approach, the whole neuronal tanslatome was screened for evidence of neurodegeneration. To this end, RNA was collected from spinal cord homogenates ('SC') and TRAP-purified motor neurons ('MN') from healthy mice and mice in the acute stage of EAE. Five such probe sets were collected on different days and used as input for deep sequencing analysis. The four different groups of material (SC, MN, iSC, iMN) were analysed in detail. First, the changes in the global transcriptome were considered, which yielded 1345 significantly up-regulated and 119 down-regulated transcripts.

3.4.1 Changes in global transcription during EAE

Cell composition

In order to illuminate the changes in cell composition during CNS inflammation, the expression levels of known cell markers were determined. Furthermore, sets of marker genes for immune cells, astrocytes, oligodendrocytes and neurons were compiled from the literature (Lein et al., 2006) and used as input for gene set enrichment analysis (GSEA). GSEA is a method that determines wether two probe sets (in this case iSC vs SC) show statistically significant, concordant differences in the expression of genes in a given gene set S. This gene set can be a group of genes that shares a common biological function, chromosomal location, or regulation (Subramanian et al., 2005). *Aif1* (Allograft inflammatory factor 1, a.k.a. *Iba1*) is specifically expressed by innate leucocytes, such as monocytes, granulocytes, macrophages, and natural killer cells. It marks microglial activation during spinal cord injury (Schwab et al., 2001). *Pecam-1* (*Cd31*) is found on the surface of immune cells and endothelial cells, while *Cd3d* is specific for leucocytes and *Gfap* is expressed by astrocytes and other CNS-resident cells. *Rbfox3* (*NeuN*) is expressed in *Chat*-negative neurons. As 3.6 shows, the cell type distribution changed significantly during EAE. GSEA showed that while signatures from immune cells and astrocytes were enriched during inflammation, those from oligodendrocytes and neurons were depleted. The analysis of individual marker genes confirmed the strong over-representation of immune cells and astrocytes in the inflamed spinal cord. This finding was confirmed using the cell-type specific expression analysis (CSEA, supplementary fig. 7.2).

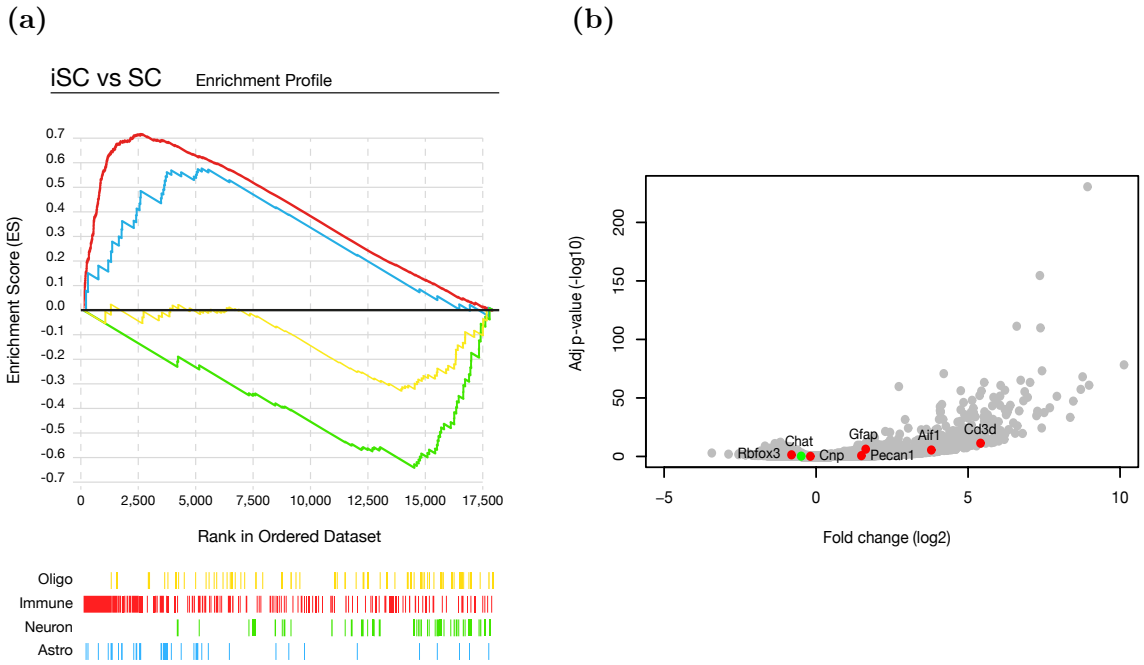

Figure 3.6: Changes in cell composition during CNS inflammation. (a) Gene-set enrichment analysis of cell-specific marker gene-sets for neurons, oligodendrocytes, astrocytes and immune cells. The maximum deviation from 0 is the enrichment score (ES), it reflects the over-expression of a gene-subset in one condition. (b) Volcano plot depicting the changes in abundance of cell type markers in spinal cord tissue during neuroinflammation. *Rbfox3* (*NeuN*): *Chat*$^-$-neurons; *Chat*: motor neurons; *Cnp*: Oligodendrocytes; *Gfap*: Astrocytes; *Pecam1*: immune and endothelial cells; *Aif1* (*Iba1*): Innate leucocytes; *Cd3d*: Leucocytes.

Activated pathways

The following heatmap (Fig. 3.7) depicts the expression levels of the 25 most significantly differentially expressed transcripts of the inflamed spinal cord tissue. The yellow side markers represent an association with the GO term 'immune' , the high contamination of the EAE probes with immune cell mRNA is further represented by a high percentage (26%) of genes within this list that carry the GO-term 'immune'. The most significantly up-regulated genes in the whole tissue material involve *Cxcl9*, a T-cell chemoattractant; *Gm4841*: Interferon-gamma-inducible GTPase Ifgga3 protein; *Iigp1*: Interferon-inducible GTPase 1. These changes in expression levels cannot be traced back to their respective

cell type as whole tissue RNA was compared in this analysis.

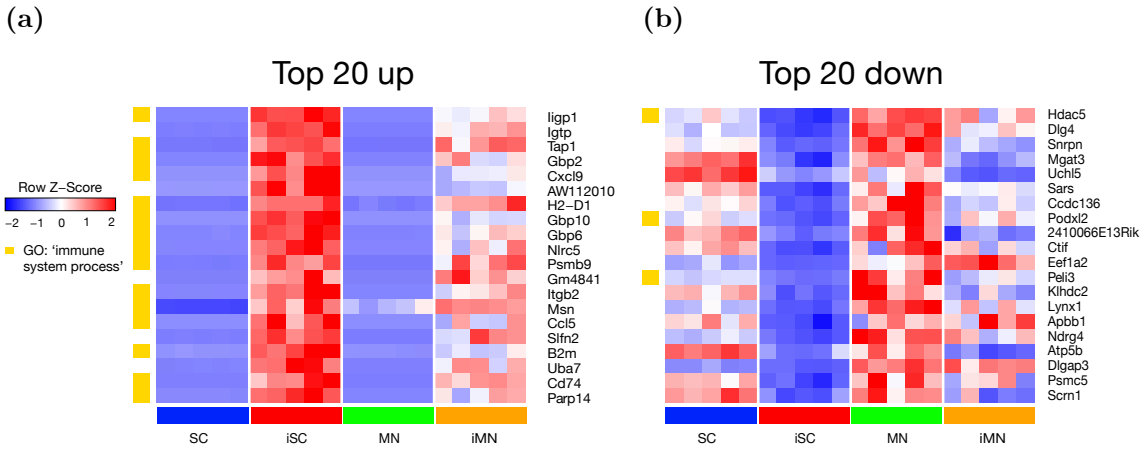

Figure 3.7: Heatmap depicting the top 25 highest hits when comparing EAE spinal cord and healthy spinal cord material. A high z-score (red) represents a high level of gene expression. The yellow side maker indicates an association with a GO term 'immune system process'. (b) Expression levels of genes with the annotation of GO 'immune system process'.

In order to analyse the biological processes that are activated during spinal cord inflammation, gene enrichment analysis was performed using the GeneAnswers package in R Studio (Feng et al., 2010). The tool allows for the analysis of three different domains: Biological process, molecular function and cellular component. Fig. 3.8a shows the biological processes up-regulated during EAE. Networks of gene sets are presented as nodes that are clustered together based on overlap in gene expression. Furthermore, the KEGG-network was analysed in order to learn about underlying metabolic processes and human diseases that have previously been described in context with these genes. Pathway analysis was repeated for biological process (BP), molecular function (MF) and cellular component (CC). It yielded 2594 significantly enriched terms for BP, 270 for MF and 254 for CC, for a FDR correction with p-value < 0.1 (Supplementary figures 7.1, 7.2, 7.3). The most significantly overrepresented GO term was 'immune system process' (p-value 8.787×10^{-169}).

(a)

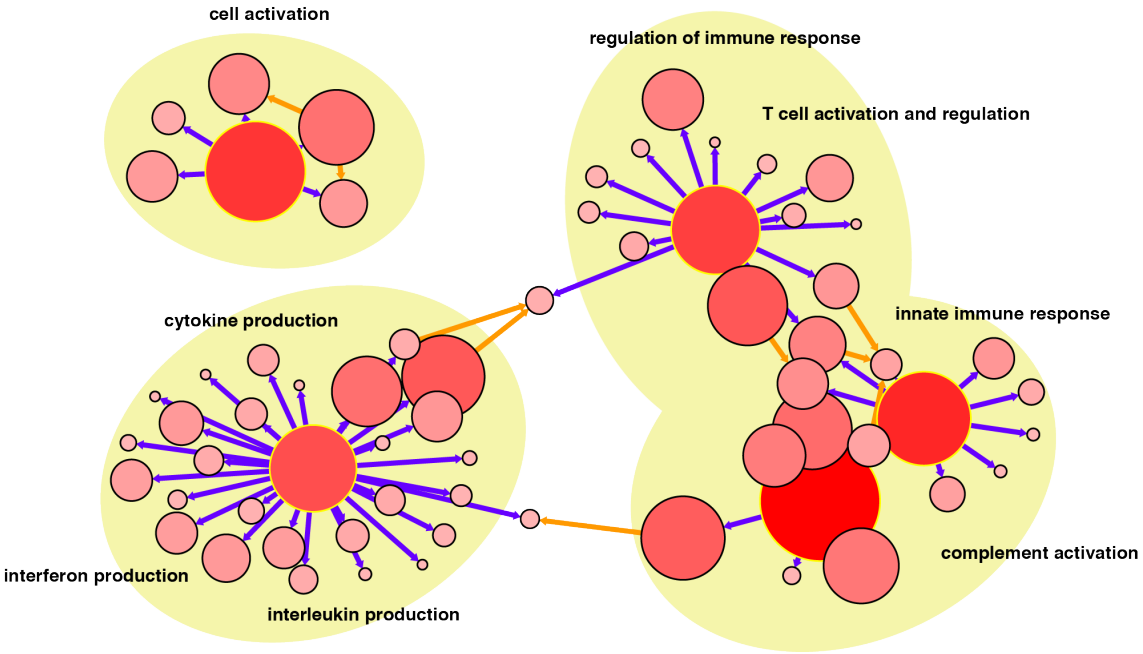

(b)

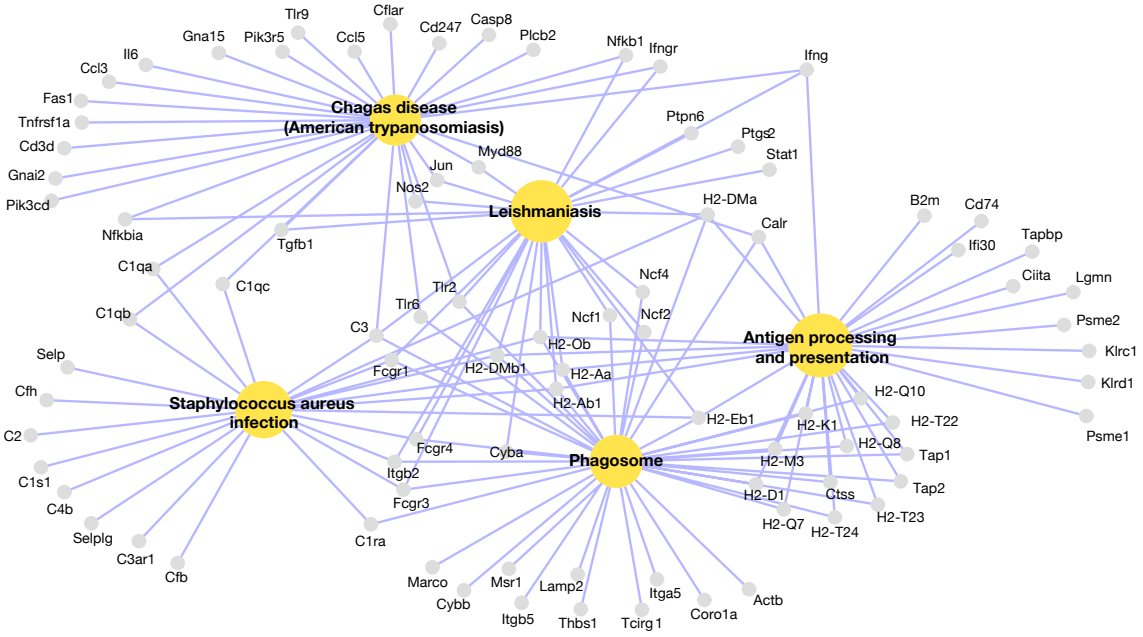

Figure 3.8: (a) Biological process GO structure network of up-regulated genes during EAE. The size of the nodes are proportional to the number of genes in a GO category, the color of nodes stands for how relative the given genes are to the GO categories. The more red, the more relative. The given GO categories are yellow framed dots with dark purple edges connections (Feng et al., 2010). (b) Top KEGG-terms associated with up-regulated genes in whole tissue material.

In the domain of biological processes, genes related to immune response, activation of innate and adaptive immune responses, T cell proliferation and differentiation, antigen processing and presentation, cell-mediated immunity, response to wounding and inflammatory response were highly over-represented. For molecular function, protein binding, cytokine activity, major histocompatibility complex (MHC) protein binding, scavenger and chemokine receptor activity were represented amongst others. In the cellular component, external side of plasma membrane, focal adhesion, lysosome, MHC protein complex and T cell receptor complex were among the highly significantly represented terms (Supplementary figures 7.1, 7.2, 7.3). The KEGG analysis showed an enrichment of genes that have been associated with infectious diseases like Leishmaniosis, Herpes, Measles, Chagas disease, Tuberculosis and Influenza A. Further, several autoimmune diseases like Lupus erythematodes, rheumatoid arthritis, autoimmune thyroid disease and inflammatory bowel disease were annotated. Other annotated pathways involved phagosomes and antigen processing and presentation, cytokines, cell adhesion molecules, TNF signalling pathway and Toll-like receptor signalling pathway. These results concur with the notion of immune cells migrating into the CNS and causing these translational changes. It is therefore virtually impossible to identify gene translational changes in neurons during EAE using whole tissue homogenates. This underlines the necessity for a different approach in order to identify inflammation-induced changes in neuronal gene expression.

3.4.2 Efficacy of pull-down

In order to verify the efficacy of the immunoprecipitation and thus the quality of the TRAP-enriched RNA material used as input for the RNA-seq, the intra-individual probes before and after TRAP were compared. First, the expression levels of control genes as published by Doyle (2008) were considered, namely *Calca*, *Calcb*, *Chat*, *Isl1*, *Mnx1* and *Lhx3* for the positive control and *Cnp*, *Gfap*, *Mbp*, *Plp1*, *Slc1a3* and *Vim* for the negative control. Figure 3.9 depicts the expression levels of those genes in the spinal cord tissue before (SC) and after immunoprecipitation via TRAP (MN). As shown in fig. 3.9, the affinity purification of the spinal cord material yielded a highly significant enrichment of positive control genes, whereas genes used as negative controls were depleted. In the healthy probes, the enrichment and depletion was significant for all controls, in the inflamed probe set the depletion of two negative controls was non-significant and one control gene, *Cnp*, was nearly unchanged in concentration.

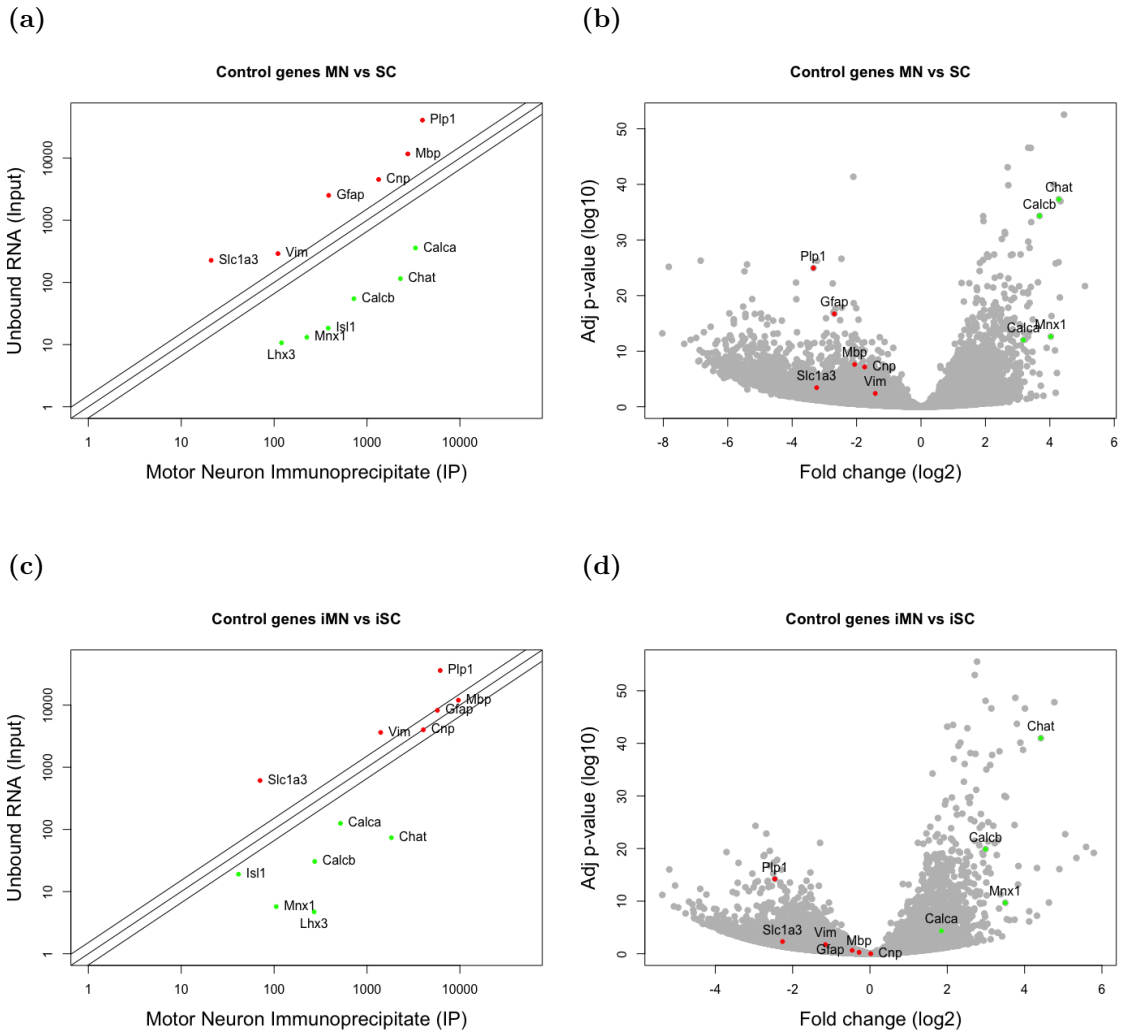

Figure 3.9: Scatter plot (a) and volcano plot (b) depicting the expression levels and fold changes of transcript abundance in the IP material versus whole tissue RNA and the respective adjusted p-values for healthy and EAE mice. Coloured and labelled are positive (green) and negative (red) control genes. Missing values are due to missing p-values in the analysis.

Secondly, a gene-set enrichment analysis (GSEA) (Subramanian et al., 2005) was performed to determine the cell-specificity of the harvested probes based on gene lists from the literature. A list of neuronal markers was chosen as a positive control and lists of astrocyte and oligodendrocyte markers (Lein et al., 2006), as well as all genes annotated to the GO term 'immune system process' were chosen as negative controls. The gene-set enrichment analysis (Figures 3.10a and 3.10b) shows the enrichment of neuron-specific transcripts, with enrichment scores of 0.48 for the heathy and 0.67 for the inflamed spinal cord (FDR (false discovery rate) q-value = 0.045 (MN vs SC), 0.023 (iMN vs iSC)). Negative control gene lists of astrocyte markers (FDR q-value = 0.008 (MN vs SC), 0.313 (iMN vs iSC)), oligodendrocyte markers (FDR q-value = 0.024 (MN vs SC), 0.170 (iMN vs iSC)) and 'immune system process' (FDR q-value = 0.008 (MN vs SC) , 0.010 (iMN vs iSC)) were depleted. The depletion was not statistically significant for astrocyte markers and oligodendrocyte markers in the inflamed tissue.

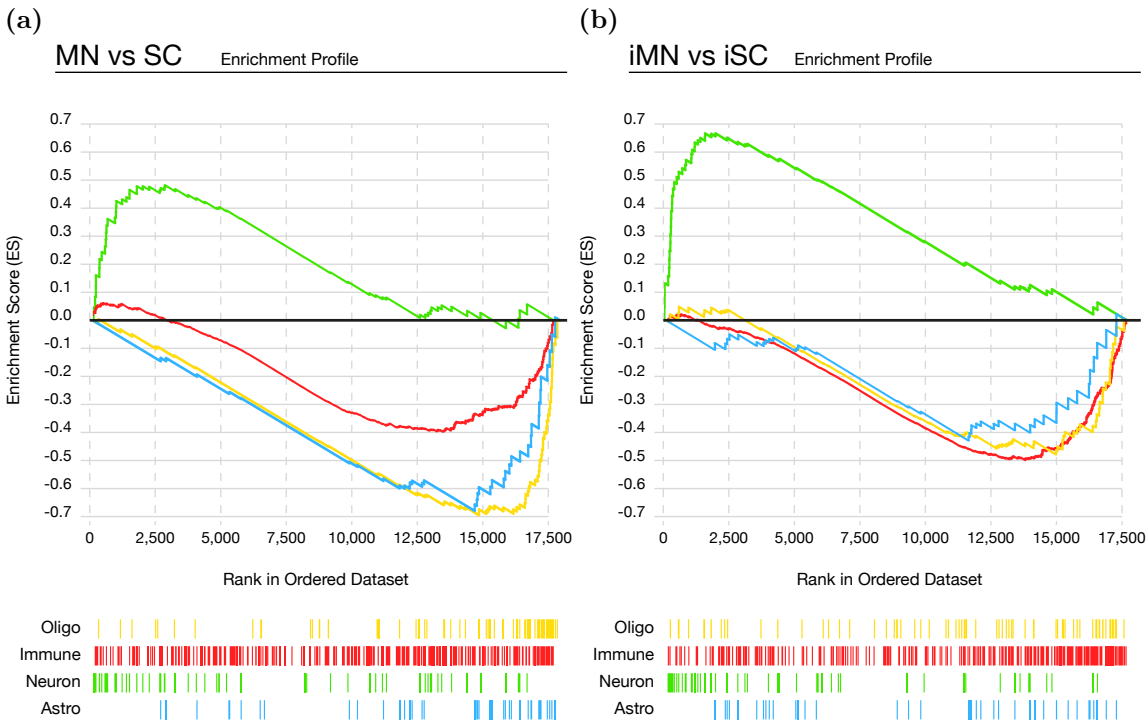

Figure 3.10: Gene-set enrichment analysis for gene lists of neurons, oligodendrocytes, astrocytes and immune cells. MN vs SC (a) and iMN vs iSC (b). The maximum deviation from 0 is the enrichment score (ES), it reflects the over-expression of a gene-subset in one condition.

Thirdly, the cell type-specific expression analysis (CSEA) was implemented, which determines the specificity of gene transcripts for certain cell types based on a database of in situ hybridisation and bacTRAP data. The gene list of significantly enriched transcripts (MN/SC > 2, Adj.P < 0.05) was used as input for further analysis. Figure 3.11 depicts the Benjamini-Hochberg corrected p-values of the gene list depending on the stringency for enrichment p(SI) for several CNS cell types. A high enrichment level was detected for genes specific to cholinergic (motor) neurons, Purkinje neurons, granule neurons and hypocretinergic neurons. No non-neuronal cells were over-represented in the MN probes (For iMN vs iSC see supplementary figure 7.1). The enrichment of genes specific to cholinergic motor neurons of the brain stem was highly significant (reaching from 2.49×10^{-99} to 8.13×10^{-17}, depending on the chosen p(SI)).

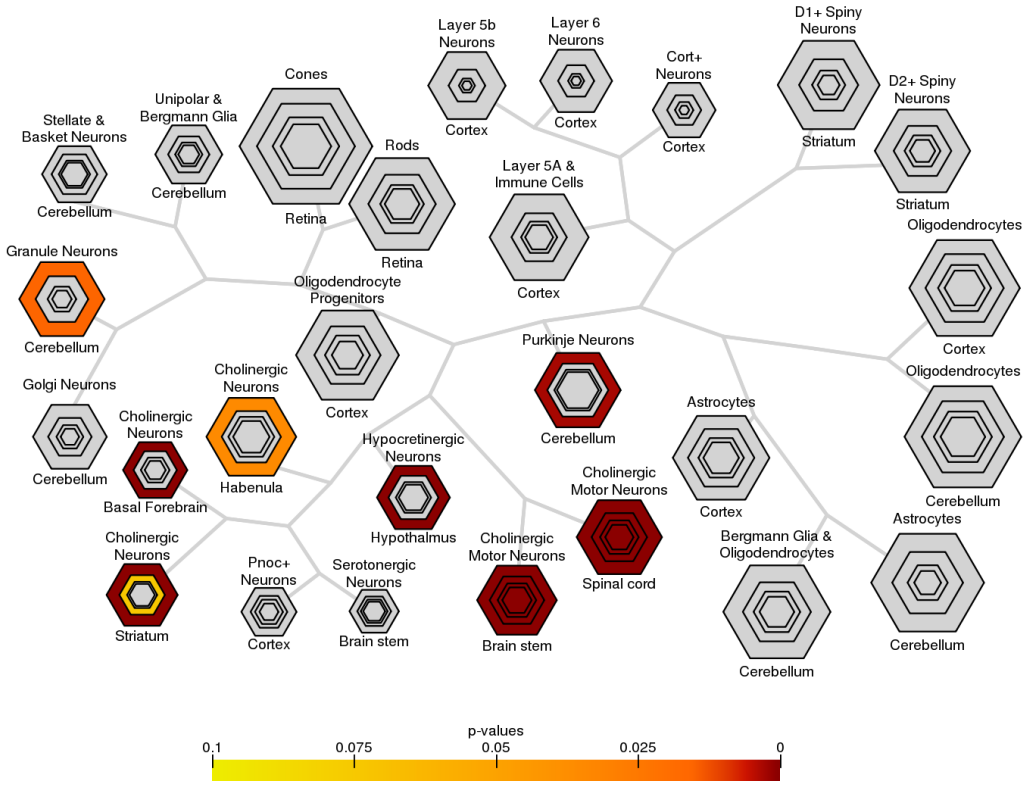

Figure 3.11: Topographical bullseye map of cell-specific and enriched transcripts showing enrichment for differentially expressed cholinergic neuron transcripts in healthy mice, Benjamini-Hochberg p-values are plotted by color. Varying stringencies for enrichment (pSI) are represented by the size of the hexagons going from least specific lists (outer hexagons) to most specific (center). Hexagons scaled to size of gene lists.

3.4.3 Neuronal translational changes during EAE

As the previous analyses showed the high degree of neuron-specificity of the MN and iMN mRNA probes, the next goal was to identify the significant differences between these conditions. This comparison yielded a list of 3074 significantly up-regulated (iMN/MN > 2, Adj.P < 0.05) and 1382 significantly down-regulated (iMN/MN < 0.5, Adj.P < 0.05) genes. For these lists the possibility of false positive results could not be ruled out completely, as mRNA immunoprecipitation via bacTRAP is not 100% cell-specific and the cellular composition of the spinal cord changed drastically during EAE (See fig. 3.6). The method does however extract neuronal mRNA with a much higher affinity than that

of other cells, the neuronal mRNA is thus overrepresented in the IP material. In order to minimise non-specific background, a lower threshold was set based on negative control genes determined by the Heintz workgoup (Doyle, 2008). This threshold was calculated as described in the methods section based on the enrichment levels of negative control genes. The threshold was rounded up and the restriction was set to iMN/iSC $>$ 2.0, Adj.P $<$ 0.05 for up-regulated (iMN $>$ MN) genes and accordingly MN/SC $>$ 2.0, Adj.P $<$ 0.05 for down-regulated (iMN $<$ MN) genes. Neuronally up-regulated genes were thus required to be neuron-specific in the EAE material, down-regulated transcripts were required to be neuron-specific in the healthy material. The adjusted p-value was consequently calculated as described in the methods section. This approach yielded a list of 327 up-regulated and 389 down-regulated genes. Those genes that met either requirement received the annotation 'neuron up' and 'neuron down', respectively. The following Venn diagram depicts the quantitive overlap of significantly up-/down-regulated genes (Fold change $>$ 2 and Adj.P $<$ 0.05).

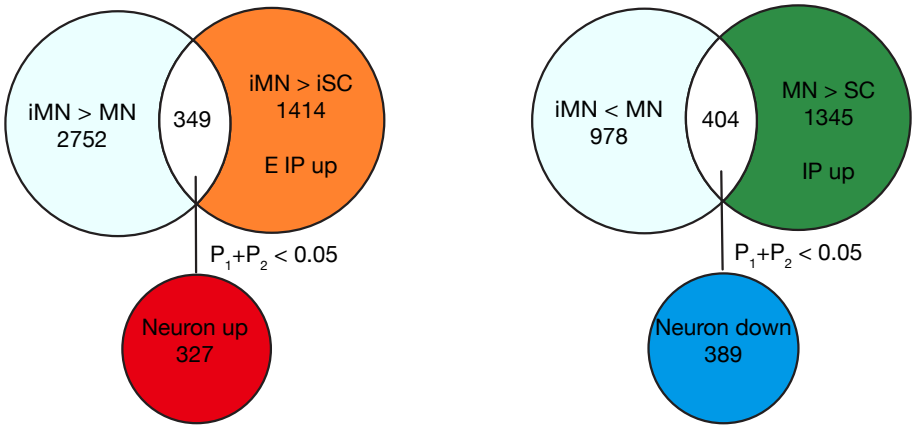

Figure 3.12: Venn diagram illustrating the number of genes that are significantly enriched by the immunoprecipitation via TRAP of EAE spinal cord tissue ('iMN $>$ iSC', orange) and healthy spinal cord tissue ('MN $>$ SC', green) and those that are significantly increased or decreased in the immunoprecipitated material of EAE versus healthy mice ('iMN $>$ MN', 'iMN $<$ MN', grey circles). Genes that fulfilled two criteria ('iMN $>$ MN' and 'iMN $>$ iSC' with adjusted p-value $p_1+p_2 < 0.05$: 'Neuron up', 'iMN $<$ MN' and 'MN $>$ SC' with adjusted p-value $p_1+p_2 < 0.05$: 'Neuron down') were used for further analysis.

The following heatmaps show the top 25 genes tagged 'neuron up' and 'neuron down' swhen ordering for the adjusted p-value. The sidebar marks the GO annotation 'immune system process'.

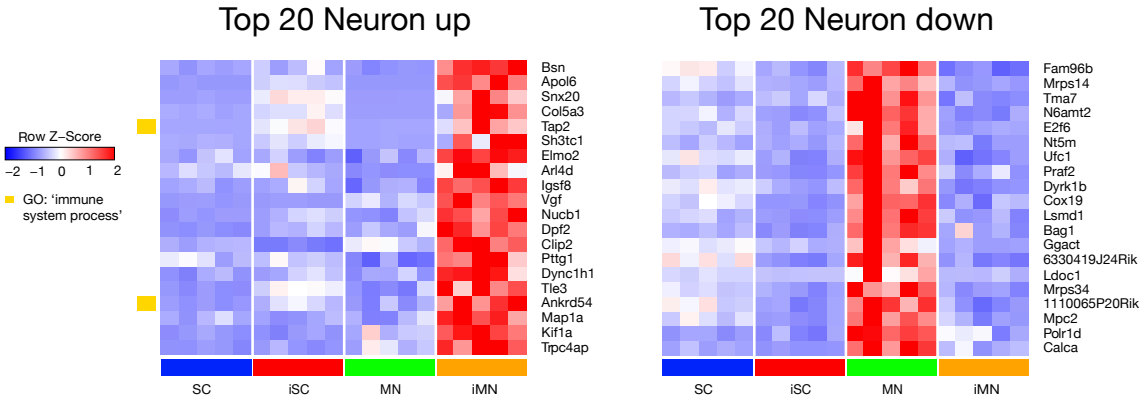

Figure 3.13: Neuronal changes in gene expression during EAE. Gene expression levels of the 25 genes with the lowest p-value that met above-mentioned criteria for 'neuron up' (a) or 'neuron down' (b). The yellow sidebar tags genes with GO annotation 'immune system process'.

Neuronally up-regulated pathways

The most significantly up-regulated gene in the analysis was *Bsn*. The encoded protein Bsn is a very large scaffolding protein, that is located at the presynapses of neurons. Bsn is known to be involved in the assembly of active zone scaffolds, neurotransmitter release, signalling processes and maintenance of synapse integrity (Gundelfinger et al., 2016). Loss of Bsn leads to the aberrant degradation of multiple presynaptic proteins, culminating in synapse degeneration (Waites et al., 2013), it has further been shown to inhibit synaptic autophagy in neurons through Atg5 (Okerlund et al., 2017). Vgf, which was also among the 25 top up-regulated transcripts, is a neuropeptide precursor that regulates energy metabolism in rodents and its deletion results in higher energy expenditure independent of activity. In the brown adipose tissue of *Vgf*-knockout mice, uncoupling protein 1 (Ucp1) and Ucp2 protein levels, mitochondrial number, and mitochondrial cristae density were found to be up-regulated (Watson et al., 2009). The up-regulation of Vgf could therefore be a marker for a heightened energy efficiency. Next, a GO term enrichment analysis was performed on the 327 up-regulated genes using the GeneAnswers package in R to identify aberrant gene clusters. GeneAnswers identifies enriched gene annotations in a given gene list by means of a hypergeometric statistic. Depicted below are the results when considering biological processes.

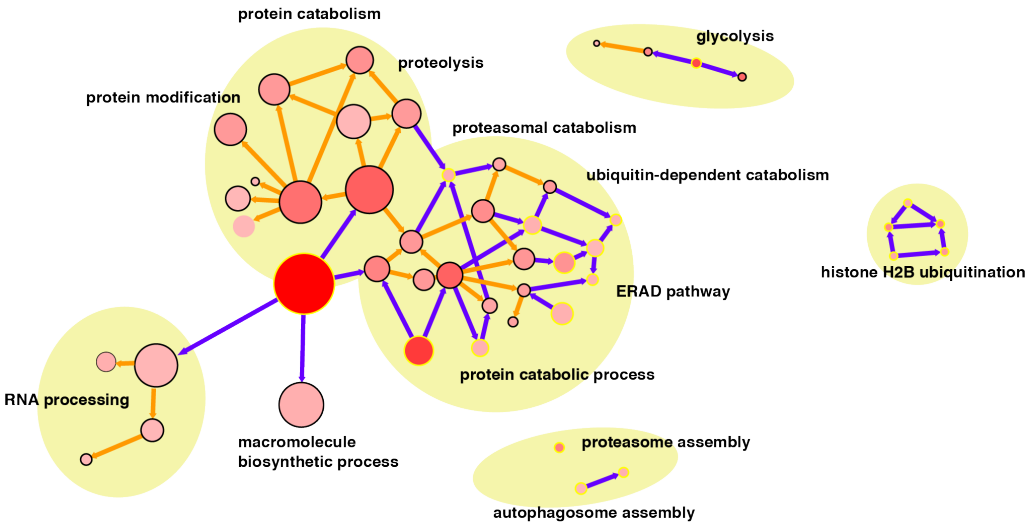

Figure 3.14: GO structure network. Biological processes of genes that were up-regulated in motor neurons during EAE. The size of nodes is proportional to the number of genes in a GO category. The color of nodes stands for how relative the given genes are to the GO categories. The more red, the more relative. The given GO categories are yellow framed dots with dark purple edges connections.

GO annotation analysis showed a de-regulation of genes involved in protein catabolism, particularly ubiquitin-mediated and proteasomal protein degradation, RNA processing, autophagy, glycolysis and microtubule function (Fig. 3.1, supplementary figures 7.7, 7.8, 7.9) amongst others. Interestingly, the GO term 'unfolded protein binding' was enriched, which could be a hint for an increased demand for protein clearance due to the accumulation of misfolded proteins. In line with this, an up-regulation of genes annotated to 'chaperone binding' (GO:0051087, data not shown) was detected.

category	genes in category	p-value	FDR p-value
macromolecule catabolic process::GO:0009057	27	1.204×10^{-05}	0.001241
proteasome assembly::GO:0043248	3	0.0004333	0.01384
proteasome complex::GO:0000502	4	0.01068	0.04759
ubiquitin-dependent protein catabolic process::GO:0006511	14	0.00123	0.02789
proteasome-mediated ubiquitin-dependent protein catabolic process::GO:0043161	9	0.009437	0.09965
positive regulation of proteasomal ubiquitin-dependent protein catabolic process::GO:0032436	4	0.007345	0.08752
proteasome regulatory particle::GO:0005838	3	0.002421	0.01749
ER-associated ubiquitin-dependent protein catabolic process::GO:0030433	4	0.006298	0.08118
regulation of histone ubiquitination::GO:0033182	2	0.004096	0.06147
positive regulation of histone ubiquitination::GO:0033184	2	0.001744	0.0352
autophagosome assembly::GO:0000045	4	0.01022	0.09965
regulation of autophagosome assembly::GO:2000785	3	0.006062	0.07985
lysosome::GO:0005764	13	0.005409	0.0311
lytic vacuole::GO:0000323	13	0.005409	0.0311
glycolytic process through glucose-6-phosphate::GO:0061620	3	2.541×10^{-05}	0.002147
glycolytic process through fructose-6-phosphate::GO:0061615	3	0.0002013	0.008477
glycolytic process through glucose-1-phosphate::GO:0061622	2	0.0007078	0.01906
microtubule-based process::GO:0007017	15	0.002503	0.04334
unfolded protein binding::GO:0051082	5	0.002428	0.06215

Table 3.1: Candidate GO terms in biological process up-regulated in neurons during EAE.

In search for further evidence of protein misfolding, the PONDR algorithm was applied in order to predict the naturally disordered regions of the top candidate genes. A high percentage of intrinsically disordered residues predisposes proteins to malformation and aggregation. Depicted below are the PONDR scores for the top 14 up-regulated transcripts (Fig. 3.15). Several of these proteins were found to contain a high percentage of intrinsically disordered residues, particularly Bsn, Apol6, Col5a3, Vgf, Nucb1, Dpf2, Clip2 and Pttg1. The up-regulation of protein catabolic pathways may thus be a reaction to the over-expression and toxic accumulation of these proteins.

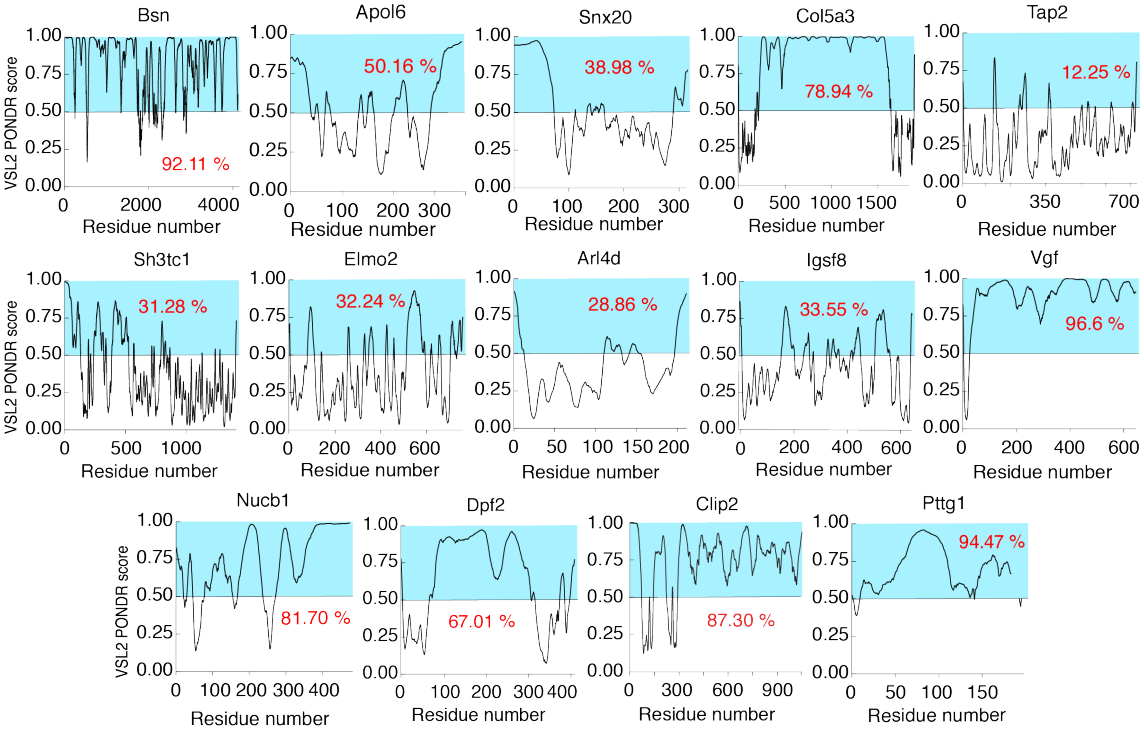

Figure 3.15: Analysis of top 14 up-regulated genes for disordered residues by PONDR VSL2 algorithm. The light blue area represents the disordered residues of the protein. The numbers represent the overall percentage of disordered regions. Long regions of prediction are more likely to be disordered than short regions of prediction.

Neuronally down-regulated pathways

After the analysis of the up-regulated neuronal pathways during EAE, the down-regulated candidate genes were considered. 389 genes met the criteria MN/SC >2.0 and MN/iMN> 2 with the sum of the p-values <0.05. The most significantly down-regulated gene was *Nt5m* (5',3'-nucleotidase, mitochondrial), which is a 5'-nucleotidase that localises to the mitochondrial matrix. It catalyses the dephosphorylation of thymidine and deoxyuridine monophosphates and participates in the regulation of the dTTP pool in mitochondria, which is necessary for mtDNA replication (Walldén et al., 2005). This may thus indicate a mitochondrial dysfunction or down-regulation of mtDNA replication. Again, the GeneAnswers package in R was used for gene network analysis using the Gene Ontology and KEGG library. Depicted below are the networks related to biological processes and the KEGG library.

(a)

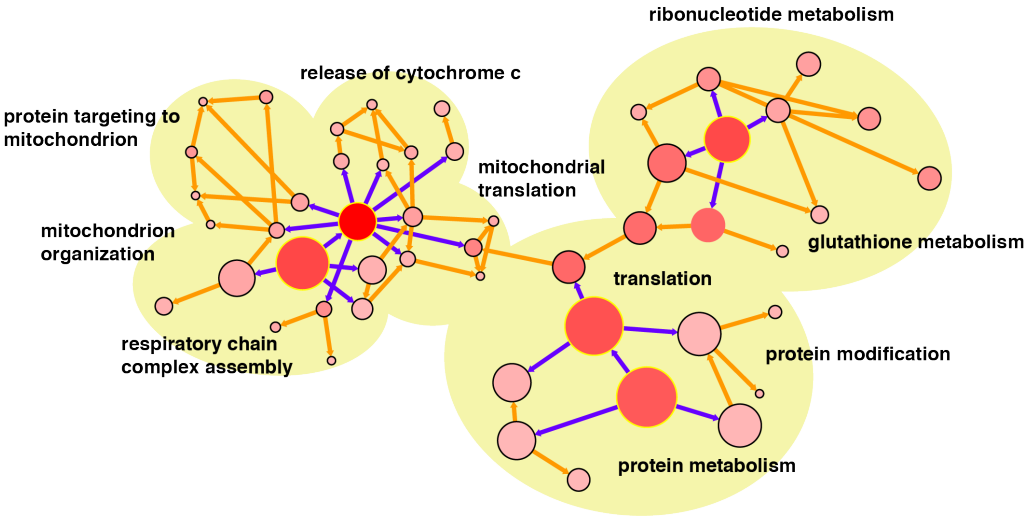

(b)

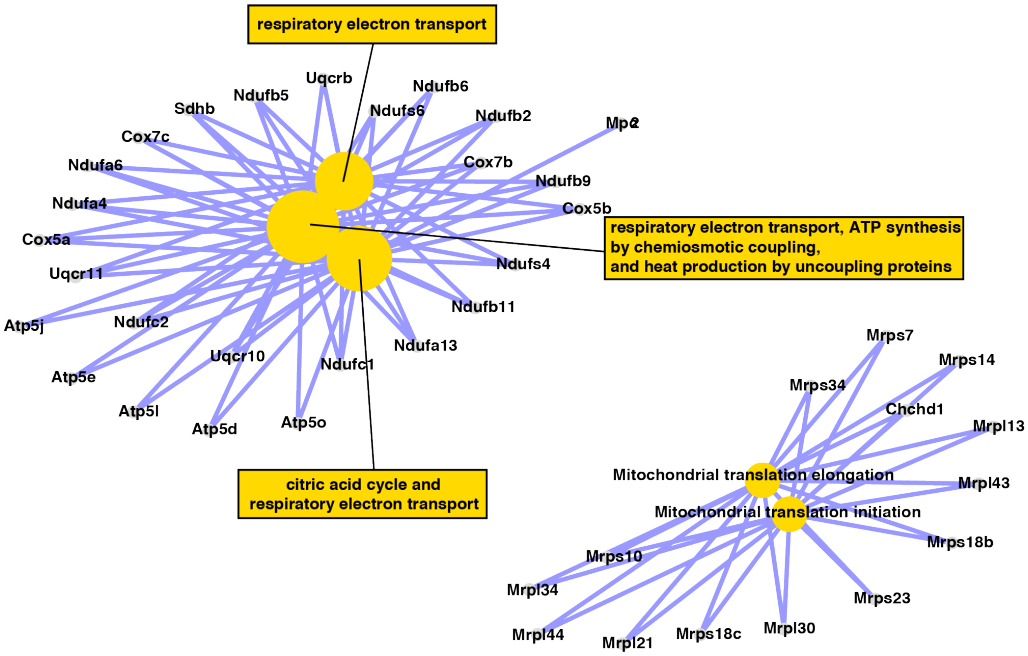

Figure 3.16: (a) GO structure network. Biological processes of genes that were down-regulated in motor neurons during EAE. The size of the nodes is proportional to the number of genes in a GO category. The color of nodes stand for how relative the given genes are to the GO categories. More red, more relative. The given GO categories are yellow framed dots. Lower image (b) shows the results of KEGG pathway analysis of neuronally down-regulated transcripts during EAE. The size of the nodes is relative to the number of genes in that KEGG category.

The analysis revealed a deregulation of proteins involved in biosynthesis and energy metabolism pathways (Fig. 3.16). Particularly, a down-regulation of genes involved in ribonucleotide metabolism, protein metabolism and translation as well as mitochondrial genes (Supplementary figures 7.10, 7.11, 7.12) was found. The strong reduction in genes involved in ATP synthesis and the electron transport chain may indicate an energy shortage, while the reduction of protein translation and depletion of structural molecules of ribosomes may highlight a disruption in protein synthesis. 91 of the 389 genes tagged 'neuron down' were found to be associated with the GO-term 'mitochondrion', indicating a mitochondrial hypo-function. The ATP synthase complex and the respiratory chain pathway showed a reduction, which could indicated an increased energy demand. Specifically, the mitochondrial complexes I-V were all reduced. Furthermore, a number of ribosomal proteins were strongly suppressed (Figure 3.17). Aberrance in mitochondrial ribosomal proteins has been shown to cause disruptions in oxidative phosphorylation and ATP synthesis (Menezes et al., 2015).

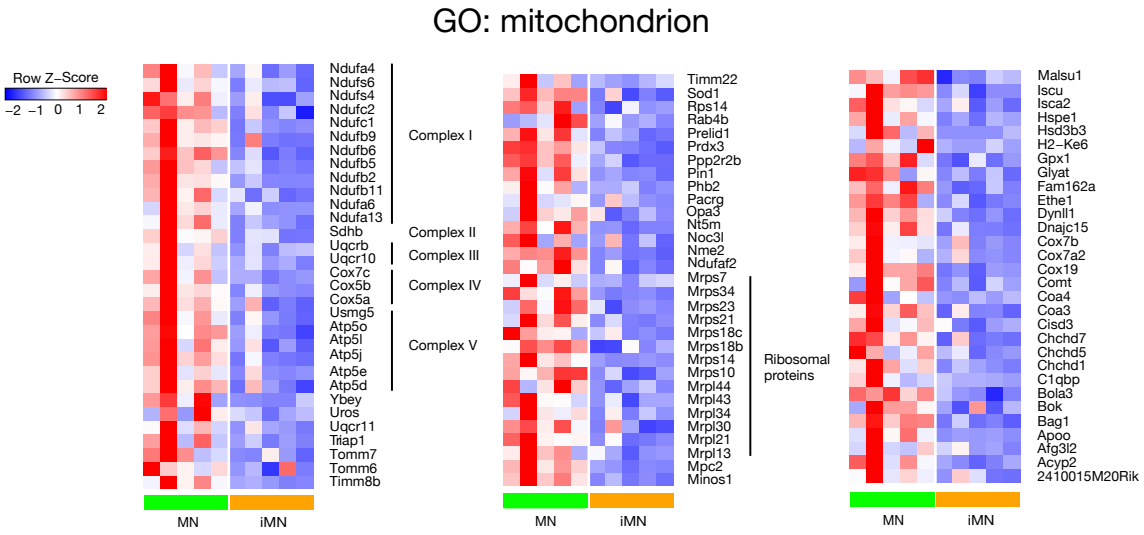

Figure 3.17: Expression levels of differentially expressed candidate genes attached to GO terms 'mitochondrion'. The side bars indicate functional gene clusters.

3.5 Immunohistochemical validation of the sequencing results

Following the analysis of the deep sequencing results, the aim was to validate the results. To this end, immunohistochemical stainings of spinal cord sections of healthy and EAE mice were conducted, staining for Bsn and its co-localisation with neuronal marker NeuN.

The protein Bsn was chosen as an example, because it showed the most significant up-regulation in the analysis and good antibodies are available for IHC. As figure 3.18 shows, the IHC stainings confirmed the predicted augmented neuronal expression of Bsn during EAE in motor neurons of the spinal cord, which supports the validity of the bacTRAP approach and the employed data analysis method.

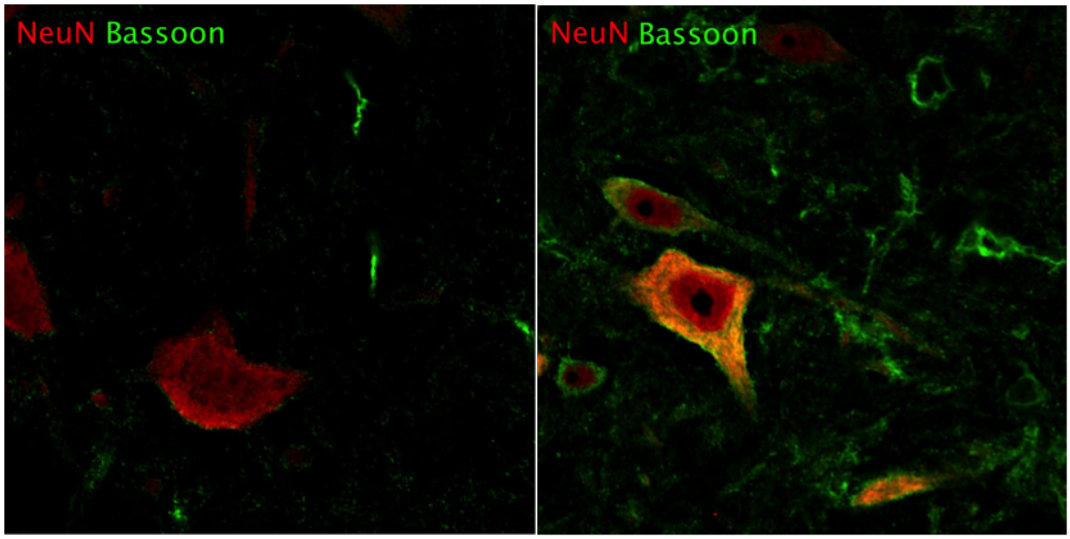

Figure 3.18: Immunohistochemical stainings of spinal cord tissue of healthy mice (left) and mice suffering from EAE (right). Red: neuronal marker NeuN, green: Bsn. This experiment was conducted in collaboration with Dr. Benjamin Schattling.

4 Discussion

Multiple sclerosis is a chronic disease causing substantial suffering and disability. It is historically considered an inflammatory disease, in which a dys-regulation of the immune system leads to immune cell infiltration and subsequently inflammatory lesions in the CNS, accounting for the wide range of clinically observed neurological symptoms (Compston and Coles, 2016). In recent years, the co-existence of two distinct processes, namely inflammatory and neurodegenerative, has been postulated (Scalfari et al., 2010). Neuronal cell death, due to primary neurodegenerative processes and/or inflammation-induced neuronal damage, are thought to be responsible for the long-term disability of MS patients (Friese et al., 2014). Although the importance of neurodegeneration in the pathogenesis of multiple sclerosis has been known for some time (Friese et al., 2014), methodological difficulties have thus far limited the insight into pathomechanisms on the cellular level, because the extraction of cell-specific mRNA transcripts poses a major technical challenge. The goal of this thesis was to apply a sophisticated neuron-specific mRNA isolation technique (*Chat* bacTRAP) in a mouse model of multiple sclerosis (EAE) in order to discriminate the translatome profile of cholinergic neurons from the total transcriptome of the spinal cord. This enabled a comprehensive insight into the pathophysiology of neurodegeneration in EAE mice, hereby overcoming hitherto existing methodological challenges.

4.1 Establishment of the bacTRAP methodology

In this study, transgenic C57BL/6 mice were used which express a fusion protein of a ribosomal protein L10a and green-fluorescent protein eGFP (L10a-eGFP) under the choline acetyltransferase (*Chat*) promotor. The *Chat* promotor was chosen for its neuron-specificity (Naciff et al., 1999), since the aim was to investigate neuronal processes contributing to neurodegeneration. By implementation of the *Chat* bacTRAP method, the isolation of highly neuron-specific mRNA material of high quality was achieved. The concentration of *Chat* after immunoprecipitation resulted in a 14-15 fold enrichment. This is in the range of former publications (Doyle, 2008). None of the cell markers used as negative controls were enriched in the qPCR analysis, while *Cd45* (lymphocytes, 15%) and *Gfap* (astrocytes, 31%) were depleted significantly. However, some contamination with non-neuronal transcripts remained after immunoprecipitation. Higher levels of contamination by other cells have been reported for the bacTRAP methodology in comparison to immuno-panning and manual sorting (Okaty et al., 2011). The negative control genes reported in the initial bacTRAP publication (Doyle, 2008) showed a slightly less efficient

depletion in the EAE condition, but the fold enrichment was below the predefined cutoff (fold change > 2.0) for all genes. The gene-set enrichment analysis (GSEA) confirmed the significant depletion of signatures from non-neuronal cells and the strong enrichment of neuronal signals. On the other hand, the cell-type specific enrichment analysis (CSEA) showed weak signals from non-neuronal cells, particularly immune cells, in the EAE condition. The cellular expression profiles used for CSEA were compiled using bacTRAP data from healthy mice (Xu et al., 2014). The application of CSEA in pathological conditions like EAE might therefore be of limited validity.

The slightly inferior purification in the EAE condition could be due to a confounding impact of inflammation on the TRAP immunoprecipitation, as factors like pH affect antibody-antigen binding affinity (Reverberi and Reverberi, 2007). Furthermore, *Chat* expression in non-neuronal cells during EAE could have affected the presented results. Low levels of Chat expression in activated leucocytes, such as macrophages, T cells and B cells, have been reported in different mammals, including in C57BL/6 mice (Kawashima et al., 2007; Fujii et al., 2017). In order to rule out this source of bias, we verified the cell-specific expression of the *Chat* promotor by conducting immunohistochemical stainings of cervical spinal cord sections of *Chat* bacTRAP transgenic mice. No co-localisation of eGFP with non-neuronal cells, including migrating immune cells during CNS inflammation, was detected. The eGFP-L10a fusion protein was expressed specifically in NeuN-positive neurons. This result is in line with previous publications (Dougherty et al., 2010; McKeever et al., 2017; Brichta et al., 2015). In addition, immunological signals were reliably depleted in the TRAP-enriched mRNA samples as determined by RNA-seq.

Taken together, these results support the notion of neuronal specificity of the TRAP-enriched mRNA material. In view of the above-mentioned considerations, false positive results cannot be entirely ruled out. A validation of the presented results is therefore necessary.

4.2 Whole transcriptome analysis during CNS inflammation

Whole transcriptome analysis of spinal cord tissue of healthy and EAE mice was conducted in order to identify whole tissue transcriptional changes during neuroinflammation. The analysis yielded 1345 up-regulated and 119 down-regulated transcripts during EAE (For Adj.P < 0.05). To investigate the relative contribution of different cell types

to the whole transcriptomal changes, sets of marker genes for immune cells, astrocytes, oligodendrocytes and neurons were compiled from the literature and used as input for gene set enrichment analysis (GSEA). Signatures from neurons and oligodendrocytes were found to be depleted, while those of astrocytes and immune cells were enriched. Cell-type specific enrichment analysis (CSEA) confirmed the strong predomination of immune and other non-neuronal cells in the nervous tissue of EAE mice, thereby obscuring possible changes in neuronal translational profiles.

GO term enrichment analysis yielded a strong up-regulation of immunological genes during CNS inflammation. Up-regulated GO terms involved 'adaptive immune response', 'innate immune response', 'lymphocyte activation' and 'positive regulation of adaptive immune response' among others. These observed changes in the whole transcriptome concur with previous studies in the multiple sclerosis literature. Specifically, a transcriptomic meta-analysis of multiple sclerosis and its experimental models (Raddatz et al., 2014) reported 12 genes which were commonly affected in MS and in its animal models. All these 12 genes were up-regulated in this analysis, 11 out of 12 significantly ($p < 0.05$). Of those 12 genes, 8 are expressed in microglia (Ramsey et al., 2008), which underlines the importance of microglial cells in MS pathology (Luo et al., 2017). All studies included in the meta-analysis investigated alterations in whole tissue gene expression and showed an up-regulation of predominantly immunological genes. This is in line with the results of this study.

GO terms associated with neuronal function, such as 'regulation of neuron differentiation', 'cell morphogenesis involved in neuron differentiation' and 'axon part' were down-regulated in the whole tissue analysis. This demonstrates that neuronal signals were concealed by the dominance of immunological signals. Intriguingly, the analysis of the whole tissue transcriptome yielded a down-regulation for multiple gene clusters, which were up-regulated in the TRAP-enriched neuronal samples. Particularly, the GO terms 'unfolded protein binding' was down-regulated in the whole transcriptome, but up-regulated in neurons. The same antithetical changes were detected for proteasomal transcripts. This implies that the up-regulation of neuronal genes during EAE was obscured by the predomination of signatures from other cell types. This highlights the value of the TRAP methodology in detecting differentially expressed genes in neuronal cells *in vivo* during CNS inflammation.

In summary, a drastic alteration in the cell composition of the spinal cord during EAE was detected. This was confirmed via immunohistochemisty, qPCR and RNA-seq, by the

application of sophisticated methods, such as GO analysis, CSEA and GSEA. The contamination of spinal cord tissue with immunological genes due to migrating and activated immune cells obscured the signals from cholinergic neurons. This underpins the need for a neuron-specific analysis approach in order to fathom the neuronal translational changes contributing to neurodegeneration.

4.3 Neuronal translational changes during CNS inflammation

This study is the first to conduct a motor neuron-specific translatome analysis in murine EAE. Cell-specific transcriptome analysis has previously been conducted for immune cells (Didonna et al., 2016) and retinal ganglion cells (Isolated via LCM) in a rat model of EAE (Herold et al., 2015). Here, a cell-specific isolation of translating ribosomes was applied to isolate neuronal mRNA from a mixed CNS tissue. Sets of up- and down-regulated candidate genes were compiled in order to identify de-regulated biological pathways in motor neurons during CNS inflammation. To minimise false positive results due to non-specific background by other cell types, a conservative filtering approach was applied. The application of this filtering method yielded 327 up-regulated and 389 down-regulated genes. By contrast, only 37 (ca. 5%) of these 716 translational changes were detected by whole tissue comparison. Due to the cellular composition of the spinal cord, no firm conclusion on the origin of these changes could have been drawn from the whole tissue analysis alone.

The compiled lists of up- and down-regulated candidate genes were used as input for GO term over-representation analysis, whereby aberrant gene clusters involved in a number of biological processes were identified. The differentially expressed genes and their associated biological processes are discussed in detail below.

4.3.1 Disruptions in protein catabolism and protein folding

Quality control of cellular components and proteins of neurons are ensured by the ubiquitin-proteasome and the autophagy-lysosome system. Disruptions in these systems are known to contribute to the pathogenesis of several neurodegenerative disorders by the accumulation and aggregation of misfolded proteins (Ghavami et al., 2014).

GO enrichment analysis yielded an up-regulation of genes involved in both degradation systems, suggesting an increased demand for the clearance of damaged organelles and defective proteins. The activation of proteolytic pathways may be the result of a patho-

logical accumulation of misfolded proteins, like in other neurodegenerative disorders such as Parkinson's disease (Dehay et al., 2010) and Alzheimer's disease (Gontier et al., 2015). Furthermore, evidence for an impairment in the process of protein folding was detected. The ER-associated protein degradation (ERAD) pathway was activated in neurons during EAE. The ERAD pathway recognises newly synthesised proteins that are not properly folded. These proteins are tagged via ubiquitination and translocated back into the cytosol for degradation by the ubiquitin-proteasome system (Ruggiano et al., 2014). The Bcl2-associated athanogene 1 (Bag1), a neuroprotective and anti-apoptotic protein with co-chaperone features, was strongly down-regulated in the analysis. Bag1 induces chaperone-dependent protein degradation of misfolded substrates (Elliott et al., 2007; Kermer et al., 2015). Additionally, the down-regulation of genes annotated to 'chaperone-mediated protein folding' and 'chaperone binding' suggests an impairment of protein folding. The role of the chaperone machinery has been implied in proteopathies (Shelton et al., 2017). In line with the notion of impaired protein folding, the GO term 'unfolded protein binding' was significantly up-regulated in neurons during EAE in this study.

Further evidence for the accumulation of misfolded proteins was detected, such that several proteins with a high percentage of intrinsically disordered residues were found among the top up-regulated transcripts. Specifically, Bsn (92.1%), Vgf (96.6%) and Pttg1 (94.5%) possess a high percentage of disordered residues, which implies a lack of fixed tertiary protein structure and therefore a predisposition to malformation and aggregation (Chiti and Dobson, 2017). The most significantly up-regulated gene was *Bsn*. The encoded protein Bsn is a presynaptic, giant protein, which is essential for the fusion of presynaptic vesicles (Altrock et al., 2003). Its increased neuronal expression was confirmed using immunohistochemical stainings. Bsn is a critical regulator of presynaptic ubiquitination and proteostasis (Waites et al., 2013), while aberrance in ubiquitination can trigger neurodegeneration (Lehman, 2009). BSN has recently been shown to be involved in neurodegenerative processes. Notably, missense mutations in *BSN* can cause or increase the risk of syndromes of progressive supranuclear palsy (PSP), multiple system atrophy and Alzheimer's disease by leading to an increased tau accumulation (Yabe et al., 2018). The neuronal up-regulation of Bsn likely leads to an inhibition of autophagy via interaction with Atg5 (Okerlund et al., 2017) and Siah (Waites et al., 2013). Autophagy may therefore be simultaneously induced and impaired during EAE, as has been shown for Alzheimer's disease (Yu et al., 2005). Autophagy is generally neuroprotective and disruptions may lead to neurodegeneration (Ghavami et al., 2014) by causing mitochondrial dysfunction and disturbances in the processing of misfolded proteins (Salminen et al., 2013).

Taken together, a down-regulation of protein folding and an up-regulation of protein degradation was detected. The increased demand for protein degradation may be a result of the impaired protein folding and an increased expression of proteins that are prone to malformation.

4.3.2 Apoptosis and excitotoxicity

The second strongest neuronal up-regulation was detected for *Apol6*, which is induced by IFN-γ (Zhaorigetu et al., 2011). IFN-γ plays a pivotal role in the pathology of MS and it was strongly up-regulated in the whole transcriptome. IFN-γ has been shown to directly affect neurons in EAE by mediating glutamate neurotoxicity via AMPA receptors (Mizuno et al., 2008). Apol6 promotes mitochondria-induced apoptosis in cancer cells (Liu et al., 2005) and in smooth muscle cells during atherosclerosis (Zhaorigetu et al., 2011) via the binding of Bcl-xL (Zhaorigetu et al., 2011). Interestingly, *Bcl2l1*, which encodes for both Bcl-xL and Bcl-xS (Boise et al., 1993), was also up-regulated in motor neurons in the analysis. Both are proteins of the Bcl2 family which are located at the outer mitochondrial membrane. They have been shown to regulate neuronal metabolism by interacting with the ATP synthase F(1)F(0), increasing mitochondrial efficiency as a result (Alavian et al., 2011). Bcl-xL acts as an anti-apoptotic agent by increasing mitochondrial ATP release upon death stimuli (Jonas, 2014). It interacts with Vdac (voltage-dependent anion channel), thereby modulating ATP release from mitochondria into the cytosol to help the cell overcome stress (Vander Heiden et al., 2001). It protects against programmed cell death by decreasing the probability of mitochondrial outer membrane permeabilisation (MOMP), which can be triggered by energy depletion during excitotoxicity (Jonas et al., 2014). Transgenic mice neuronally over-expressing Bcl2 display a reduced EAE severity and less axonal loss in comparison to control mice without changes in the immune response (Offen et al., 2000). The up-regulation of *Bcl2l1* might therefore be a neuroprotective reaction to an apoptotic signal, cellular stress and energy depletion during EAE. Bcl2 is also involved in the regulation of autophagy by interaction with the Beclin-1 complex (Ghavami et al., 2014).

Evidence for excitotoxicity was drawn from the increased neuronal expression of ion channel proteins. Notably, *Grin1* and *Grin2a*, which encode for subunits of the NMDA receptor, were both significantly up-regulated in the analysis (Supplementary figure 7.3). This is in line with a recent study that applied the bacTRAP approach in a mouse model

of Alzheimer's disease. It reported an up-regulation of the NMDA receptor subunits in cholinergic neurons (McKeever et al., 2017), implying common pathophysiological pathways between MS and Alzheimer's disease. The NMDA receptor has been linked to neurodegeneration in Alzheimer's (Tackenberg et al., 2013) and benzo(a)pyrene induced neurotoxicity (Chepelev et al., 2016). An association to MS severity has been suggested for *GRIN2A* in GWAS studies (Baranzini et al., 2009; IMSGC, 2011). Increased glutamate signalling may therefore mediate neuronal cell death by excitotoxicity during EAE.

$Na_{(v)}1.2$ type sodium channels are redistributed along the axon during demyelination (Craner et al., 2004). Enhanced $Na_{(v)}1.2$ currents may result in an increased energy consumption and axonal degeneration in EAE without affecting the immune response (Schattling et al., 2016). In the present study, no up-regulation of the encoding gene *Scn2a1* was detected. The redistribution might therefore occur via previously synthesised and stored ion channels, which is not reflected in changes in mRNA translation. As Schattling et al. (2012) have shown, Trpm4 mediates neurodegeneration caused by excitotoxicity in EAE. No alteration in the ribosome-bound mRNA-levels of *Trpm4* was detected in this study. The excitotoxic process does therefore not seem to be mediated by an increased expression in Trpm4 channel proteins.

4.3.3 Axonal transport

Evidence for disruptions in neuronal axonal transport during inflammation was found. This may be caused by the above-mentioned disruptions in neuronal proteolysis (Lee et al., 2011). Axonal transport dysfunction has been postulated as a possible pathomechanism of neuronal damage in several neurodegenerative disorders like MS (van den Berg et al., 2017), Huntington's disease (Bucci et al., 2014) and Alzheimer's disease (Lee et al., 2011). Microtubular axonal transport is necessary for proteostasis by facilitating the fusion of lysosomes and autophagosomes (Ghavami et al., 2014). Disruption in retrograde axonal transport is known to result in the accumulation of misfolded and aggregated proteins (Millecamps and Julien, 2013), as soma are the primary site of degradation of autophagic cargo (Maday and Holzbaur, 2016). The activation of axonal transport might therefore be a result of an increased demand for protein degradation.

Amongst the up-regulated transcripts in the analysis were two kinesin family member proteins (KIFs), Kif1a and Kif5a, which are involved in anterograde microtubule transport (van den Berg et al., 2017). Kif5a is responsible for anterograde transport of mitochondria

(Schwarz, 2013; Campbell et al., 2014) and neurofilament proteins (Xia et al., 2003). A SNP in its gene has been identified as a risk factor for MS (Alcina et al., 2010) and a reduction of axonal expression has been found in the WM of MS patients (Hares et al., 2017a). Reduced expression of Kif5a is correlated with an accumulation of APP and phosphorylated neurofilaments (NF), a hallmark of MS (Gray et al., 2012). Up-regulation of KIFs may be an adaptive response to impaired axonal transport, as has been postulated for AD (Hares et al., 2017b). Increased KIF expression may further indicate an increased transport of mitochondria in order to meet local energy requirements (Millecamps and Julien, 2013).

An increased neuronal expression of the intermediate filament Nefm was detected in the TRAP-seq analysis. The accumulation of neurofilaments due to increased genomic expression can cause disturbed microtubule dynamics in motor neurons (Yadav et al., 2016). The depletion of axonal intermediate filaments in neurons leads to improved axonal transport of mitochondria and lysosomes (Perrot and Julien, 2009) and attenuates neurodegeneration (Ishihara et al., 2001). The elevated levels of Nefm might therefore contribute to microtubule dysfunction, ATP depletion and impaired protein degradation in motor neurons during EAE.

4.3.4 Energy deficit and mitochondrial dysfunction

Mitochondrial dysfunction and consequent energy deprivation are likely to contribute to neurodegeneration in EAE via several different mechanisms and changes in the morphology of axonal mitochondria during EAE have been described in previous studies (Bando et al., 2015). Applying GO term over-/under-representation analysis, a strong down-regulation of multiple gene clusters indicating energy shortage and mitochondrial dysfunction was detected. Particularly, a down-regulation of the gene clusters 'ATP synthesis', 'electron transport chain', 'respiratory transport chain', 'proton transport' and 'ribonucleotide metabolism' was identified. Key components of all mitochondrial electron transport chain complexes and a number of mitochondrial ribosomal proteins (MRPs) were depleted in neurons during EAE. Mitochondrial ribosomal proteins are required for mitochondrial translation of mtDNA-encoded OXPHOS components (Sylvester et al., 2004). Dysfunction in MRPS7, which was among the down-regulated transcripts, leads to a severe familial form of combined OXPHOS deficiency due to a shortage of mitochondrial protein synthesis, complex I and IV activity and ATP production rate (Menezes et al., 2015). The energy deficit might be further exacerbated by the detected malfunction in

axonal transport, which may lead to a reduced mitochondrial motility, resulting in a reduction in axonally available ATP (van den Berg et al., 2017). Mitochondrial dysfunction and consequently decreased ATP levels might in turn result in microtubule and autophagy dysfunction (F F Silva et al., 2011).

More evidence for neuronal energy deficiency was drawn from the up-regulation of gene clusters involved in glycolysis. Particularly, the GO terms 'glycolytic process through glucose-6-phosphate', 'glycolytic process through fructose-6-phosphate' and 'glycolytic process through glucose-1-phosphate' were significantly over-represented in cholinergic neurons during EAE. Glycolysis is possibly up-regulated in order to compensate for the impaired mitochondrial ATP production and the increased energy demand during CNS inflammation. Cellular energy deficit leads to the activation of AMPK, which in turn can activate the PGC1α/FNDC5 axis. In neurodegenerative disorders like Parkinson's and Alzheimer's disease, PGC1α-overexpression is neuroprotective (Farshbaf et al., 2016). It was therefore hypothesised that neuronal energy deficit in EAE may induce similar mechanisms. However, no changes in expression levels of *Ampk*, *Fndc5* or *Pgc1α* were found in neurons during EAE as anticipated. Possibly, the pathomechanism in EAE differs from that of other neurodegenerative disorders in this regard, or the induction of this pathway is in fact localised in other cell types. Hypoxia-Inducible factor-1 (Hif-1) is activated by hypoxia and up-regulated in neurons in neurodegenerative disorder ALS (Sato et al., 2012). Uncoupling-protein 2 (Ucp2) has been shown to be neuroprotective by promoting mitochondrial uncoupling and is induced during hypoxia and hypoglycaemia in neurons (Mattiasson et al., 2003). No neuronal induction of *Ucp2* or *Hif-1* during EAE was found, however. The reported *Ucp2* up-regulation in inflamed spinal cord may thus be due to expression in activated T-lymphocytes (Smorodchenko et al., 2017) and not representative of a neuronal gene-induction.

These findings imply a severely impaired neuronal energy metabolism during EAE, which is in line with previous publications that reported a mitochondrial dysfunction in neurons of MS patients (Campbell et al., 2011; Witte et al., 2014; Dutta et al., 2006). Disturbed neuronal energy metabolism has been linked to neurodegeneration also in different contexts (Nikic et al., 2011; Lin and Beal, 2006).

4.4 Conclusion

In this study, evidence for a neuronal energy deficit, mitochondrial dysfunction, impaired protein metabolism, degradation and transport was detected. Concordant with the induction of protein degradation pathways, a strong up-regulation of several proteins with a high percentage of intrinsically disorders residues was found, indicating a hitherto unknown role of misfolded proteins in the pathophysiology of EAE and MS. These findings suggest a pathogenic overlap between inflammatory neurodegeration and primary neurodegenerative disorders such as Parkinson's and Alzheimer's disease. Future research should focus on investigating the role of pathological protein accumulation, the interaction between energy deficit and impaired protein degradation and their contribution to the pathology of EAE and MS. This could lead to more efficacious treatment options for MS patients, that target the neurodegenerative component of inflammatory neurodegeneration.

5 Summary

Multiple sclerosis (MS) is the most frequent inflammatory disease affecting the central nervous system (CNS). Alongside the inflammatory lesions due to infiltrating immune cells, there seems to be a chronic neurodegenerative process driving disease progression and longterm disability. Precise mechanisms contributing to neurodegeration are incompletely understood. The goal of this thesis was to investigate the underlying molecular mechanisms that mediate this progressive neuronal damage in a mouse model of MS (EAE). To accomplish this, a cell-specific translating mRNA extraction method termed bacTRAP was used to extract and consequently analyse whole tissue and neuronal mRNA of inflamed and healthy spinal cords. Using qPCR and deep sequencing analysis, multiple gene clusters that are activated in the CNS and particularly in motor neurons during experimental autoimmune encephalomyelitis (EAE) were identified. Gene signatures from immune cells and astrocytes were found to be enriched during inflammation and those from oligodendrocytes and neurons to be depleted. Through the analysis of the neuron-specific translatome during EAE, hundreds of de-regulated transcripts including key components of neurodegenerative pathways were identified. The most significant up-regulation was found for the presynaptic and intrinsically disordered protein Bassoon. Furthermore, among the top up-regulated candidates were several others with a high percentage of intrinsically disordered residues, a common feature of pathologically accumulating proteins. The neuronal deposition of misfolded proteins may result in an increased demand in protein clearance, signified by the activation of pathways involved in proteostasis including ubiquitin- and proteasome-dependent protein degradation. Moreover, evidence for neuronal energy deficit, reduced ATP synthesis, activation of glycolysis and mitochondrial dysfunction was found. This energy shortage may be the driver of impaired protein metabolism and the accumulation of misfolded proteins. These results imply hitherto unappreciated common pathological pathways of EAE/MS with other neurodegenerative disorders such as Parkinson's disease and Alzheimer's disease. More research is needed in order to illuminate the role of these de-regulated pathways and their contribution to inflammatory neurodegeneration in order to develop more efficacious treatments for MS patients.

6 *Zusammenfassung*

Multiple Sklerose (MS) ist die häufigste entzündliche Erkrankung des zentralen Nervensystems (ZNS). Neben entzündlichen Läsionen, welche durch migrierende Immunzellen verursacht werden, scheint es einen chronisch ablaufenden, neurodegenerativen Prozess zu geben, welcher das Fortschreiten der Erkrankung und die langfristige Behinderung bedingt. Die genauen Mechanismen, welche zur Neurodegeneration beitragen, sind nicht vollständig verstanden. Das Ziel dieser Arbeit war es, die zugrundeliegenden molekularen Mechanismen, welche diesen progressiven neuronalen Verlust vermitteln, zu studieren. Um dies zu erreichen, wurde eine Methode namens bacTRAP genutzt, welche eine zellspezifische Extraktion translatierender mRNA erlaubt, um neuronale mRNA aus entzündetem und gesundem Rückenmark zu extrahieren und zu analysieren. Mittels qPCR und deep-sequencing analysis konnten multiple Gen-Cluster identifiziert werden, welche im Gesamtgewebe sowie in Neuronen des Rückenmarks während der sogenannten experimental autoimmune encephalomyelitis (EAE) aktiviert werden. Insbesondere waren Signaturen von Immunzellen und Astrozyten im entzündlichen Gewebe angereichert, während diejenigen von Neuronen und Oligodendrozyten reduziert waren. Durch die neuronenspezifische Translatomanalyse während der EAE gelang es, verschiedene Schlüsselbestandteile neurodegenerativer Signalwege zu identifizieren. Die stärkste Hochregulation wurde für das präsynaptische und intrinsisch ungeordnete Protein Bassoon gefunden. Unter den hochregulierten Genen waren einige weitere mit einem hohen Grad intrinsischer Unordnung, ein gemeinsames Merkmal pathologisch akkumulierender Proteine. Die neuronale Ablagerung dieser fehlgefalteten Proteine führt möglicherweise zu einem erhöhten Bedarf des Proteinabbaus, welcher in unserer Analyse durch die Aktivierung von Signalwegen der Proteostase, insbesondere Ubiquitin- und Proteasom-abhängiger Proteindegradation, angezeigt wurde. Des Weiteren fand sich Evidenz für ein neuronales Energiedefizit, eine reduzierte ATP-Produktion, die Aktivierung von Glykolyse und eine mitochondriale Dysfunktion. Dieser Energiemangel ist möglicherweise Ursache des gestörten Proteinmetabolismus und der Akkumulation fehlgefalteter Protein. Diese Ergebnisse implizieren bisher unbeachtete gemeinsame pathologische Signalwege zwischen EAE/MS und anderen neurodegenerativen Störungen wie der Parkinson-Krankheit und der Alzheimer-Krankheit. Weitere Forschung ist nötig, um die Rolle dieser fehlregulierten Signalwege und ihren Beitrag zur entzündlichen Neurodegeneration besser zu verstehen, mit dem Ziel, wirksamere Behandlungen für MS-Patienten zu entwickeln.

7 Supplementary figures

7.1 TRAP

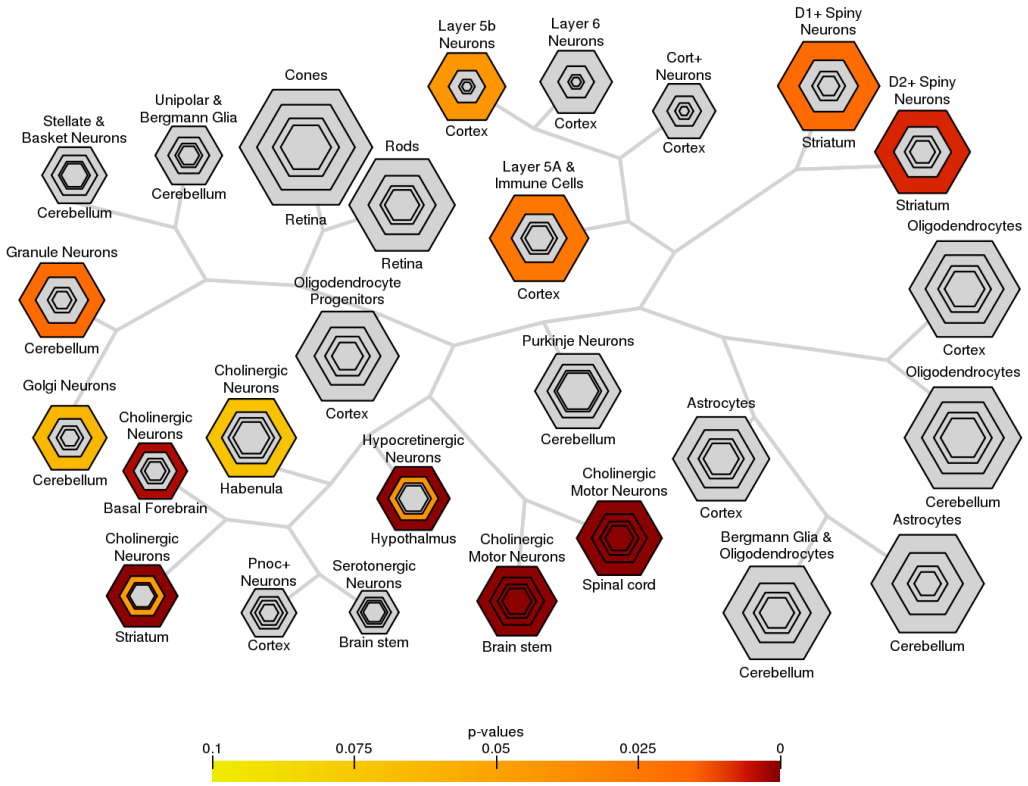

Figure 7.1: Cell-type Specific Expression Analysis (CSEA) of gene list up-regulated in iMN vs iSC. The gene list of all significantly enriched transcripts (iMN/iSC > 2, adj.p-value < 0.05) was used as input for the analysis. Bullseyeplot with Benjamini-Hochberg p-values plotted by color. Varying stringencies for enrichment (pSI) are represented by the size of the hexagons going from least specific lists (outer hexagons) to most specific (center). Hexagons scaled to size of gene lists.

7.2 Whole transcriptome

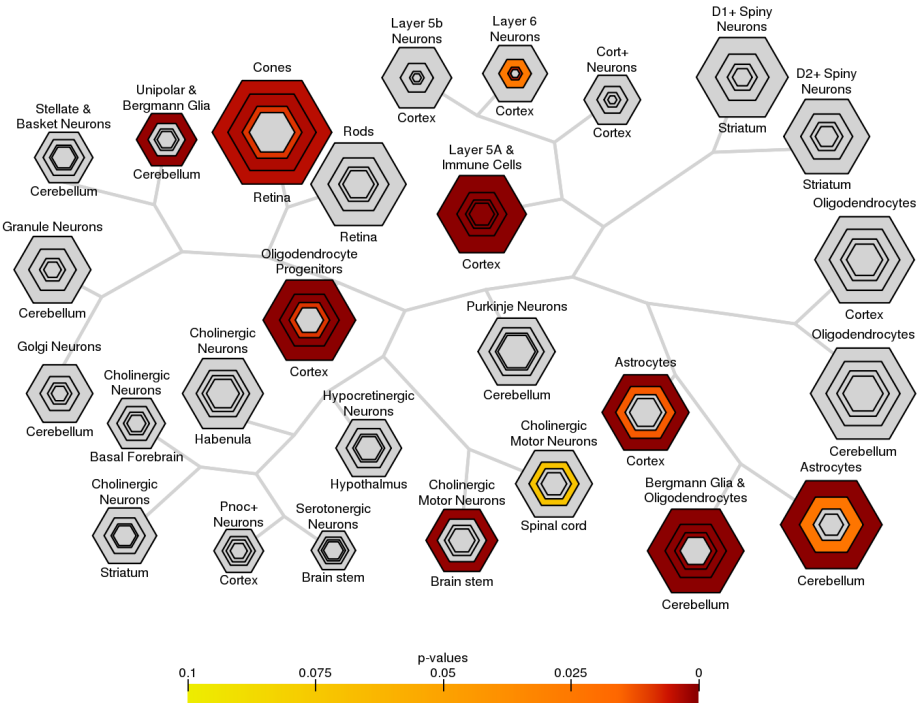

Figure 7.2: Cell-type Specific Expression Analysis (CSEA) of gene list up-regulated in iSC vs SC. The CSEA determines the specificity of gene transcripts for certain cell types based on a database of in situ hybridisation and bacTRAP data. It compares each cell profile to all other profiles in the database and identifies transcripts that are enriched in each cell type, calculates an enrichment score (the SI), and ascribes a pSI value (Xu et al., 2014). The gene list of all significantly enriched transcripts (iSC/SC > 2, adj.p-value < 0.05) was used as input for the analysis. Bullseyeplot with Benjamini-Hochberg p-values plotted by color. Varying stringencies for enrichment (pSI) are represented by the size of the hexagons going from least specific lists (outer hexagons) to most specific (center). Hexagons scaled to size of gene lists.

7.3 EAE up

category	genes in category	p-value	FDR p-value
defense response::GO:0006952	285	2.727×10^{-121}	1.978×10^{-117}
innate immune response::GO:0045087	174	7.073×10^{-97}	2.566×10^{-93}
cell activation::GO:0001775	198	1.251×10^{-87}	3.025×10^{-84}
regulation of immune response::GO:0050776	156	1.633×10^{-80}	2.962×10^{-77}
cytokine production::GO:0001816	149	3.58×10^{-71}	5.195×10^{-68}
lymphocyte activation::GO:0046649	153	2.141×10^{-69}	2.589×10^{-66}
positive regulation of immune response::GO:0050778	125	1.997×10^{-65}	2.07×10^{-62}
regulation of cytokine production::GO:0001817	135	9.266×10^{-65}	8.404×10^{-62}
inflammatory response::GO:0006954	138	8.904×10^{-62}	7.179×10^{-59}
response to external biotic stimulus::GO:0043207	164	2.824×10^{-61}	2.049×10^{-58}
hemopoiesis::GO:0030097	162	9.179×10^{-61}	6.055×10^{-58}
response to cytokine::GO:0034097	131	5.275×10^{-60}	3.189×10^{-57}
hematopoietic or lymphoid organ development::GO:0048534	164	8.777×10^{-59}	4.899×10^{-56}
leukocyte differentiation::GO:0002521	125	1.386×10^{-58}	7.186×10^{-56}
leukocyte cell-cell adhesion::GO:0007159	121	6.941×10^{-58}	3.358×10^{-55}
single organismal cell-cell adhesion::GO:0016337	140	5.728×10^{-54}	2.597×10^{-51}
cellular response to chemical stimulus::GO:0070887	267	4.122×10^{-53}	1.759×10^{-50}
leukocyte aggregation::GO:0070486	112	9.103×10^{-53}	3.67×10^{-50}
T cell activation::GO:0042110	111	1.062×10^{-52}	3.854×10^{-50}
T cell aggregation::GO:0070489	111	1.062×10^{-52}	3.854×10^{-50}
lymphocyte aggregation::GO:0071593	111	1.353×10^{-52}	4.674×10^{-50}
regulation of defense response::GO:0031347	124	2.35×10^{-52}	7.752×10^{-50}
response to organic substance::GO:0010033	275	1.631×10^{-51}	5.144×10^{-49}
regulation of response to stress::GO:0080134	172	4.346×10^{-50}	1.314×10^{-47}
positive regulation of cytokine production::GO:0001819	97	7.769×10^{-50}	2.255×10^{-47}
regulation of cell activation::GO:0050865	111	1.889×10^{-48}	5.273×10^{-46}
regulation of cell proliferation::GO:0042127	198	7.931×10^{-48}	2.131×10^{-45}
cell-cell adhesion::GO:0098609	156	1.47×10^{-47}	3.809×10^{-45}
regulation of leukocyte activation::GO:0002694	104	5.022×10^{-46}	1.256×10^{-43}
defense response to other organism::GO:0098542	112	1.193×10^{-44}	2.885×10^{-42}
leukocyte mediated immunity::GO:0002443	86	1.384×10^{-44}	3.238×10^{-42}

Table 7.1: Top 35 GO annotations involved in biological process in whole tissue material during EAE (iSC vs SC) when sorting for FDR corrected p-value and after removal of 3 layers. Determined by GeneAnswers in R Studio using a hypergeometric statistic.

category	genes in category	p-value	FDR p-value
cell::GO:0005623	959	6.867×10^{-51}	5.184×10^{-48}
cell part::GO:0044464	958	1.476×10^{-50}	5.57×10^{-48}
extracellular region part::GO:0044421	360	3.131×10^{-41}	7.88×10^{-39}
extracellular organelle::GO:0043230	279	4.681×10^{-39}	8.835×10^{-37}
extracellular vesicle::GO:1903561	275	1.793×10^{-37}	2.326×10^{-35}
extracellular exosome::GO:0070062	274	1.848×10^{-37}	2.326×10^{-35}
cell periphery::GO:0071944	408	2.236×10^{-37}	2.411×10^{-35}
extracellular region::GO:0005576	381	1.897×10^{-36}	1.791×10^{-34}
vesicle::GO:0031982	331	4.943×10^{-36}	4.146×10^{-34}
cell surface::GO:0009986	134	9.996×10^{-36}	7.547×10^{-34}
plasma membrane::GO:0005886	395	4.039×10^{-35}	2.772×10^{-33}
membran-bounded vesicle::GO:0031988	305	8.043×10^{-34}	5.061×10^{-32}
side of membrane::GO:0098552	99	9.035×10^{-34}	5.247×10^{-32}
cytoplasm::GO:0005737	684	1.346×10^{-32}	7.257×10^{-31}
membrane-bounded organelle::GO:0043227	745	4.432×10^{-32}	2.231×10^{-30}
external side of plasma membrane::GO:0009897	77	5.557×10^{-32}	2.622×10^{-30}
membrane::GO:0016020	637	2.391×10^{-30}	1.062×10^{-28}
organelle::GO:0043226	779	9.143×10^{-30}	3.835×10^{-28}
intracellular::GO:0005622	797	3.829×10^{-24}	1.521×10^{-22}
intracellular part::GO:0044424	790	1.389×10^{-23}	5.245×10^{-22}
extracellular space::GO:0005615	158	2.391×10^{-22}	8.596×10^{-21}
plasma membrane part::GO:0044459	224	3.119×10^{-22}	1.07×10^{-20}
focal adhesion::GO:0005925	61	3.808×10^{-18}	1.25×10^{-16}
cell-substrate adherens junction::GO:0005924	61	7.75×10^{-18}	2.438×10^{-16}
lysosome::GO:0005764	69	8.922×10^{-18}	2.587×10^{-16}
lytic vacuole::GO:0000323	69	8.922×10^{-18}	2.587×10^{-16}
cytoplasmic part::GO:0044444	455	9.251×10^{-18}	2.587×10^{-16}
cell-substrate junction::GO:0030055	61	1.784×10^{-17}	4.81×10^{-16}
intracellular organelle::GO:0043229	681	3.151×10^{-17}	8.204×10^{-16}
MHC protein complex::GO:0042611	15	6.299×10^{-17}	1.585×10^{-15}
membrane part::GO:0044425	460	1.022×10^{-16}	2.489×10^{-15}
intracellular membrane-bounded organelle::GO:0043231	625	1.433×10^{-15}	3.381×10^{-14}
adherens junction::GO:0005912	79	2.547×10^{-14}	5.827×10^{-13}
anchoring junction::GO:0070161	80	3.678×10^{-14}	8.167×10^{-13}
vacuole::GO:0005773	103	4.068×10^{-12}	8.775×10^{-11}
cytosol::GO:0005829	130	2.079×10^{-11}	4.359×10^{-10}
plasma membrane protein complex::GO:0098797	55	6.843×10^{-10}	1.396×10^{-08}
intrinsic component of membrane::GO:0031224	371	1.16×10^{-09}	2.305×10^{-08}
cell leading edge::GO:0031252	43	1.829×10^{-09}	3.542×10^{-08}
endomembrane system::GO:0012505	238	3.543×10^{-09}	6.688×10^{-08}
integral component of membrane::GO:0016021	360	4.347×10^{-09}	8.004×10^{-08}

Table 7.2: Top 40 GO annotations involved in cellular component in whole tissue material during EAE (iSC vs SC) when sorting for FDR corrected p-value. Determined by GeneAnswers in R Studio using a hypergeometric statistic.

category	genes in category	p-value	FDR p-value
protein binding::GO:0005515	673	1.176×10^{-70}	2.183×10^{-67}
binding::GO:0005488	859	1.048×10^{-58}	9.722×10^{-56}
receptor binding::GO:0005102	168	1.862×10^{-24}	1.152×10^{-21}
protein complex binding::GO:0032403	106	2.691×10^{-18}	1.249×10^{-15}
macromolecular complex binding::GO:0044877	140	1.799×10^{-15}	6.678×10^{-13}
cytokine receptor activity::GO:0004896	26	2.3×10^{-14}	7.114×10^{-12}
carbohydrate derivative binding::GO:0097367	176	7.633×10^{-14}	2.024×10^{-11}
enzyme regulator activity::GO:0030234	97	1.037×10^{-13}	2.406×10^{-11}
cell adhesion molecule binding::GO:0050839	61	1.739×10^{-13}	3.586×10^{-11}
enzyme binding::GO:0019899	162	2.893×10^{-13}	5.37×10^{-11}
cytokine binding::GO:0019955	26	4.099×10^{-13}	6.916×10^{-11}
identical protein binding::GO:0042802	122	5.596×10^{-13}	8.524×10^{-11}
cytokine receptor binding::GO:0005126	46	5.971×10^{-13}	8.524×10^{-11}
molecular function regulator::GO:0098772	113	5.618×10^{-12}	7.447×10^{-10}
protein dimerization activity::GO:0046983	113	6.247×10^{-12}	7.729×10^{-10}
carbohydrate binding::GO:0030246	39	4.037×10^{-11}	4.683×10^{-09}
kinase binding::GO:0019900	72	8.758×10^{-11}	9.562×10^{-09}
actin binding::GO:0003779	50	1.535×10^{-10}	1.583×10^{-08}
protein kinase binding::GO:0019901	66	3.036×10^{-1} 0	2.966×10^{-08}
cytokine activity::GO:0005125	34	1.345×10^{-09}	1.248×10^{-07}
antigen binding::GO:0003823	25	1.612×10^{-09}	1.425×10^{-07}
integrin binding::GO:0005178	22	2.438×10^{-09}	2.057×10^{-07}
protein homodimerization activity::GO:0042803	76	3.826×10^{-09}	3.088×10^{-07}
organic cyclic compound binding::GO:0097159	335	1.047×10^{-08}	8.095×10^{-07}
enzyme activator activity::GO:0008047	49	1.155×10^{-08}	8.575×10^{-07}
heterocyclic compound binding::GO:1901363	330	1.235×10^{-08}	8.817×10^{-07}
peptide antigen binding::GO:0042605	13	5.33×10^{-08}	3.664×10^{-06}
peptidase regulator activity::GO:0061134	32	6.107×10^{-08}	4.048×10^{-06}
cytoskeletal protein binding::GO:0008092	76	6.73×10^{-08}	4.204×10^{-06}
chemokine receptor binding::GO:0042379	14	6.796×10^{-08}	4.204×10^{-06}
glycosaminoglycan binding::GO:0005539	28	8.887×10^{-08}	5.321×10^{-06}
cysteine-type endopeptidase activity::GO:0004197	17	1.897×10^{-07}	1.1×10^{-05}
small molecule binding::GO:0036094	165	5.273×10^{-07}	2.863×10^{-05}
RNA polymerase II regulatory region DNA binding::GO:0001012	56	5.313×10^{-07}	2.863×10^{-05}
purine nucleotide binding::GO:0017076	129	5.448×10^{-07}	2.863×10^{-05}
nucleoside binding::GO:0001882	127	5.553×10^{-07}	2.863×10^{-05}
ribonucleotide binding::GO:0032553	129	6.357×10^{-07}	3.189×10^{-05}
purine ribonucleoside binding::GO:0032550	126	6.653×10^{-07}	3.25×10^{-05}
purine ribonucleoside triphosphate binding::GO:0035639	125	7.259×10^{-07}	3.306×10^{-05}

Table 7.3: Top 40 GO annotations involved in molecular function in whole tissue material during EAE (iSC vs SC) when sorting for FDR corrected p-value. Determined by GeneAnswers in R Studio using a hypergeometric statistic.

7.4 EAE down

Category	genes in Category	p value	fdr p value
cellular metabolic process::GO:0044237	59	2.832×10^{-5}	0.05059
negative regulation of cyclic-nucleotide phosphodiesterase activity::GO:0051344	2	5.473×10^{-5}	0.05059
cellular process::GO:0009987	82	7.58×10^{-5}	0.05059
metabolic process::GO:0008152	62	0.0001065	0.05218
aerobic respiration::GO:0009060	4	0.0001303	0.05218
regulation of cyclic-nucleotide phosphodiesterase activity::GO:0051342	2	0.0001814	0.06054
dicarboxylic acid metabolic process::GO:0043648	4	0.0003253	0.09305

Table 7.4: Downregulated GO annotations involved in biological process in whole tissue material during EAE (iSC vs SC) when sorting for FDR corrected p-value. Determined by GeneAnswers in R Studio using a hypergeometric statistic.

Category	genes in Category	p value	FDR p value
mitochondrial protein complex::GO:0098798	7	2.975×10^{-6}	8.033×10^{-5}
inner mitochondrial membrane protein complex::GO:0098800	6	8.088×10^{-6}	0.0002028
mitochondrial inner membrane::GO:0005743	9	5.637×10^{-5}	0.001099
mitochondrial part::GO:0044429	12	8.374×10^{-5}	0.001547
mitochondrial membrane part::GO:0044455	6	9.722×10^{-5}	0.001706
organelle inner membrane::GO:0019866	9	0.0001187	0.001944
mitochondrial membrane::GO:0031966	10	0.0001219	0.001944
mitochondrion::GO:0005739	19	0.0001399	0.002135
mitochondrial proton-transporting ATP synthase complex, catalytic core F(1)::GO:0000275	2	0.0001813	0.002546
proton-transporting ATP synthase complex, catalytic core F(1)::GO:0045261	2	0.0001813	0.002546
mitochondrial envelope::GO:0005740	10	0.0002188	0.002953
myelin sheath::GO:0043209	6	0.0002965	0.003652
membrane-bounded vesicle::GO:0031988	27	0.0002988	0.003652
nucleus::GO:0005634	44	0.0003017	0.003652
mitochondrial matrix::GO:0005759	6	0.0003799	0.004445
nuclear proteasome complex::GO:0031595	2	0.0005035	0.005701
organelle envelope::GO:0031967	12	0.0006797	0.007351
organelle membrane::GO:0031090	16	0.0007104	0.007351
envelope::GO:0031975	12	0.0007121	0.007351
cytosolic proteasome complex::GO:0031597	2	0.001174	0.01177
extracellular exosome::GO:0070062	22	0.001219	0.01189
extracellular vesicle::GO:1903561	22	0.001309	0.01214
vesicle::GO:0031982	27	0.001324	0.01214
extracellular organelle::GO:0043230	22	0.001349	0.01214
proton-transporting two-sector ATPase complex, catalytic domain::GO:0033178	2	0.001609	0.01412
catalytic complex::GO:1902494	12	0.002142	0.01833
protein complex::GO:0043234	29	0.002215	0.01851
nucleoplasm::GO:0005654	18	0.002294	0.01873
mitochondrial proton-transporting ATP synthase complex::GO:0005753	2	0.002675	0.02109
nuclear part::GO:0044428	25	0.002734	0.02109
dendritic spine::GO:0043197	4	0.002765	0.02109
proteasome complex::GO:0000502	3	0.002897	0.02118
endopeptidase complex::GO:1905369	3	0.002897	0.02118
neuron spine::GO:0044309	4	0.003071	0.022
respiratory chain complex::GO:0098803	3	0.003153	0.02214
mitochondrial respiratory chain::GO:0005746	3	0.003286	0.0223
proton-transporting ATP synthase complex::GO:0045259	2	0.003304	0.0223
proteasome regulatory particle::GO:0005838	2	0.003641	0.02411
nuclear lumen::GO:0031981	22	0.00387	0.02515
main axon::GO:0044304	3	0.004158	0.02653
proteasome accessory complex::GO:0022624	2	0.004362	0.02734
presynapse::GO:0098793	5	0.005081	0.03129
respiratory chain::GO:0070469	3	0.005336	0.03229
peptidase complex::GO:1905368	3	0.005519	0.03283
axon part::GO:0033267	5	0.006529	0.03757
ionotropic glutamate receptor complex::GO:0008328	2	0.01959	0.07395
proteasome regulatory particle, lid subcomplex::GO:0008541	1	0.0297	0.09309
endosome::GO:0005768	7	0.03259	0.0986

Table 7.5: Top downregulated GO annotations involved in cellular component in whole tissue material during EAE (iSC vs SC) when sorting for FDR corrected p-value. Determined by GeneAnswers in R Studio using a hypergeometric statistic.

Category	genes in category	p value	FDR p value
purine nucleotide binding::GO:0017076	23	1.195×10^{-6}	0.0001575
ribonucleotide binding::GO:0032553	23	1.256×10^{-6}	0.0001575
nucleotide binding::GO:0000166	26	1.288×10^{-6}	0.0001575
nucleoside phosphate binding::GO:1901265	26	1.288×10^{-6}	0.0001575
small molecule binding::GO:0036094	27	1.892×10^{-6}	0.0001585
purine ribonucleoside triphosphate binding::GO:0035639	22	2.545×10^{-6}	0.0001585
purine ribonucleoside binding::GO:0032550	22	2.916×10^{-6}	0.0001585
purine nucleoside binding::GO:0001883	22	3.002×10^{-6}	0.0001585
ribonucleoside binding::GO:0032549	22	3.002×10^{-6}	0.0001585
nucleoside binding::GO:0001882	22	3.242×10^{-6}	0.0001585
purine ribonucleotide binding::GO:0032555	22	4.034×10^{-6}	0.0001793
catalytic activity::GO:0003824	45	4.609×10^{-6}	0.0001878
carbohydrate derivative binding::GO:0097367	23	2.424×10^{-5}	0.0009118
protein binding::GO:0005515	55	3.666×10^{-5}	0.001281
binding::GO:0005488	74	5.261×10^{-5}	0.001715
adenyl nucleotide binding::GO:0030554	17	0.0001215	0.003713
G-protein coupled receptor binding::GO:0001664	7	0.0001352	0.003888
nucleoside-triphosphatase activity::GO:0017111	11	0.0002443	0.006637
ATP binding::GO:0005524	16	0.0002662	0.006852
beta-amyloid binding::GO:0001540	3	0.000335	0.007903
adenyl ribonucleotide binding::GO:0032559	16	0.0003649	0.007903
pyrophosphatase activity::GO:0016462	11	0.0003874	0.007903
hydrolase activity, acting on acid anhydrides, in phosphorus-containing anhydrides::GO:0016818	11	0.0003963	0.007903
hydrolase activity, acting on acid anhydrides::GO:0016817	11	0.0004008	0.007903
NADH dehydrogenase activity::GO:0003954	3	0.000404	0.007903
ATPase activity, coupled::GO:0042623	7	0.000458	0.008613
heterocyclic compound binding::GO:1901363	37	0.0008238	0.01492
organic cyclic compound binding::GO:0097159	37	0.001137	0.01985
proton-transporting ATP synthase activity, rotational mechanism::GO:0046933	2	0.001218	0.02053
ligase activity::GO:0016874	7	0.001554	0.02533
ATPase activity::GO:0016887	7	0.002126	0.03354
ATP-dependent RNA helicase activity::GO:0004004	3	0.002797	0.04145
RNA-dependent ATPase activity::GO:0008186	3	0.002797	0.04145
TBP-class protein binding::GO:0017025	2	0.003426	0.04199
unfolded protein binding::GO:0051082	3	0.003753	0.04199
proton-transporting ATPase activity, rotational mechanism::GO:0046961	2	0.003776	0.04199
GTP binding::GO:0005525	6	0.004015	0.04199
RNA helicase activity::GO:0003724	3	0.004058	0.04199
ATPase regulator activity::GO:0060590	2	0.004142	0.04199
hydrolase activity::GO:0016787	20	0.004148	0.04199
chaperone binding::GO:0051087	3	0.004217	0.04199

Table 7.6: Top downregulated GO annotations involved in molecular function in whole tissue material during EAE (iSC vs SC) when sorting for FDR corrected p-value. Determined by GeneAnswers in R Studio using a hypergeometric statistic.

7.5 Neuron up

category	genes in category	p-value	FDR p-value
protein localization::GO:0008104	60	1.279×10^{-10}	2.713×10^{-07}
multicellular organism development::GO:0007275	97	1.645×10^{-10}	2.713×10^{-07}
transport::GO:0006810	87	2.255×10^{-10}	2.713×10^{-07}
establishment of protein localization::GO:0045184	50	1.054×10^{-09}	9.506×10^{-07}
system development::GO:0048731	86	2.912×10^{-09}	2.102×10^{-06}
cellular component assembly::GO:0022607	56	5.106×10^{-09}	3.071×10^{-06}
regulation of cell communication::GO:0010646	62	6.604×10^{-09}	3.405×10^{-06}
cellular protein localization::GO:0034613	41	2.481×10^{-08}	1.024×10^{-05}
regulation of cellular component organization::GO:0051128	54	2.553×10^{-08}	1.024×10^{-05}
cellular macromolecule localization::GO:0070727	41	3.056×10^{-08}	1.103×10^{-05}
nervous systemwdevelopment::GO:0007399	49	1.795×10^{-07}	5.889×10^{-05}
regulation of intracellular signal transduction::GO:1902531	39	2.498×10^{-07}	7.513×10^{-05}
regulation of signal transduction::GO:0009966	53	3.035×10^{-07}	8.425×10^{-05}
neuron differentiation::GO:0030182	36	3.901×10^{-07}	0.0001006
intracellular signal transduction::GO:0035556	51	4.388×10^{-07}	0.0001056
neuron development::GO:0048666	31	5.729×10^{-07}	0.0001292
cellular macromolecule metabolic process::GO:0044260	117	7.942×10^{-07}	0.0001648
organic substance transport::GO:0071702	52	8.221×10^{-07}	0.0001648
cell communication::GO:0007154	101	1.033×10^{-06}	0.0001961
organelle organization::GO:0006996	60	1.414×10^{-06}	0.0002551
generation of neurons::GO:0048699	37	1.679×10^{-06}	0.0002885
protein transport::GO:0015031	40	1.875×10^{-06}	0.0003075
cell part morphogenesis::GO:0032990	26	2.137×10^{-06}	0.0003353
neurogenesis::GO:0022008	38	2.876×10^{-06}	0.0004325
intracellular transport::GO:0046907	33	3.258×10^{-06}	0.0004703
cell morphogenesis::GO:0000902	31	4.21×10^{-06}	0.0005755
establishment of localization in cell::GO:0051649	39	4.306×10^{-06}	0.0005755
macromolecule metabolic process::GO:0043170	123	6.142×10^{-06}	0.0007656
neuron projection development::GO:0031175	26	6.152×10^{-06}	0.0007656
macromolecular complex subunit organization::GO:0043933	45	7.094×10^{-06}	0.0008363
cellular component morphogenesis::GO:0032989	32	7.183×10^{-06}	0.0008363
protein complex subunit organization::GO:0071822	33	8.629×10^{-06}	0.0009608
single-organism organelle organization::GO:1902589	39	8.785×10^{-06}	0.0009608
response to organic substance::GO:0010033	51	9.12×10^{-06}	0.0009681
macromolecule catabolic process::GO:0009057	27	1.204×10^{-05}	0.001241
protein localization to organelle::GO:0033365	23	1.248×10^{-05}	0.001251
cell projection morphogenesis::GO:0048858	24	1.306×10^{-05}	0.001274
cellular response to chemical stimulus::GO:0070887	48	1.471×10^{-05}	0.001397
regulation of TOR signalling::GO:0032006	7	1.541×10^{-05}	0.001426

Table 7.7: GO annotations involved in biological process in 'neuron up' list sorted for FDR corrected p-values. Determined by GeneAnswers in R Studio using a hypergeometric statistic.

category	genes in category	p-value	FDR p-value
cytoplasm::GO:0005737	199	8.722×10^{-16}	2.922×10^{-13}
intracellular::GO:0005622	235	1.016×10^{-15}	2.922×10^{-13}
cell part::GO:0044464	257	2.347×10^{-15}	3.705×10^{-13}
cell::GO:0005623	257	2.577×10^{-15}	3.705×10^{-13}
intracellular part::GO:0044424	231	1.617×10^{-14}	1.86×10^{-12}
cell projection part::GO:0044463	42	6.154×10^{-12}	5.898×10^{-10}
neuron part::GO:0097458	51	1.67×10^{-10}	1.371×10^{-08}
cell projection::GO:0042995	62	2.269×10^{-10}	1.631×10^{-08}
organelle::GO:0043226	211	4.299×10^{-10}	2.746×10^{-08}
intracellular organelle::GO:0043229	197	6.674×10^{-10}	3.837×10^{-08}
macromolecular complex::GO:0032991	108	1.452×10^{-09}	7.588×10^{-08}
protein complex::GO:0043234	93	3.227×10^{-09}	1.546×10^{-07}
axon::GO:0030424	26	3.535×10^{-09}	1.564×10^{-07}
neuron projection::GO:0043005	41	5.551×10^{-09}	2.28×10^{-07}
organelle part::GO:0044422	128	6.444×10^{-09}	2.47×10^{-07}
cytoplasmic part::GO:0044444	131	2.288×10^{-08}	8.221×10^{-07}
intracellular organelle part::GO:0044446	122	6.769×10^{-08}	2.289×10^{-06}
membrane-bounded organelle::GO:0043227	191	2.082×10^{-07}	6.65×10^{-06}
somatodendritic compartment::GO:0036477	31	2.897×10^{-07}	8.767×10^{-06}
growth cone::GO:0030426	12	9.79×10^{-07}	2.815×10^{-05}
cell body::GO:0044297	26	1.337×10^{-06}	3.576×10^{-05}
site of polarized growth::GO:0030427	12	1.368×10^{-06}	3.576×10^{-05}
cytoskeleton::GO:0005856	50	1.555×10^{-06}	3.887×10^{-05}
intracellular membrane-bounded organelle::GO:0043231	172	1.8×10^{-06}	4.314×10^{-05}
vesicle::GO:0031982	75	4.537×10^{-06}	0.0001037
non-membrane-bounded organelle::GO:0043228	79	4.869×10^{-06}	0.0001037
intracellular non-membrane-bounded organelle::GO:0043232	79	4.869×10^{-06}	0.0001037
neuronal cell body::GO:0043025	23	5.962×10^{-06}	0.0001224
bounding membrane of organelle::GO:0098588	29	8.019×10^{-06}	0.000159
synapse::GO:0045202	27	9.672×10^{-06}	0.0001854
excitatory synapse::GO:0060076	13	1.017×10^{-05}	0.0001887
cell projection membrane::GO:0031253	13	1.829×10^{-05}	0.0003271
synapse part::GO:0044456	22	1.94×10^{-05}	0.0003271
postsynaptic density::GO:0014069	12	1.991×10^{-05}	0.0003271
postsynaptic specialization::GO:0099572	12	1.991×10^{-05}	0.0003271
spectrin::GO:0008091	3	2.124×10^{-05}	0.0003392
dendrite::GO:0030425	20	6.512×10^{-05}	0.001012
organelle membrane::GO:0031090	38	7.521×10^{-05}	0.001138
lysosomal membrane::GO:0005765	10	0.0001016	0.001443
lytic vacuole membrane::GO:0098852	10	0.0001016	0.001443
membrane-bounded vesicle::GO:0031988	65	0.0001041	0.001443

Table 7.8: GO annotations involved in cellular component in 'neuron up' list, sorted by FDR corrected p-values. Determined by GeneAnswers in R Studio using a hypergeometric statistic.

category	genes in category	p-value	FDR p-value
protein binding::GO:0005515	166	5.172×10^{-13}	5.56×10^{-10}
binding::GO:0005488	221	7.225×10^{-12}	3.883×10^{-09}
macromolecular complex binding::GO:0044877	46	2.188×10^{-08}	7.84×10^{-06}
protein complex binding::GO:0032403	32	2.017×10^{-07}	4.949×10^{-05}
enzyme binding::GO:0019899	52	2.302×10^{-07}	4.949×10^{-05}
carbohydrate derivative binding::GO:0097367	52	4.144×10^{-06}	0.0007424
kinase binding::GO:0019900	24	6.933×10^{-06}	0.001065
purine ribonucleoside triphosphate binding::GO:0035639	43	1.734×10^{-05}	0.001978
purine ribonucleoside binding::GO:0032550	43	2.117×10^{-05}	0.001978
ATP binding::GO:0005524	37	2.195×10^{-05}	0.001978
purine nucleoside binding::GO:0001883	43	2.209×10^{-05}	0.001978
ribonucleoside binding::GO:0032549	43	2.209×10^{-05}	0.001978
nucleoside binding::GO:0001882	43	2.471×10^{-05}	0.002043
purine ribonucleotide binding::GO:0032555	43	3.394×10^{-05}	0.00242
purine nucleotide binding::GO:0017076	43	3.887×10^{-05}	0.00242
adenyl ribonucleotide binding::GO:0032559	37	4.009×10^{-05}	0.00242
ribonucleotide binding::GO:0032553	43	4.157×10^{-05}	0.00242
protein kinase binding::GO:0019901	21	4.217×10^{-05}	0.00242
enzyme activator activity::GO:0008047	17	4.278×10^{-05}	0.00242
adenyl nucleotide binding::GO:0030554	37	4.519×10^{-05}	0.002429
heterocyclic compound binding::GO:1901363	97	7.045×10^{-05}	0.003606
organic cyclic compound binding::GO:0097159	98	8.11×10^{-05}	0.003963
molecular function regulator::GO:0098772	32	0.0001078	0.005038
GTPase regulator activity::GO:0030695	12	0.0001166	0.005224
protein heterodimerization activity::GO:0046982	18	0.0001309	0.005628
ankyrin binding::GO:0030506	4	0.0001464	0.006055
Ras guanyl-nucleotide exchange factor activity::GO:0005088	8	0.0001597	0.006359
nucleotide binding::GO:0000166	48	0.000196	0.007267
nucleoside phosphate binding::GO:1901265	48	0.000196	0.007267
GTPase activator activity::GO:0005096	11	0.0002289	0.008203
nucleoside-triphosphatase regulator activity::GO:0060589	12	0.0002563	0.008888
poly(A) RNA binding::GO:0044822	30	0.00027	0.009071
Rho guanyl-nucleotide exchange factor activity::GO:0005089	6	0.0002926	0.009533
transcription factor binding::GO:0008134	18	0.0003246	0.01026
small molecule binding::GO:0036094	50	0.0004027	0.01237
receptor binding::GO:0005102	36	0.0004475	0.01336
RNA binding::GO:0003723	37	0.0005298	0.01539
enzyme regulator activity::GO:0030234	24	0.0008393	0.02374
ATPase activity::GO:0016887	14	0.001082	0.02982
Rab GTPase binding::GO:0017137	7	0.001221	0.03282
protein dimerization activity::GO:0046983	28	0.002282	0.05984

Table 7.9: GO annotations involved in molecular function in 'neuron up' list, sorted by FDR corrected p-values. Determined by GeneAnswers in R Studio using a hypergeometric statistic.

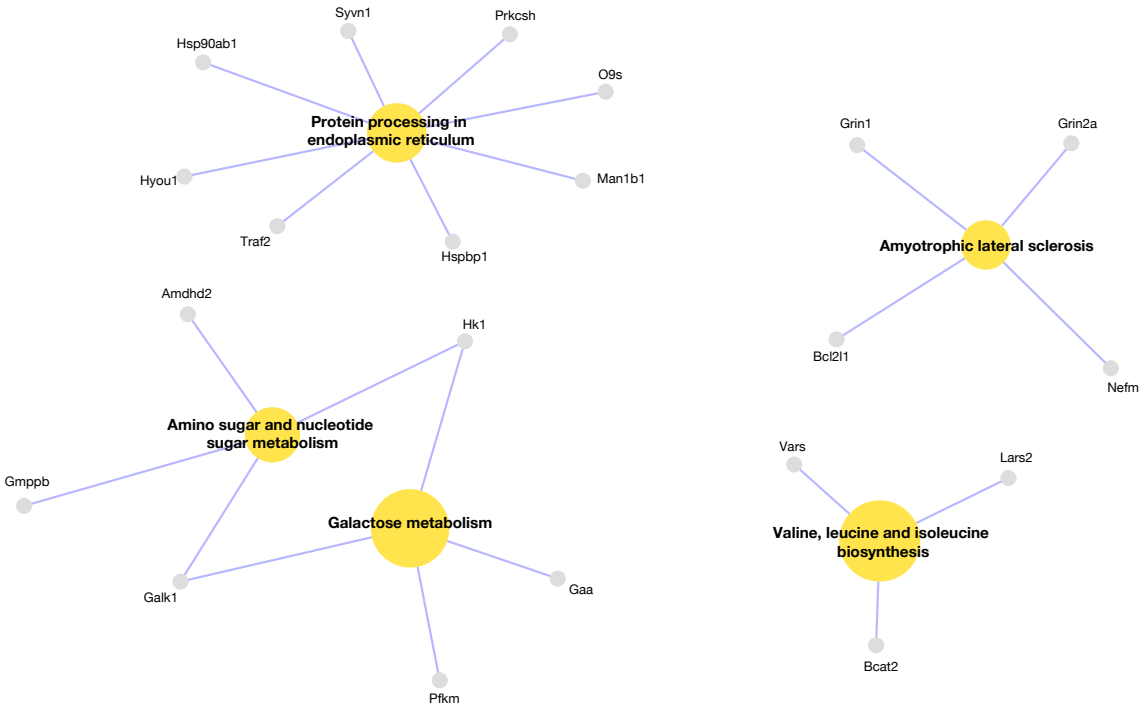

Figure 7.3: KEGG annotations over-represented in 'neuron up' list.

7.6 Neuron down

category	genes in category	p-value	FDR p-value
mitochondrion organization::GO:0007005	43	3.232×10^{-17}	1.062×10^{-13}
organonitrogen compound metabolic process::GO:1901564	63	3.146×10^{-10}	5.166×10^{-07}
organelle organization::GO:0006996	84	1.233×10^{-09}	1.35×10^{-06}
electron transport chain::GO:0022900	11	2.527×10^{-09}	2.075×10^{-06}
metabolic process::GO:0008152	200	4.459×10^{-09}	2.542×10^{-06}
peptide metabolic process::GO:0006518	35	4.644×10^{-09}	2.542×10^{-06}
translation::GO:0006412	31	6.114×10^{-09}	2.868×10^{-06}
cellular respiration::GO:0045333	14	1.252×10^{-08}	4.385×10^{-06}
peptide biosynthetic process::GO:0043043	31	1.297×10^{-08}	4.385×10^{-06}
respiratory electron transport chain::GO:0022904	10	1.335×10^{-08}	4.385×10^{-06}
amide biosynthetic process::GO:0043604	32	3.558×10^{-08}	1.035×10^{-05}
cellular component organization or biogenesis::GO:0071840	128	3.78×10^{-08}	1.035×10^{-05}
cellular amide metabolic process::GO:0043603	36	4.33×10^{-08}	1.094×10^{-05}
cellular component organization::GO:0016043	125	5.025×10^{-08}	1.179×10^{-05}
cellular protein metabolic process::GO:0044267	102	5.609×10^{-08}	1.228×10^{-05}
organonitrogen compound biosynthetic process::GO:1901566	43	7.649×10^{-08}	1.57×10^{-05}
mitochondrial ATP synthesis coupled electron transport::GO:0042775	8	1.004×10^{-07}	1.939×10^{-05}
mitochondrial transmembrane transport::GO:1990542	8	1.232×10^{-07}	2.247×10^{-05}
ATP synthesis coupled electron transport::GO:0042773	8	1.822×10^{-07}	3.046×10^{-05}
mitochondrial translation::GO:0032543	9	1.855×10^{-07}	3.046×10^{-05}
cellular metabolic process::GO:0044237	178	2.069×10^{-07}	3.236×10^{-05}
protein metabolic process::GO:0019538	109	3.952×10^{-07}	5.899×10^{-05}
purine ribonucleoside triphosphate metabolic process::GO:0009205	15	4.791×10^{-07}	6.841×10^{-05}
ribonucleoside triphosphate metabolic process::GO:0009199	15	5.752×10^{-07}	7.341×10^{-05}
ATP synthesis coupled proton transport::GO:0015986	6	5.812×10^{-07}	7.341×10^{-05}
energy coupled proton transport, down electrochemical gradient::GO:0015985	6	5.812×10^{-07}	7.341×10^{-05}
purine nucleoside triphosphate metabolic process::GO:0009144	15	7.745×10^{-07}	9.42×10^{-05}
ATP metabolic process::GO:0046034	14	8.932×10^{-07}	0.0001048
energy derivation by oxidation of organic compounds::GO:0015980	15	9.765×10^{-07}	0.0001106
nucleoside monophosphate metabolic process::GO:0009123	15	1.295×10^{-06}	0.0001406
oxidation-reduction process::GO:0055114	33	1.327×10^{-06}	0.0001406
mitochondrial respiratory chain complex assembly::GO:0033108	7	1.406×10^{-06}	0.0001443
nucleoside triphosphate metabolic process::GO:0009141	15	2.111×10^{-06}	0.0002101
iron-sulfur cluster assembly::GO:0016226	5	3.519×10^{-06}	0.0003218
metallo-sulfur cluster assembly::GO:0031163	5	3.519×10^{-06}	0.0003218
organic substance metabolic process::GO:0071704	182	3.528×10^{-06}	0.0003218
purine ribonucleoside monophosphate metabolic process::GO:0009167	14	3.847×10^{-06}	0.0003415
purine nucleoside monophosphate metabolic process::GO:0009126	14	4.06×10^{-06}	0.0003509
oxidative phosphorylation::GO:0006119	8	4.256×10^{-06}	0.0003584
ribonucleoside metabolic process::GO:0009119	16	4.493×10^{-06}	0.0003619
ribonucleoside monophosphate metabolic process::GO:0009161	14	4.518×10^{-06}	0.0003619

Table 7.10: GO annotations involved in biological process down-regulated in neurons during EAE, sorted by FDR corrected p-values. Determined by GeneAnswers in R Studio using a hypergeometric statistic.

Category	genes in category	p value	FDR p value
cytoplasm::GO:0005737	241	2.534×10^{-35}	1.031×10^{-33}
mitochondrial part::GO:0044429	66	2.09×10^{-27}	4.253×10^{-33}
mitochondrion::GO:0005739	93	1.628×10^{-32}	2.208×10^{-09}
intracellular membrane-bounded organelle::GO:0043231	231	4.042×10^{-30}	4.113×10^{-27}
cytoplasmic part::GO:0044444	180	5.981×10^{-24}	4.868×10^{-28}
mitochondrial envelope::GO:0005740	51	7.42×10^{-27}	5.033×10^{-26}
inner mitochondrial membrane protein complex::GO:0098800	27	9.3×10^{-25}	5.407×10^{-25}
mitochondrial protein complex::GO:0098798	29	5.463×10^{-26}	2.779×10^{-22}
mitochondrial inner membrane::GO:0005743	39	1.71×10^{-22}	7.735×10^{-20}
mitochondrial membrane::GO:0031966	44	6.493×10^{-21}	2.643×10^{-20}
organelle envelope::GO:0031967	56	1.762×10^{-21}	6.52×10^{-20}
organelle inner membrane::GO:0019866	39	5.812×10^{-21}	1.971×10^{-19}
ribosome::GO:0005840	29	1.454×10^{-20}	4.553×10^{-18}
mitochondrial respiratory chain::GO:0005746	19	3.201×10^{-19}	9.305×10^{-19}
ribosomal subunit::GO:0044391	25	3.495×10^{-19}	9.483×10^{-17}
respiratory chain complex::GO:0098803	18	7.039×10^{-19}	1.791×10^{-11}
mitochondrial respiratory chain complex I::GO:0005747	11	4.207×10^{-12}	9.012×10^{-11}
respiratory chain complex I::GO:0045271	11	4.207×10^{-12}	9.012×10^{-11}
NADH dehydrogenase complex::GO:0030964	11	4.207×10^{-29}	9.012×10^{-11}
cytosol::GO:0005829	54	8.115×10^{-12}	1.651×10^{-10}
mitochondrial ribosome::GO:0005761	13	1.882×10^{-11}	3.648×10^{-10}
cytosolic part::GO:0044445	20	2.027×10^{-11}	3.75×10^{-11}
cytosolic ribosome::GO:0022626	15	2.477×10^{-11}	4.384×10^{-11}
intracellular ribonucleoprotein complex::GO:0030529	38	3.62×10^{-11}	6.14×10^{-11}
large ribosomal subunit::GO:0015934	14	8.246×10^{-10}	1.342×10^{-09}
small ribosomal subunit::GO:0015935	11	1.485×10^{-09}	2.324×10^{-08}
mitochondrial matrix::GO:0005759	17	7.003×10^{-08}	1.056×10^{-07}
catalytic complex::GO:1902494	39	1.209×10^{-08}	1.701×10^{-07}
nucleus::GO:0005634	131	1.212×10^{-08}	1.701×10^{-07}
cytosolic large ribosomal subunit::GO:0022625	10	1.386×10^{-08}	1.88×10^{-07}
intracellular organelle lumen::GO:0070013	77	4.733×10^{-08}	6.214×10^{-07}
mitochondrial small ribosomal subunit::GO:0005763	7	6.346×10^{-08}	7.827×10^{-07}
organellar small ribosomal subunit::GO:0000314	7	6.346×10^{-08}	7.827×10^{-07}
mitochondrial proton-transporting ATP synthase complex::GO:0005753	6	8.484×10^{-08}	1.016×10^{-06}
proton-transporting ATP synthase complex::GO:0045259	6	1.732×10^{-07}	2.014×10^{-05}
intracellular non-membrane-bounded organelle::GO:0043232	84	4.543×10^{-06}	5.137×10^{-06}
cytochrome complex::GO:0070069	6	1.223×10^{-06}	1.346×10^{-05}
vesicle::GO:0031982	77	2.976×10^{-06}	3.187×10^{-05}

Table 7.11: GO annotations involved in cellular component down-regulated in neurons during EAE, sorted by FDR corrected p-values. Determined by GeneAnswers in R Studio using a hypergeometric statistic.

category	genes in category	p-value	FDR p-value
structural constituent of ribosome::GO:0003735	24	5.561×10^{-10}	4.927×10^{-13}
hydrogen ion transmembrane transporter activity::GO:0015078	14	1.732×10^{-08}	7.672×10^{-08}
structural molecule activity::GO:0005198	30	5.139×10^{-09}	1.518×10^{-06}
electron carrier activity::GO:0009055	10	1.741×10^{-07}	3.856×10^{-05}
cytochrome-c oxidase activity::GO:0004129	6	2.451×10^{-06}	0.0003102
heme-copper terminal oxidase activity::GO:0015002	6	2.451×10^{-06}	0.0003102
oxidoreductase activity, acting on a heme group of donors, oxygen as acceptor::GO:0016676	6	2.451×10^{-06}	0.0003102
oxidoreductase activity, acting on a heme group of donors::GO:0016675	6	3.08×10^{-06}	0.0003411
NADH dehydrogenase (ubiquinone) activity::GO:0008137	6	7.043×10^{-06}	0.000624
NADH dehydrogenase (quinone) activity::GO:0050136	6	7.043×10^{-06}	0.000624
NADH dehydrogenase activity::GO:0003954	6	8.5×10^{-06}	0.000682
monovalent inorganic cation transmembrane transporter activity::GO:0015077	17	9.236×10^{-06}	0.000682
oxidoreductase activity::GO:0016491	28	2.092×10^{-05}	0.001426
oxidoreductase activity, acting on NAD(P)H, quinone or similar compound as acceptor::GO:0016655	6	3.594×10^{-05}	0.002275
ubiquinol-cytochrome-c reductase activity::GO:0008121	3	0.0001114	0.006171
oxidoreductase activity, acting on diphenols and related substances as donors, cytochrome as acceptor::GO:0016681	3	0.0001114	0.006171
oxidoreductase activity, acting on diphenols and related substances as donors::GO:0016679	3	0.0001763	0.00919
oxidoreductase activity, acting on NAD(P)H::GO:0016651	7	0.0001978	0.009736
acylphosphatase activity::GO:0003998	2	0.0002236	0.01043
4 iron, 4 sulfur cluster binding::GO:0051539	5	0.000313	0.01387
inorganic cation transmembrane transporter activity::GO:0022890	18	0.0003581	0.01501
iron-sulfur cluster binding::GO:0051536	6	0.0003898	0.01501
metal cluster binding::GO:0051540	6	0.0003898	0.01501
poly(A) RNA binding::GO:0044822	32	0.0005576	0.02018
2 iron, 2 sulfur cluster binding::GO:0051537	4	0.0005694	0.02018
proton-transporting ATP synthase activity, rotational mechanism::GO:0046933	3	0.0006625	0.02258
chaperone binding::GO:0051087	6	0.00085	0.02789
cation transmembrane transporter activity::GO:0008324	19	0.0008926	0.02824
RNA binding::GO:0003723	39	0.001704	0.05207
phosphatidic acid transporter activity::GO:1990050	2	0.00217	0.0641
binding::GO:0005488	213	0.002527	0.07224
nucleoside-triphosphatase regulator activity::GO:0060589	11	0.002647	0.0733

Table 7.12: GO annotations involved in molecular function in 'neuron down' list, sorted by FDR corrected p-values, based on the p-value as determined by a hypergeometric statistic.

8 Abbreviations

Ab Antibody

Aif1 allograft inflammatory factor 1

AMPK AMP-activated protein kinase

Apol6 apolipoprotein L6

APP amyloid precursor protein

Asic1 acid-sensing ion channel subunit 1

BAC bacterial artificial chromosome

Bag1 Bcl2-associated athanogene 1

Bcl2 B-cell lymphoma 2

BDNF brain-derived neurotrophic factor

BP biological process

BSA bovine serum albumin

Bsn bassoon

°C degree Celcius

Calca calcitonin related polypeptide alpha

Calcb calcitonin related polypeptide beta

CC cellular component

Chat choline acetyltransferase

Clip2 CAP-Gly domain-containing linker protein 2

CSEA cell-type specific expression analysis

CSF cerebrospinal fluid

Cxcl9 chemokine (C-X-C motif) ligand 9

Cypd cyclophilin D

DEPC diethyldicarbonat

DNA deoxyribonucleic acid

Dpf2 zinc finger protein ubi-d4

dTTP desoxythymidintriphosphate

EAE experimental autoimmune encephalomyelitis

EGF epidermal growth factor

EGFP enhanced green fluorescent protein

ER endoplasmatic reticulum

ES enrichment score

FACS fluorescence activated cell sorting

FDR false discovery rate

FNDC5 fibronectin type III domain-containing protein 5

g gravitational force

GALC galactosylceramidase

Gm4841 predicted gene 4841

GO Gene Ontology

GSEA gene set enrichment analysis

GWAS genome-wide-association-studies

HBSS Hank's balanced salt solution

HEPES 4-(2-hydroxyethyl)-1-piperazineethanesulfonic acid

Hif-1a hypoxia-inducible factor 1a

Ig immunoglobuline

IHC immunohistochemistry

Iigp1 interferon-inducible GTPase 1

iMN inflamed motor neuron

IP Immunoprecipitation

iSC inflamed spinal cord

Isl1 insulin gene enhancer protein Isl1

KCl potassium chloride

Kcnn1 potassium intermediate/small conductance calcium-activated channel subfamily N member 1

KEGG Kyoto encyclopedia of genes and genomes

Kif kinesin family member

l litre

LCM laser-capture microdissection

Lhx3 LIM homeobox 3

m milli (10^{-3})

MBP myelin basic protein

MF molecular function

$MgCl_2$ magnesium chloride

MHC major histocompatibility complex

min minutes

ml millilitre

MN motor neurons

Mnx1 motor neuron and pancreas homeobox 1

MOG myelin oligodendrocyte glycoprotein

MOMP mitochondrial outer membrane permeabilisation

mPT mitochondria permeability transition

MRI magnet resonance imaging

mRNA messenger RNA

MS multiple sclerosis

mt mitochondrial

μ micro (10^{-6})

NAD nicotinamide adenine dinucleotide

$NaHCO_3$ sodium bicarbonate

NAWM normal appearing white matter

NCX Na^+/Ca^{2+} exchanger

NeuN neuronal nuclei

NF neurofilaments

NP-40 4-nonylphenyl poly(ethylene glycol)

Nt5m 5' 3'-nucleotidase mitochondrial

Nucb1 nucleobindin-1

PBS phosphate-buffered saline

PCR polymerase chain reaction

Pecam1 platelet endothelial cell adhesion molecule 1

PFA paraformaldehyde

PLP proteolipid protein

PONDR predictor of natural disordered regions

PPMS primary progressive MS

Pttg1 securin

Rbfox3 RNA binding Fox-1 homolog 3

RNA ribonucleic acid

RNS reactive nitrogen species

ROS radical oxygen species

RRMS relapse-remitting MS

SC spinal cord

SCN2A sodium voltage-gated channel alpha subunit 2

Scn2a1 sodium channel voltage-gated type II alpha subunit

SEM standard error of mean

SI specificity index

Slc1a3 solute carrier family 1 member 3

SNP single nucleotide polymorphism

SPMS secondary progressive MS

TNF tumor necrosis factor

TRAP translating ribosome affinity purification

Trpm4 transient receptor potential cation channel subfamily M member 4

UCP uncoupling proteins

Ucp2 uncoupling protein 2

Vgf vascular growth factor

Vim Vimentin

WT wild type

9 References

Alavian KN et al. (2011). Bcl-xl regulates metabolic efficiency of neurons through interaction with the mitochondrial f1fo atp synthase. *Nature Cell Biology*, **13**: 1224 – 1233.

Alcina A et al. (2010). The autoimmune disease-associated kif5a, cd226 and sh2b3 gene variants confer susceptibility for multiple sclerosis. *Genes And Immunity*, **11**: 439–445.

Altrock WD et al. (2003). Functional inactivation of a fraction of excitatory synapses in mice deficient for the active zone protein bassoon. *Neuron*, **37**(5): 787–800.

Anderson JM et al. (2008). Abnormally phosphorylated tau is associated with neuronal and axonal loss in experimental autoimmune encephalomyelitis and multiple sclerosis. *Brain*, **131**(7): 1736–1748.

Andrews ZB, Diano S, Horvath TL (2005). Mitochondrial uncoupling proteins in the cns: in support of function and survival. *Nature Reviews Neuroscience*, **6**: 829–840.

Arsenijevic D et al. (2000). Disruption of the uncoupling protein-2 gene in mice reveals a role in immunity and reactive oxygen species production. *Nature Genetics*, **26**: 435–439.

Ashburner M et al. (2000). Gene ontology: tool for the unification of biology. *Nature Genetics*, **25**: 25–29.

Bae BI et al. (2005). p53 mediates cellular dysfunction and behavioral abnormalities in huntington's disease. *Neuron*, **47**(1): 29–41.

Bando Y et al. (2015). Abnormal morphology of myelin and axon pathology in murine models of multiple sclerosis. *Neurochemistry International*, **81**: 16–27.

Baranzini SE et al. (2009). Genome-wide association analysis of susceptibility and clinical phenotype in multiple sclerosis. *Human Molecular Genetics*, **18**(4): 767–778.

Baranzini et al SE (2010). Genetic variation influences glutamate concentrations in brains of patients with multiple sclerosis. *Brain*, **133**(9): 2603–2611.

Baxter AG (2007). The origin and application of experimental autoimmune encephalomyelitis. *Nature reviews Immunology*, **7**(november): 904–912.

Black JA et al. (2007). Exacerbation of experimental autoimmune encephalomyelitis after withdrawal of phenytoin and carbamazepine. *Annals of Neurology*, **62**(1): 21–33.

Boise LH et al. (1993). *bcl-x*, a *bcl-2*-related gene that functions as a dominant regulator of apoptotic cell death. *Cell*, **74**(4): 597–608.

Brichta L et al. (2015). Identification of neurodegenerative factors using translatome–regulatory network analysis. *Nature Neuroscience*, **18**: 1325–1333.

Bucci A C, P, Cogli L (2014). The role of rab proteins in neuronal cells and in the trafficking of neurotrophin receptors. *Membranes*, **4**(4): 642–677.

Campbell GR et al. (2011). Mitochondrial dna deletions and neurodegeneration in multiple sclerosis. *Annals of Neurology*, **69**(3): 481–492.

Campbell PD et al. (2014). Unique function of kinesin kif5a in localization of mitochondria in axons. *The Journal of Neuroscience*, **34**(44): 14717.

Cantó C, Auwerx J (2009). Pgc-1α, sirt1 and ampk, an energy sensing network that controls energy expenditure. *Current Opinion in Lipidology*, **20**(2): 98–105.

Chepelev NL et al. (2016). Transcriptional profiling of the mouse hippocampus supports an nmdar-mediated neurotoxic mode of action for benzo[a]pyrene. *Environmental and Molecular Mutagenesis*, **57**(5): 350–363.

Chiti F, Dobson CM (2017). Protein misfolding, amyloid formation, and human disease: A summary of progress over the last decade. *Annual Review of Biochemistry*, **86**(1): 27–68.

Chitnis T et al. (2007). Elevated neuronal expression of cd200 protects wld mice from inflammation-mediated neurodegeneration. *The American Journal of Pathology*, **170**(5): 1695–1712.

Ciechanover A, Kwon YT (2017). Protein quality control by molecular chaperones in neurodegeneration. *Frontiers in Neuroscience*, **11**: 185.

Compston A (1988). The 150th anniversary of the first depiction of the lesions of multiple sclerosis. *Journal of neurology, neurosurgery, and psychiatry*, **51**(10): 1249–1252.

Compston A, Coles A (2002). Multiple sclerosis. *The Lancet*, **359**(9313): 1221–1231.

Compston A, Coles A (2008). Multiple sclerosis. *The Lancet*, **372**(9648): 1502–1517.

Compston A, Coles A (2016). Multiple sclerosis. *The Lancet*, **372**(9648): 1502–1517.

Confavreux C, Vukusic S, Moreau T, Adeleine P (2000). Relapses and progression of disability in multiple sclerosis. *New England Journal of Medicine*, **343**(20): 1430–1438.

Craner MJ et al. (2004). Molecular changes in neurons in multiple sclerosis: Altered axonal expression of $na_v1.2$ and $na_v1.6$ sodium channels and na^+/ca^{2+} exchanger. *Proceedings of the National Academy of Sciences of the United States of America*, **101**(21): 8168–8173.

Croxford JL et al. (2008). Cannabinoid-mediated neuroprotection, not immunosuppression, may be more relevant to multiple sclerosis. *Journal of Neuroimmunology*, **193**(1): 120–129.

Dehay B et al. (2010). Pathogenic lysosomal depletion in parkinson's disease. *The Journal of Neuroscience*, **30**(37): 12535.

Dhingra V, Gupta M, Andacht T, Fu ZF (2005). New frontiers in proteomics research: A perspective. *International Journal of Pharmaceutics*, **299**(1): 1–18.

Didonna A, Cekanaviciute E, Oksenberg JR, Baranzini SE (2016). Immune cell-specific transcriptional profiling highlights distinct molecular pathways controlled by tob1 upon experimental autoimmune encephalomyelitis. *Scientific Reports*, **6**: 31603.

Dougherty JD, Schmidt EF, Nakajima M, Heintz N (2010). Analytical approaches to rna profiling data for the identification of genes enriched in specific cells. *Nucleic Acids Research*, **38**(13): 4218–4230.

Doyle JP (2008). Application of a translational profiling approach for the comparative analysis of cns cell types. *Cell*, **135**(4): 749–762.

Dutta R et al. (2006). Mitochondrial dysfunction as a cause of axonal degeneration in multiple sclerosis patients. *Annals of Neurology*, **59**(3): 478–489.

Eichhorst H (1896). Über infantile und heriditäre multiple Sklerose. *Archiv für pathologische Anatomie und Physiologie und für klinische Medicin*, **146**(2): 173–192.

Elliott E, Tsvetkov P, Ginzburg I (2007). Bag-1 associates with hsc70Âůtau complex and regulates the proteasomal degradation of tau protein. *Journal of Biological Chemistry*, **282**(51): 37276–37284.

F F Silva D et al. (2011). Amyloid-β-induced mitochondrial dysfunction impairs the autophagic lysosomal pathway in a tubulin dependent pathway. *Journal of Alzheimer's disease : JAD*, **26**: 565–81.

Farshbaf JM et al. (2016). Does pgc1α/fndc5/bdnf elicit the beneficial effects of exercise on neurodegenerative disorders? *NeuroMolecular Medicine*, **18**(1): 1–15.

Feng G et al. (2010). A collection of bioconductor methods to visualize gene-list annotations. *BMC research notes*, **3**: 10–10.

Fischer MT et al. (2012). Nadph oxidase expression in active multiple sclerosis lesions in relation to oxidative tissue damage and mitochondrial injury. *Brain*, **135**(3): 886–899.

Fischer MT et al. (2013). Disease-specific molecular events in cortical multiple sclerosis lesions. *Brain*, **136**(6): 1799–1815.

Fonseca-Kelly Z et al. (2012). Resveratrol neuroprotection in a chronic mouse model of multiple sclerosis. *Frontiers in Neurology*, **3**: 84.

Forte M et al. (2007). Cyclophilin d inactivation protects axons in experimental autoimmune encephalomyelitis, an animal model of multiple sclerosis. *Proceedings of the National Academy of Sciences*, **104**(18): 7558.

Friese MA, Schattling B, Fugger L (2014). Mechanisms of neurodegeneration and axonal dysfunction in multiple sclerosis. *Nat Rev Neurol*, **10**(4): 225–238.

Friese MA et al. (2007). Acid-sensing ion channel-1 contributes to axonal degeneration in autoimmune inflammation of the central nervous system. *Nature Medicine*, **13**: 1483–1489.

Fujii T et al. (2017). Expression and function of the cholinergic system in immune cells. *Frontiers in Immunology*, **8**: 1085.

Ghavami S et al. (2014). Autophagy and apoptosis dysfunction in neurodegenerative disorders. *Progress in Neurobiology*, **112**: 24–49.

Gontier G et al. (2015). Blocking igf signaling in adult neurons alleviates alzheimer's disease pathology through amyloid-β clearance. *The Journal of Neuroscience*, **35**(33): 11500.

Gray E et al. (2012). Accumulation of cortical hyperphosphorylated neurofilaments as a marker of neurodegeneration in multiple sclerosis. *Multiple Sclerosis Journal*, **19**(2): 153–161.

Gundelfinger ED, Reissner C, Garner CC (2016). Role of bassoon and piccolo in assembly and molecular organization of the active zone. *Frontiers in Synaptic Neuroscience*, **7**: 19.

Haghikia A, Hohlfeld R, Gold R, Fugger L (2013). Therapies for multiple sclerosis: translational achievements and outstanding needs. *Trends in Molecular Medicine*, **19**(5): 309–319.

Haider L et al. (2011). Oxidative damage in multiple sclerosis lesions. *Brain*, **134**(7): 1914–1924.

Hardingham GE, Bading H (2010). Synaptic versus extrasynaptic NMDA receptor signalling: implications for neurodegenerative disorders. *Nat Rev Neurosci*, **11**(10): 682–696.

Hares K et al. (2017a). Axonal motor protein kif5a and associated cargo deficits in multiple sclerosis lesional and normal-appearing white matter. *Neuropathology and Applied Neurobiology*, **43**(3): 227–241.

Hares K et al. (2017b). Overexpression of kinesin superfamily motor proteins in alzheimer's disease. *Journal of Alzheimer's Disease*, **60**(4): 1511–1524.

Hawkes CH (2007). Smoking is a risk factor for multiple sclerosis : a metanalysis. *Multiple Sclerosis*, **13**(September 2006): 610–615.

Heiman M et al. (2008). A translational profiling approach for the molecular characterization of cns cell types. *Cell*, **135**(4): 738–748.

Herold S et al. (2015). Neurodegeneration in autoimmune optic neuritis is associated with altered app cleavage in neurons and up-regulation of p53. *PLOS ONE*, **10**(10): e0138852–.

Hollander M, Wolfe D (1973). Nonparametric statistical methods. *Wiley New York*.

IMSGC (2005). A high-density screen for linkage in multiple sclerosis. *The American Journal of Human Genetics*, **77**(3): 454–467.

IMSGC (2011). Genome-wide association study of severity in multiple sclerosis. *Genes Immun*, **12**(8): 615–625.

IMSGC, WTCCC (2011). Genetic risk and a primary role for cell-mediated immune mechanisms in multiple sclerosis. *Nature*, **476**(7359): 214–219.

Ishihara T et al. (2001). Attenuated neurodegenerative disease phenotype in tau transgenic mouse lacking neurofilaments. *The Journal of Neuroscience*, **21**(16): 6026–6035.

Jonas EA (2014). Contributions of bcl-xl to acute and long term changes in bioenergetics during neuronal plasticity. *Biochimica et Biophysica Acta (BBA) - Molecular Basis of Disease*, **1842**(8): 1168–1178.

Jonas EA, Porter GA, Alavian KN (2014). Bcl-xl in neuroprotection and plasticity. *Frontiers in Physiology*, **5**: 355.

Kamoshita M et al. (2016). Neuroprotective effect of activated 5'-adenosine monophosphate-activated protein kinase on cone system function during retinal inflammation. *BMC Neuroscience*, **17**(1): 32.

Kawashima K et al. (2007). Expression and function of genes encoding cholinergic components in murine immune cells. *Life Sciences*, **80**(24): 2314–2319.

Kermer P et al. (2015). Bag1 is neuroprotective in in vivo and in vitro models of parkinson's disease. *Journal of Molecular Neuroscience*, **55**(3): 587–595.

Kingwell E et al. (2013). Incidence and prevalence of multiple sclerosis in europe: a systematic review. *BMC Neurology*, **13**(1): 128.

Kutzelnigg A et al. (2005). Cortical demyelination and diffuse white matter injury in multiple sclerosis. *Brain*, **128**(11): 2705–2712.

Lassmann H (1999). The pathology of multiple sclerosis and its evolution. *Philosophical transactions of the Royal Society of London Series B, Biological sciences*, **354**(1390): 1635–1640.

Lee S, Sato Y, Nixon RA (2011). Lysosomal proteolysis inhibition selectively disrupts axonal transport of degradative organelles and causes an alzheimer's-like axonal dystrophy. *The Journal of Neuroscience*, **31**(21): 7817.

Lehman NL (2009). The ubiquitin proteasome system in neuropathology. *Acta Neuropathologica*, **118**(3): 329–347.

Lein ES et al. (2006). Genome-wide atlas of gene expression in the adult mouse brain. *Nature*, **445**: 168–176.

Lin MT, Beal MF (2006). Mitochondrial dysfunction and oxidative stress in neurodegenerative diseases. *Nature*, **443**: 787–795.

Lin SC, Hardie DG (2018). Ampk: Sensing glucose as well as cellular energy status. *Cell Metabolism*, **27**(2): 299–313.

Lindholm D, Eriksson O, Korhonen L (2004). Mitochondrial proteins in neuronal degeneration. *Biochemical and Biophysical Research Communications*, **321**(4): 753–758.

Linker RA et al. (2011). Fumaric acid esters exert neuroprotective effects in neuroinflammation via activation of the nrf2 antioxidant pathway. *Brain*, **134**(3): 678–692.

Liu Z et al. (2005). Apolipoprotein l6, a novel proapoptotic bcl-2 homology 3–only protein, induces mitochondria-mediated apoptosis in cancer cells. *Molecular Cancer Research*, **3**(1): 21.

Lobo MK et al. (2006). FACS-array profiling of striatal projection neuron subtypes in juvenile and adult mouse brains. *Nat Neurosci*, **9**(3): 443–452.

Lovas G et al. (2000). Axonal changes in chronic demyelinated cervical spinal cord plaques. *Brain*, **123**(12): 308–317.

Luo C et al. (2017). The role of microglia in multiple sclerosis. *Neuropsychiatric disease and treatment*, **13**: 1661–1667.

Maday S, Holzbaur ELF (2016). Compartment-specific regulation of autophagy in primary neurons. *The Journal of Neuroscience*, **36**(22): 5933.

Mattiasson G et al. (2003). Uncoupling protein-2 prevents neuronal death and diminishes brain dysfunction after stroke and brain trauma. *Nature Medicine*, **9**: 1062–1068.

McKeever PM et al. (2017). Cholinergic neuron gene expression differences captured by translational profiling in a mouse model of alzheimer's disease. *Neurobiology of Aging*, **57**: 104–119.

Menezes MJ et al. (2015). Mutation in mitochondrial ribosomal protein s7 (mrps7) causes congenital sensorineural deafness, progressive hepatic and renal failure and lactic acidemia. *Human Molecular Genetics*, **24**(8): 2297–2307.

Millecamps S, Julien JP (2013). Axonal transport deficits and neurodegenerative diseases. *Nature Reviews Neuroscience*, **14**: 161 EP –.

Mizuno T et al. (2008). Interferon-γdirectly induces neurotoxicity through a neuron specific, calcium-permeable complex of ifn-γ receptor and ampa glur1 receptor. *The FASEB Journal*, **22**(6): 1797–1806.

Morsali D et al. (2013). Safinamide and flecainide protect axons and reduce microglial activation in models of multiple sclerosis. *Brain*, **136**(4): 1067–1082.

MS F, EJ T, F D, et al (2005). Recommended standard of cerebrospinal fluid analysis in the diagnosis of multiple sclerosis: A consensus statement. *Archives of Neurology*, **62**(6): 865–870.

Naciff JM, Behbehani MM, Misawa H, Dedman JR (1999). Identification and transgenic analysis of a murine promoter that targets cholinergic neuron expression. *Journal of Neurochemistry*, **72**(1): 17–28.

Nakagawa T et al. (2005). Cyclophilin d-dependent mitochondrial permeability transition regulates some necrotic but not apoptotic cell death. *Nature*, **434**: 652–658.

Nath N et al. (2009). Loss of ampk exacerbates experimental autoimmune encephalomyelitis disease severity. *Biochemical and Biophysical Research Communications*, **386**(1): 16–20.

Newcombe J et al. (2008). Glutamate receptor expression in multiple sclerosis lesions. *Brain Pathology*, **18**(1): 52–61.

Nikic et al I (2011). A reversible form of axon damage in experimental autoimmune encephalomyelitis and multiple sclerosis. *Nature medicine*, **17**(4): 495–499.

Noseworthy JH, Lucchinetti C, Rodriguez M, Weinshenker BG (2000). Multiple sclerosis. *New England Journal of Medicine*, **343**(13): 938–952.

Offen D et al. (2000). Mice overexpressing bcl-2 in their neurons are resistant to myelin oligodendrocyte glycoprotein (mog)-induced experimental autoimmune encephalomyelitis (eae). *Journal of Molecular Neuroscience*, **15**(3): 167–176.

Okaty BW, Sugino K, Nelson SB (2011). A quantitative comparison of cell-type-specific microarray gene expression profiling methods in the mouse brain. *PLOS ONE*, **6**(1): 1–10.

Okerlund ND et al. (2017). Bassoon controls presynaptic autophagy through atg5. *Neuron*, **93**(4): 897–913.e7.

O'Malley HA et al. (2009). Loss of Na+ channel $\beta 2$ subunits is neuroprotective in a mouse model of multiple sclerosis. *Molecular and Cellular Neuroscience*, **40**(2): 143–155.

Peng K et al. (2006). Length-dependent prediction of protein intrinsic disorder. *BMC Bioinformatics*, **7**(1): 208.

Pennisi G et al. (2011). Redox regulation of cellular stress response in multiple sclerosis. *Biochemical Pharmacology*, **82**(10): 1490–1499.

Perrot R, Julien JP (2009). Real-time imaging reveals defects of fast axonal transport induced by disorganization of intermediate filaments. *The FASEB Journal*, **23**(9): 3213–3225.

Peter Bassoe RRG (1929). Human Rabies and Rabies vaccine encephalomyelitis. *Archives of Neurology and Psychiatry*.

Polman CH et al. (2011). Diagnostic criteria for multiple sclerosis: 2010 revisions to the mcdonald criteria. *Annals of Neurology*, **69**(2): 292–302.

Popescu BFG, Lucchinetti CF (2012). Pathology of demyelinating diseases. *Annual Review of Pathology: Mechanisms of Disease*, **7**(1): 185–217.

Quintanilla RA, Johnson GVW (2009). Role of mitochondrial dysfunction in the pathogenesis of huntington's disease. *Brain Research Bulletin*, **80**(4): 242–247.

Raddatz BBR et al. (2014). Transcriptomic meta-analysis of multiple sclerosis and its experimental models. *PLOS ONE*, **9**(1): 1–15.

Ramsey SA et al. (2008). Uncovering a macrophage transcriptional program by integrating evidence from motif scanning and expression dynamics. *PLOS Computational Biology*, **4**(3): 1–25.

Ray PD, Huang BW, Tsuji Y (2012). Reactive oxygen species (ros) homeostasis and redox regulation in cellular signaling. *Cellular signalling*, **24**(5): 981–990.

Reverberi R, Reverberi L (2007). Factors affecting the antigen-antibody reaction. *Blood Transfusion*, **5**(4): 227–240.

Robinson AP, Harp CT, Noronha A, Miller SD (2014). The experimental autoimmune encephalomyelitis (EAE) model of MS. utility for understanding disease pathophysiology and treatment. *Handbook of Clinical Neurology*, **122**: 179–189.

Rossner MJ et al. (2006). Global transcriptome analysis of genetically identified neurons in the adult cortex. *The Journal of Neuroscience*, **26**(39): 9956.

Ruggiano A, Foresti O, Carvalho P (2014). Er-associated degradation: Protein quality control and beyond. *The Journal of Cell Biology*, **204**(6): 869–879.

Salmen A, Gold R (2014). Mode of action and clinical studies with fumarates in multiple sclerosis. *Experimental Neurology*, **262**(Part A): 52–56.

Salminen A et al. (2013). Impaired autophagy and app processing in alzheimer's disease: The potential role of beclin 1 interactome. *Progress in Neurobiology*, **106-107**: 33–54.

Sarchielli P et al. (2003). Excitatory amino acids and multiple sclerosis: Evidence from cerebrospinal fluid. *Archives of Neurology*, **60**(8): 1082–1088.

Sato F et al. (2013). Resveratrol exacerbates both autoimmune and viral models of multiple sclerosis. *The American Journal of Pathology*, **183**(5): 1390–1396.

Sato K et al. (2012). Impaired response of hypoxic sensor protein hif-1α and its downstream proteins in the spinal motor neurons of als model mice. *Brain Research*, **1473**: 55–62.

Sawcer S, Franklin RJM, Ban M (2014). Multiple sclerosis genetics Sup. *Lancet neurology*, **13**(7): 700–709.

Scalfari A et al. (2010). The natural history of multiple sclerosis, a geographically based study 10: relapses and long-term disability. *Brain*, **133**(7): 1914–1929.

Schattling B et al. (2012). Trpm4 cation channel mediates axonal and neuronal degeneration in experimental autoimmune encephalomyelitis and multiple sclerosis. *Nature Medicine*, **18**: 1805–1811.

Schattling B et al. (2016). Activity of nav1.2 promotes neurodegeneration in an animal model of multiple sclerosis. *JCI Insight*, **1**(19).

Schwab JM et al. (2001). AIF-1 expression defines a proliferating and alert microglial/macrophage phenotype following spinal cord injury in rats. *Journal of Neuroimmunology*, **119**(2): 214–222.

Schwarz TL (2013). Mitochondrial trafficking in neurons. *Cold Spring Harbor Perspectives in Biology*, **5**(6).

Shelton LB, Koren J, Blair LJ (2017). Imbalances in the hsp90 chaperone machinery: Implications for tauopathies. *Frontiers in Neuroscience*, **11**: 724.

Simpson S et al. (2011). Latitude is significantly associated with the prevalence of multiple sclerosis: a meta-analysis. *Journal of neurology, neurosurgery, and psychiatry*, **82**(10): 1132–41.

Smorodchenko A et al. (2017). Ucp2 up-regulation within the course of autoimmune encephalomyelitis correlates with t-lymphocyte activation. *Biochimica et Biophysica Acta (BBA) - Molecular Basis of Disease*, **1863**(4): 1002–1012.

Spillantini MG, Goedert M (2013). Tau pathology and neurodegeneration. *The Lancet Neurology*, **12**(6): 609–622.

Sriram S, Steiner I (2005). Experimental allergic encephalomyelitis: A misleading model of multiple sclerosis. *Annals of Neurology*, **58**(6): 939–945.

Stover JF et al. (1997). Neurotransmitters in cerebrospinal fluid reflect pathological activity. *European Journal of Clinical Investigation*, **27**(12): 1038–1043.

Stranahan AM, Mattson MP (2012). Recruiting adaptive cellular stress responses for successful brain ageing. *Nat Rev Neurosci*, **13**(3): 209–216.

Stys PK, Zamponi GW, van Minnen J, Geurts JJG (2012). Will the real multiple sclerosis please stand up? *Nature Reviews Neuroscience*, **13**(7): 507–514.

Subramanian A et al. (2005). Gene set enrichment analysis: A knowledge-based approach for interpreting genome-wide expression profiles. *Proceedings of the National Academy of Sciences*, **102**(43): 15545.

Sumaya C, Myers LW, Ellison GW (1980). Epstein-barr virus antibodies in multiple sclerosis. *Archives of Neurology*, **37**(2): 94–96.

Sylvester JE, Fischel-Ghodsian N, Mougey EB, O'brien TW (2004). Mitochondrial ribosomal proteins: Candidate genes for mitochondrial disease. *Genetics In Medicine*, **6**: 73–80.

Tackenberg C et al. (2013). Nmda receptor subunit composition determines beta-amyloid-induced neurodegeneration and synaptic loss. *Cell Death Disease*, **4**: e608.

Tebaldi T et al. (2012). Widespread uncoupling between transcriptome and translatome variations after a stimulus in mammalian cells. *BMC Genomics*, **13**: 220–220.

The Gene Ontology Consortium (2017). Expansion of the gene ontology knowledgebase and resources. *Nucleic Acids Research*, **45**(D1): 331–338.

Tietjen I et al. (2003). Single-cell transcriptional analysis of neuronal progenitors. *Neuron*, **38**(2): 161–175.

Trapp BD, Stys PK (2009). Virtual hypoxia and chronic necrosis of demyelinated axons in multiple sclerosis. *The Lancet Neurology*, **8**(3): 280–291.

van den Berg R, Hoogenraad CC, Hintzen RQ (2017). Axonal transport deficits in multiple sclerosis: spiraling into the abyss. *Acta Neuropathologica*, **134**(1): 1–14.

van Horssen J et al. (2008). Severe oxidative damage in multiple sclerosis lesions coincides with enhanced antioxidant enzyme expression. *Free Radical Biology and Medicine*, **45**(12): 1729–1737.

Vander Heiden MG et al. (2001). Bcl-x l promotes the open configuration of the voltage-dependent anion channel and metabolite passage through the outer mitochondrial membrane. *Journal of Biological Chemistry*, **276**(22): 19414–19419.

Vaseva AV et al. (2012). p53 opens the mitochondrial permeability transition pore to trigger necrosis. *Cell*, **149**(7): 1536–1548.

Waites CL et al. (2013). Bassoon and piccolo maintain synapse integrity by regulating protein ubiquitination and degradation. *The EMBO Journal*, **32**(7): 954.

Walldén K et al. (2005). Structural basis for substrate specificity of the human mitochondrial deoxyribonucleotidase. *Structure*, **13**(7): 1081–1088.

Watson E et al. (2009). Analysis of knockout mice suggests a role for vgf in the control of fat storage and energy expenditure. *BMC Physiology*, **9**(1): 19.

Willer CJ et al. (2005). Timing of birth and risk of multiple sclerosis: population based study. *BMJ (Clinical research ed)*, **330**(7483): 120.

Witte ME, Mahad DJ, Lassmann H, van Horssen J (2014). Mitochondrial dysfunction contributes to neurodegeneration in multiple sclerosis. *Trends in Molecular Medicine*, **20**(3): 179–187.

Witte ME et al. (2013). Reduced expression of pgc-1α partly underlies mitochondrial changes and correlates with neuronal loss in multiple sclerosis cortex. *Acta Neuropathologica*, **125**(2): 231–243.

Xia CH et al. (2003). Abnormal neurofilament transport caused by targeted disruption of neuronal kinesin heavy chain kif5a. *The Journal of Cell Biology*, **161**(1): 55.

Xu X et al. (2014). Cell type-specific expression analysis to identify putative cellular mechanisms for neurogenetic disorders. *The Journal of Neuroscience*, **34**(4): 1420.

Yabe I et al. (2018). Mutations in bassoon in individuals with familial and sporadic progressive supranuclear palsy-like syndrome. *Scientific Reports*, **8**(1): 819.

Yadav P et al. (2016). Neurofilament depletion improves microtubule dynamics via modulation of stat3/stathmin signaling. *Acta Neuropathologica*, **132**(1): 93–110.

Yu WH et al. (2005). Macroautophagy—a novel β-amyloid peptide-generating pathway activated in alzheimer's disease. *The Journal of Cell Biology*, **171**(1): 87.

Zhaorigetu S et al. (2011). Apolipoprotein l6, induced in atherosclerotic lesions, promotes apoptosis and blocks beclin 1-dependent autophagy in atherosclerotic cells. *Journal of Biological Chemistry*, **286**(31): 27389–27398.

Zivadinov R et al. (2007). Preservation of gray matter volume in multiple sclerosis patients with the met allele of the rs6265 (val66met) snp of brain-derived neurotrophic factor. *Human Molecular Genetics*, **16**(22): 2659–2668.

10 Acknowledgement

I would like to thank my supervisor Prof. Dr. Manuel A. Friese for the opportunity to work on this exciting topic, for the great support and for his constant encouragement to extend my scientific skills.

I thank the whole Friese lab, especially Dr. Benjamin Schattling, Dr. Dr. Broder Engler, Dr. Friederike Ufer, Dr. Anne Willing and Dr. Melanie Piédavent-Salomon for teaching me the basic experimental tools and for creating a cooperative and inspiring atmosphere. I would also like to thank Dr. Katharine Miller for teaching me experimental procedures and for the collaborative work in establishing the bacTRAP methodology. Special thanks also goes to Nina Kursawe for her support with experimental procedures and to the animal caretakers for their dedicated work.

I would also like to thank Prof. Dr. Stefan M. Gold and Dr. Ole Pless for inspiring joint discussions and Dr. Schattling and Dr. Pless for proofreading the manuscript.

Finally, I am extremely grateful to my family and my friends for their love and support.

11 Curriculum vitae

Lebenslauf wurde aus datenschutzrechtlichen Gründen entfernt.

12 *Eidesstattliche Versicherung*

Ich versichere ausdrücklich, dass ich die Arbeit selbständig und ohne fremde Hilfe verfasst, andere als die von mir angegebenen Quellen und Hilfsmittel nicht benutzt und die aus den benutzten Werken wörtlich oder inhaltlich entnommenen Stellen einzeln nach Ausgabe (Auflage und Jahr des Erscheinens), Band und Seite des benutzten Werkes kentlich gemacht habe. Ferner versichere ich, dass ich die Dissertation bisher nicht einem Fachvertreter an einer anderen Hochschule zur Überprüfung vorgelegt oder mich anderweitig um Zulassung zur Promotion beworben habe. Ich erkläre mich einverstanden, dass meine Dissertation vom Dekanat der Medizinischen Fakultät mit einer gängigen Software zur Erkennung von Plagiaten überprüft werden kann.

Unterschrift: .....